Computational Approaches for Organic Semiconductors: From Chemical and Physical Understanding to Predicting New Materials

Vinayak Bhat[†], Connor P. Callaway[†], Chad Risko*

Department of Chemistry &
Center for Applied Energy Research
University of Kentucky
Lexington, KY 40506-0055, United States

KEYWORDS: π-conjugated molecules; π-conjugated polymers; organic semiconductors; computational modeling; quantum chemistry; density functional theory; atomistic molecular dynamics; coarse-grained molecular dynamics; multi-scale computational methods; virtual screening; machine learning

TOC Graphic

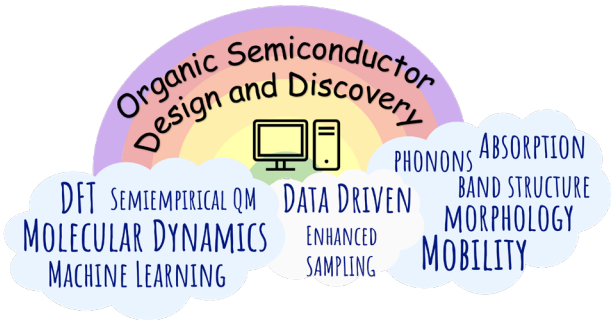
Organic Semiconductor Design and Discovery
DFT
Semiempirical QM
Molecular Dynamics
Machine Learning
Data Driven
Enhanced Sampling
Phonons
Absorption
Band Structure
Morphology
Mobility

Abstract

While a complete understanding of organic semiconductor (OSC) design principles remains elusive, computational methods – ranging from techniques based in classical and quantum mechanics to more recent data-enabled models – can complement experimental observations and provide deep physicochemical insights into OSC structure–processing–property relationships, offering new capabilities for in silico OSC discovery and design. In this Review, we trace the evolution of these computational methods and their application to OSC, beginning with early quantum-chemical methods to investigate resonance in benzene and building to recent machine learning (ML) techniques and their application to ever more sophisticated OSC scientific and engineering challenges. Along the way, we highlight the limitations of the methods and how sophisticated physical and mathematical frameworks have been created to overcome those limitations. We conclude by providing an outlook for the future development of computational techniques to discover and assess the properties of high-performing OSC with greater accuracy.

Contents

1 Introduction

Organic semiconductors (OSC), composed of π-conjugated molecules, polymers, or combinations thereof, offer distinctive tunability of their electrical, optical, and mechanical properties. Modifying these material properties begins with the initial design of the molecular and polymer constituents, wherein the synthetic chemist can alter the length, dimensionality,[1-3] and aromatic (e.g., aromatic, anti-aromatic, quinoid) character of the π-conjugated pathways defined by the carbon framework,[4-7] introduce heteroatoms (e.g., often nitrogen or sulfur) within the carbon backbone,[8-10] and append electron accepting groups, electron-donating groups, and alkyl-based chains of varying length and bulkiness along the periphery.[11-18] However, these molecular-level designs are only part of the story, as the way these molecular or polymer constituents organize in the solid state determines the hierarchical OSC properties, with this organization heavily influenced by material processing. A wide variety of processing methods are available to develop OSC, including from the vapor phase, solutions of differing complexity, or the melt;[19-24] thermal and solvent-based post-processing techniques allow for further tuning of the OSC building block organization,[25, 26] while modifications of the chemistry of the surface on which the OSC is deposited can also impact the characteristics of the final material.[27, 28] Hence, the design space for OSC, when considering the atomic-scale construction of the building blocks and the macroscale processing conditions and device architectures in which the OSC will be used, is, in a word, immense.

Further, a key feature of OSC, especially when contrasting OSC properties to those of inorganic semiconductors, stems from the fact that the molecular and polymer building blocks that comprise OSC interact solely through noncovalent (typically exchange repulsion, dispersion, and electrostatics, with some minor influence from induction) interactions;[29, 30] these noncovalent interactions are considerably weaker when compared to the covalent or ionic (or permutations thereof) bonds that form inorganic materials. The reliance of the OSC structure, from local molecular-scale packing interactions through longer-range solid-state morphologies, on noncovalent interactions has limited the advance of a priori OSC design standards

and makes the development of precise physicochemical models to understand and govern physicochemical properties, at best, difficult.

The last few decades have witnessed tremendous growth in computational power, including software and hardware development, the implementation of ever more complicated mathematical and physical functions, and the general development and application of computational approaches (including both theoretical development and modeling) in chemistry. This growth, notably, has coincided with the rise in the academic and commercial interest in OSC. Hence, the study of OSC has been an intriguing playground in which to develop, benchmark, and deploy these approaches to provide a multiscale physicochemical understanding of these hierarchical materials.[31]

In this Review, we provide an overview of computational methods used to evaluate the properties of organic π-conjugated molecules and polymers and OSC and trace their development with the ever more complex chemical and physical questions that have been posed for these systems over time. As the fundamental theory behind many of these computational methods is well documented and reviewed, we focus more on applications to further the chemical and physical understanding of OSC and provide references to the published literature that offer a more in-depth discussion of the theory. We begin this Review with an overview of quantum-chemical techniques, which evolved from applications of semiempirical wavefunction models for increasingly larger systems to the state-of-the-art density functional theory (DFT) methods readily implemented today to investigate the electronic, redox, optical, and electrical properties of molecular and polymer OSC. We note that, though we generally focus here on the use of semiempirical and DFT-based methods, (non-empirical) wavefunction-based methods do play a critical role in the study of OSC.[32-34] We then move to the description of more classical molecular dynamics and multiscale modeling approaches that have grown in use as interest has increased in understanding OSC structure–processing–function relationships. Due to advancements in computing, modern simulations often include hundreds of thousands – if not millions – of atoms. We next move to discussions of data-enabled and machine-learning approaches, which offer ever-increasing capacities for machine-informed OSC discovery and design, and

highlight novel computer architectures, including quantum computing, that will soon advance the field. Today, considerable effort is regularly expended toward increasing the length and time scales of systems studied through computational approaches, improving the accuracy with which their properties are estimated, and enabling machine-driven exploration of complex materials spaces. Considering these factors, we conclude with an outlook for the future of computational approaches in facilitating the discovery, design, and deployment of next-generation OSC.

2 Quantum-chemical approaches

We begin our discussion with quantum-chemical (QC) approaches used to study OSC, as a key driver of OSC development has been the push to rationalize the mechanisms governing material electronic, redox, optical, and electrical characteristics.[31, 35, 36] We begin by reviewing the development and application of semiempirical wavefunction methods followed by DFT-based approaches, each of which are used to investigate molecular, oligomers (as surrogates of polymers), and solid-state properties.

2.1 Semiempirical QC methods

The physical and chemical properties of materials can be exactly modeled by quantum theory by evaluating the Schrödinger equation.[37] However, the mathematical framework is still prohibitively complex even for modern computational resources, necessitating the use of approximate methods to solve the Schrödinger equation. In some approaches, termed semiempirical methods, data from experiments or model systems are used to estimate values for parameters that are entered into the Schrödinger equation.[38, 39] In this section, we discuss the origins of semiempirical methods as they relate to the study of π-conjugated systems, starting with resonance energy calculations and their subsequent evolution to provide reasonable estimates of ground- and excited-state properties.

2.1.1 Modeling resonance energy and π-conjugation

A key feature of OSC relies on distinctive features of the delocalization of π electrons across the π-conjugated carbon frameworks of the molecular, oligomer, and polymer building blocks. Early computational/modeling efforts related to organic, π-conjugated molecules can be traced back to the understanding of the resonance structures of benzene. In 1931, Hückel formulated the determination of the resonance energy based on two methods.[40] Hückel's first method was based on works by Heitler and London,[41] Heisenberg,[42] Slater,[43-45] and Bloch,[46] while the second method was inspired by Bloch[47] and Hartree.[48] We now refer to these two methods as valence bond (VB) theory and molecular orbital (MO) theory, respectively.[49] Building on Hückel, Pauling's 1933 formulation of the VB method simplified the approach, extending it to larger systems and free radicals.[50, 51] In the case of benzene, Pauling and coworkers assumed that only the interaction between the six electrons in the pure 2*p* carbon orbitals, projecting at right angles to the ring, was sufficient to evaluate the resonance energy. The choice of these orbitals was justified as the resulting energy from the in-plane orbitals only changes the arbitrarily chosen zero of energy. Moreover, the exchange energy of the chosen 2*p* orbitals is negative, while that for the in-plane orbital is positive. The method ignores the interactions between non-adjacent carbon atoms while computing the exchange integrals (α). To compute the resonance energy (*W*), Pauling and coworkers solved the secular equation using Slater's method, as shown in Figure 1.[44] The results revealed that 80% of the resonance energy is contributed by the two Kekulé structures[52] (benzene models A and B in Figure 1), while 20% comes from the three excited-state structures (additional structures shown in Figure 1).

(a)

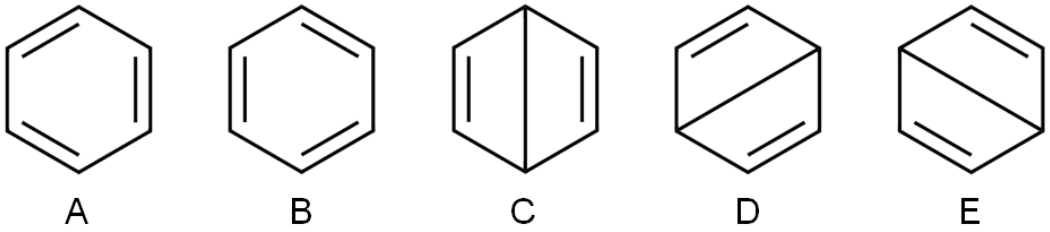

(b)

$$\begin{vmatrix} (Q-W)+3\alpha/2 & \frac{1}{4}(Q-W)+3\alpha/2 & \frac{1}{2}(Q-W)+3\alpha/2 & \frac{1}{2}(Q-W)+3\alpha/2 & \frac{1}{2}(Q-W)+3\alpha/2 \\ \frac{1}{4}(Q-W)+3\alpha/2 & (Q-W)+3\alpha/2 & \frac{1}{2}(Q-W)+3\alpha/2 & \frac{1}{2}(Q-W)+3\alpha/2 & \frac{1}{2}(Q-W)+3\alpha/2 \\ \frac{1}{2}(Q-W)+3\alpha/2 & \frac{1}{2}(Q-W)+3\alpha/2 & (Q-W) & \frac{1}{4}(Q-W)+3\alpha/2 & \frac{1}{4}(Q-W)+3\alpha/2 \\ \frac{1}{2}(Q-W)+3\alpha/2 & \frac{1}{2}(Q-W)+3\alpha/2 & \frac{1}{4}(Q-W)+3\alpha/2 & (Q-W) & \frac{1}{4}(Q-W)+3\alpha/2 \\ \frac{1}{2}(Q-W)+3\alpha/2 & \frac{1}{2}(Q-W)+3\alpha/2 & \frac{1}{4}(Q-W)+3\alpha/2 & \frac{1}{4}(Q-W)+3\alpha/2 & (Q-W) \end{vmatrix} = 0$$

Figure 1. (a) The five canonical structures contributing to the ground state of benzene. Recreated from Ref.[51] Copyright 1934 AIP Publishing. (b) The secular equation with Slater valence-bond eigenfunctions for benzene is based on the five canonical structures, where Q is the Coulomb integral, W is the resonance energy, and α is the exchange integral.

Importantly, the computed resonance energies agreed with experiments that determined the heat of combustion. The formulation was then extended to larger systems like biphenyl, terphenyl, and stilbene, which enabled the derivation of rules for π-conjugation, such as a phenyl group is 20 to 30% less effective in π-conjugation than a double bond.[51] This approach also provided a rationale for stable structures based on π-conjugation (such as the 4.9 kcal stability of 1,2-dihydronaphthalene over 1,4-dihydronaphthalene).

Though Pauling and coworkers simplified the VB method, it was still cumbersome to apply to much larger systems. Hückel's MO method was more applicable to such systems, as demonstrated in later works.[53, 54] In this method, instead of establishing VB eigenfunctions, each of the carbon 2p electrons was considered to move under the influence of the nuclei and all other 2p electrons. The eigenfunction for such a system is represented by the linear combination of atomic orbitals (LCAO), in this case, 2p orbitals. The corresponding secular equation for benzene is

$$\begin{vmatrix} Q-W & \beta & 0 & 0 & 0 & \beta \\ \beta & Q-W & \beta & 0 & 0 & 0 \\ 0 & \beta & Q-W & \beta & 0 & 0 \\ 0 & 0 & \beta & Q-W & \beta & 0 \\ 0 & 0 & 0 & \beta & Q-W & \beta \\ 0 & 0 & 0 & 0 & \beta & Q-W \end{vmatrix} = 0$$

where β is the resonance integral. This method is less rigorous and fails to account for the Pauli exclusion principle, which results in charge pileup in the molecule.[55, 56] As a result, the resonance energies determined through this approach were inferior to those derived from the VB method, as demonstrated by Wheland.[57] However, the simplicity in implementing the MO method for large molecules resulted in its wide application, namely in estimating the electron affinity (EA) of free radicals, the acid strength of hydrocarbons, and the basicity of aryl carbinols.

The methods discussed above use experimental bond dissociation energies and heats of combustion to solve the secular equations and are classified as semiempirical. It is worth nothing that both methods only considered atomic connectivity, as shown in Figure 1, to formulate the secular equation and derive physical insights. However, later works by Mülliken and coworkers improved the MO methods and investigated the alteration in bond lengths on going from localized molecular orbitals to delocalized molecular orbitals.[58, 59]

2.1.2 Understanding molecular interactions with light: Excited states

The interaction of light with matter ignites several processes, with the absorption of a photon by matter being one such process. This process is responsible for the perception of color, the theory or which for organic π-conjugated molecules was proposed by Sklar in 1937.[60] Sklar analyzed the electronic transition in the UV–visible range for benzene by applying the VB method and MO picture with the inclusion of antisymmetric LCAO functions.[60, 61] The only parameters used to compute the absorption bands were the data from the heats of hydrogenation and C–C bond distances. The VB approximation and MO method behave differently; the MO treats the bond as covalent, while the other treats it as ionic. Both fail to model electron repulsion accurately. Hence, to account for polarization, resonance structures with charges were

included. Singlet and triplet energy levels were estimated by incorporating symmetry and polarization. The UV bands observed experimentally were assigned with reasonable confidence via both methods. Mülliken and coworkers further extended the theory of electronic transitions in molecular spectra to organic molecules with double bonds and diene.[58, 59, 62]

Until the works of Coulson and coworkers in 1947,[63] all theories of π-conjugated systems concentrated on applications in hydrocarbons, namely benzene, diene, and heteroatom-containing systems. However, the work of Coulson presented a generalized theory for π-conjugated systems based on molecular orbitals. Later, terms such as electronic density, bond order, and mutual polarizability were introduced and have since played essential roles in determining chemical reactivities, force constants, and other properties.

2.1.3 Moving to larger systems

The semiempirical MO method is easy to implement in larger systems but lacks the configuration interactions (CI) that are accounted for with antisymmetric LCAO eigenfunctions. The antisymmetric LCAO method, however, is laborious to extend to larger molecules. The works of Pariser, Parr, and Pople in the early 1950s proposed a new implementation of the antisymmetrized LCAO methods that use semiempirical quantities to evaluate the electron integrals.[64, 65] This method is commonly known as PPP (named after its inventors), and several flavors of approximations for evaluating the electron integrals have resulted in the methods used in assessing the electronic properties of π-conjugated molecules, namely the Mataga–Nishimoto approximation.[66]

Even with the Mataga–Nishimoto approximation, the PPP method underestimated the absorption maxima of π-conjugated molecules, with the discrepancy increasing with extended π conjugation.[67] In 1995, Hiruta et al. introduced the concept of chemical softness for π-conjugated systems in computing the electron repulsion integral within PPP. With this approach, the calculated excitation energies of polycyclic aromatic hydrocarbons (PAH) with up to seven acene rings showed improved agreement with experiments.[68, 69] As the PPP method includes high-order CI over a large active space, several works have used the PPP method

to more recently investigate singlet fission in π-conjugated chromophores.[70, 71] Bhattacharyya et al. showed that the excitation energy of PAH using the PPP method with CI yields better results than the popular time-dependent density functional method.[72] Because computational limitations in the early 1990s rendered a full CI approach with PPP infeasible for large polyacenes beyond anthracene,[73] efforts were initiated to replace CI with the density matrix renormalization group (DMRG) method,[74] which enables the accurate calculation of low-lying states for one-dimensional and quasi-one-dimensional systems with reduced computational cost compared to a full CI calculation. This approach has been used to explore the optical, polaronic, and bipolaronic states of large π-conjugated polymers.[75-81] In recent works, Barford and coworkers explored the photoexcited-state dynamics of polyenes and carotenoids with DMRG calculation of the PPP model to describe the dark singlet states responsible for the non-emissive properties of linear polyenes.[82, 83]

2.1.4 Considering all valence electrons

All methods discussed in the previous sections, including PPP, consider only a single 2*p* orbital in computing electronic and optical properties. The restriction to 2*p* orbitals was due to limited experimental data to provide empirical parameters and inadequate computational resources to solve complex mathematical equations. Hence, these methods did not account for σ interactions while evaluating the molecular properties. After three decades of development and validation of Hückel's methods, Hoffmann proposed the extended Hückel method in 1963 that considered all valence electrons independently to calculate electronic properties.[84] However, the approach did not consider electron-electron interactions, similar to Hückel's theory. As an alternative, Pople and coworkers[85-87] proposed the neglect of diatomic differential overlap (NDDO) approximation, which is similar to the PPP method but considers all valence orbitals. Complete neglect of differential overlap (CNDO) and intermediate neglect of differential overlap (INDO) are common variations of this method. The parameterization for these methods is designed to mimic the results of Hartree–Fock calculations with a minimal basis set.[88, 89] For spectroscopic applications,

these methods were modified to CNDO/S, INDO/S, and ZINDO/S.[90] While the estimates of excitation energies were improved, these methods produced less reliable ground-state geometries.

Dewar and coworkers calibrated the parameters against experimental reference data to provide more accurate estimates. The method based on INDO was called MNDO/3[91], and that with NDDO was termed MNDO.[92] The detailed formalism for the semiempirical techniques discussed here can be found in other review articles.[93-95] The MNDO method resulted in a poor description of van der Waals interactions that was later rectified in the Austin Model 1 (AM1).[96]

The methods discussed so far employ parameters derived from experiments. Stewart proposed optimizing the parameters by using derivatives of calculated values for properties with respect to adjustable parameters.[97, 98] This method, called parametric method 3 (PM3), provided better accuracy, as shown in Figure 2, and increased the speed of results as only a simple series expression was required to be calculated. Later improvements of PM3 include PM6, which parameterized 70 additional elements,[99] and PM7, which uses experimental data and high-level ab-initio reference data for parametrization.[100] The orthogonalization-corrected methods (OM1,[101] OM2,[102, 103] and OM3[103]) include additional interactions, namely, Pauli repulsion and core–valence interactions, which improve both ground- and excited-state properties.

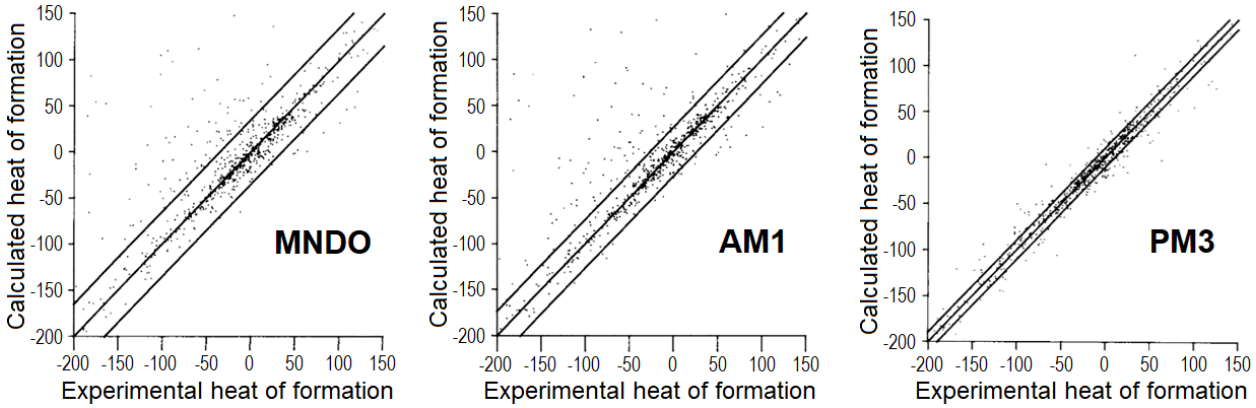

Figure 1. Calculated and experimental heats of formation with MNDO, AM1 and PM3 methods. Adapted with permission from Ref.[98] Copyright 2004 John Wiley & Sons, Inc.

Cornil et al. observed that the C-C bond lengths of poly(p-phenylene vinylene) (PPV) oligomers obtained from MNDO-based methods agreed with the X-ray diffraction data.[104] The simulated absorption spectrum of PPV with INDO/S was also observed to agree well with the experimental absorption spectrum. Hence, several studies that followed used AM1 or PM3 for geometry optimizations, followed by INDO/S calculations to obtain excitation energies.[105-112] Silva-Junior and Thiel compared the performance of OM1, OM2, and OM3 with other semiempirical methods (namely, MNDO, AM1, PM3, and INDO) and observed that orthogonalization-corrected approaches perform the best for modeling valence excited states of large organic chromophores.[113] In recent years, the approach of combining CI with the semiempirical Hamiltonians has been used to explore vertical excitation energies,[114] to optimize excited-state geometries,[115, 116] and for nonadiabatic dynamics simulations.[117-119] The benchmark study by Bruckner and Engels shows that the semiempirical methods are on par with the state-of-the-art DFT methods (*vide infra*) in estimating ground- and excited-state properties of organic π-conjugated molecules with reduced computational cost.[120]

2.1.5 Tight-binding methods

The condensed phase equivalent of semi-empirical quantum methods is the tight-binding (TB) method. The TB scheme was first proposed by Bloch in 1929; [42] a simplified version was later presented by Slater and Koster.[46, 121] The method expresses the eigenstates of the Hamiltonian with an LCAO basis and the exact many-body Hamiltonian with a parameterized matrix consisting of element fit to the electronic band structure. The early applications were centered on inorganic systems, with Leblanc first using it for anthracene crystal to obtain the electronic band structure.[122] An improved TB model for π-conjugated systems was proposed by André et al. based on valence effective Hamiltonians (VEH).[123] Several works from Brédas and coworkers use VEH-based approaches to investigate the electronic band structures of π-conjugated polymers.[112, 124-130]

In 1985, Siefert and Eschrig demonstrated that the TB method could be fit with parameters derived from DFT calculations.[131] This development paved the way for the density functional-based tight binding (DFTB) method, which consists of Taylor series expansions of the Kohn–Sham DFT total energy.[132, 133] Based on the order of the Taylor series expansion, DFTB1, DFTB2 (SCC-DFTB), and DFTB3 are derived.[134, 135] Heck et al. have extensively used DFTB in conjunction with other dynamics simulation approaches to simulate charge-carrier transport in OSC materials.[136, 137] To estimate nonlocal electron-phonon coupling in molecular crystals, Troisi and coworkers used SCC-DFTB to obtain interatomic forces.[138] Recently, Gallmetzer et al. used SCC-DFTB to investigate the redox potentials of anthraquinone and its derivatives.[139] The DFTB methods are highly sensitive to the parameters used to fit the DFT data and hence inherit their self-interaction error. A benchmarking study of DFTB methods by Gaus et al. showed that either the energy or the vibrational frequencies could be improved by reparameterization, but not both.[140] Nonetheless, these methods are two-to-three orders of magnitude faster than DFT-based methods with medium-sized basis sets.

2.2 DFT methods

Over the last few decades, DFT-based methods have generally overtaken semiempirical methods as the go-to approach for evaluating molecular and solid-state electronic, redox, and optical properties. This trend is due in large part to advances in computer technology and the development of density functionals that work well for molecular systems. DFT is based on Hohenberg and Kohn's proof that the energy of the system can be defined by its electron density;[141] the properties of the interacting many-electron system can thus be reduced to solving the non-interacting single-particle equation. The DFT formalism incorporates exchange and correlation effects and thus produces property estimates close to ab initio wave function methods. As the fundamental theory of DFT has already been thoroughly reviewed in earlier works,[142-146] here we discuss the development of DFT techniques and their application to organic π-conjugated systems.

2.2.1 Emergence of DFT and TDDFT

In 1965, the emergence of DFT from the works of Hohenberg, Kohn, and Sham paved the way for computing electronic properties at a reduced computational cost when compared to CI methods but with similar accuracy.[141, 147] The exact form of the exchange–correlation functional is not known, and approximations, namely local density and generalized gradient approximation, are used. Early implementations developed around the local density approximation (LDA)[148] were used by Albertazzi et al. to compute the vibrational frequencies of benzene and octatetracene.[149] Bylaska et al. used LDA to investigate aromaticity in organic systems as large as a 44-atom ring.[150] The generalized gradient approximation (GGA), which includes nonlocal correlation, provides an improvement over LDA.[151, 152]. Some of the popular GGA exchange–correlation functionals are PW91,[153, 154] PBE,[155] BLYP.[156-158] Pederson and coworkers used GGA to study the polarizability, charge states, and vibrational modes of fullerene.[159] They observed that the GGA framework reproduced the experimental cohesive energies to 0.05-0.1 eV while LDA overestimates the C-C bond energies by 7-20%, leading to overestimates in cohesive energy.[159, 160]

In 1984, Harris introduced the adiabatic-connection approach to the Kohn–Sham theory, which allowed for linking interacting and non-interacting systems to model inhomogeneous electron systems.[161] This paved the way for the Hartree–Fock/DFT hybrid scheme first introduced by Becke.[156, 157] The hybrid functional consists of Hartree–Fock exchange energy that accounts for a fraction of the local or semi-local DFT exchange energy. Some popular hybrid DFT functionals include B3LYP,[157, 158] PBE0,[162, 163] B3PW91,[153, 157, 164] HSE.[165] The B3LYP functional gained popularity after benchmark studies indicated that the functional yielded low errors for computed geometries, zero-point energies, and formation enthalpies.[166, 167] Recent applications of DFT include electronic and redox properties of molecules and oligomers,[168-173] analysis of molecular crystals,[174-176] and OSC interfaces,[177-182] to name a few.

The application of DFT to excited states using the time-dependent DFT (TDDFT) formalism was envisioned in 1984 by Runge and Gross.[183] While the initial work of Runge and Gross focused on small

organic molecules, the TDDFT method was later used for π-conjugated systems like pyridine and naphthalene.[184] In 2000, Guillaumont and Nakamura used TDDFT for large organic dyes and observed reasonable agreement, for most systems, with experimental absorption wavelength, spectral shift, and intensity.[185] TDDFT is now applied to investigate excited-state phenomena like charge transfer,[186-193] singlet fission,[194-203] and thermally activated delayed fluorescence (TADF)[204-209] in π-conjugated molecules, crystals, and polymers.

2.2.2 Tamm–Dancoff approximation

The typical implementation of TDDFT uses Kohn–Sham formalism with an adiabatic approximation.[210, 211] This approximation assumes that the self-consistent field responds instantaneously without any temporal change in the charge density.[212] With this approximation, Casida's approach can obtain excited state energies, where random phase approximation-like equations are solved.[213] However, these implementations predict low energies for triplet states, termed the triplet instability, as shown in Figure 3.[214, 215] To overcome this problem, Head-Gordon and coworkers proposed the Tamm–Dancoff approximation (TDA) to TDDFT, a truncated form of Casida's equations.[216] This method improves the predicted excited-state energies and reduces the computational cost.[212, 215, 217, 218] Brédas and coworkers demonstrated that TDA-TDDFT can be used for large complexes of C_{60} with a π-conjugated molecule/oligomer for investigation of triplet exciton formation and for TADF.[219-221]

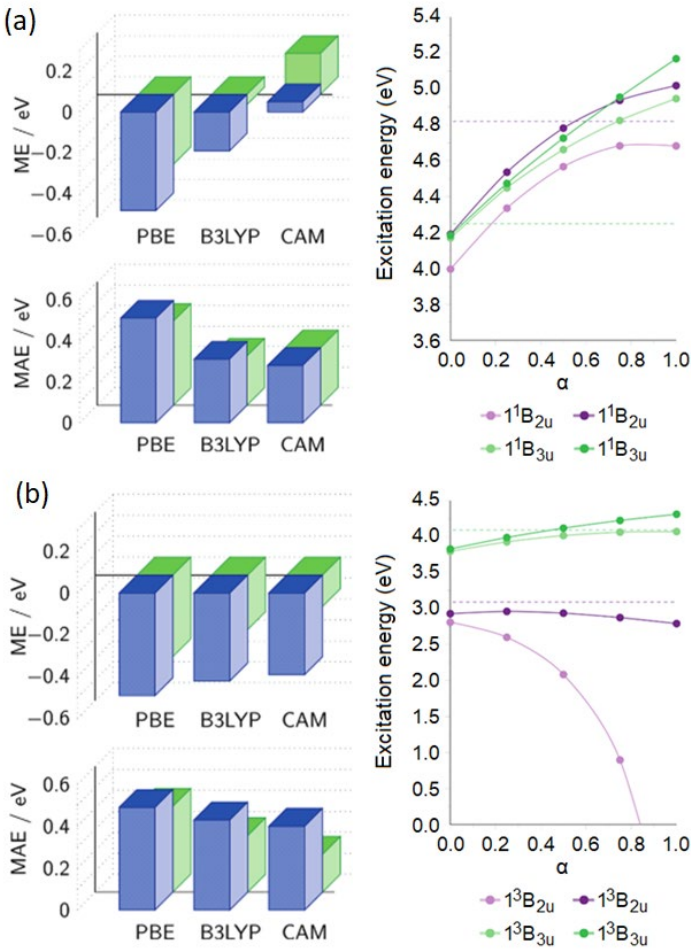

Figure 3. (*Left*) Mean errors (ME) and mean absolute errors (MAE) relative to the reference values of Ref.[222], for (a) 57 singlet and (b) 63 triplet vertical excitation energies. Blue bars represent conventional TDDFT errors; green bars represent TDA errors. CAM denotes CAM-B3LYP. (*Right*) The variation of (a) singlet and (b) triplet excitation energies in naphthalene as a function of the amount of exact exchange α. The lighter version of the color represents the TDDFT results, and the darker version the TDA results. Dashed lines represent reference values. Adapted with permission from Ref.[223] Copyright 2011 American Chemical Society.

2.2.3 Long-range corrections to the density functional

The hybrid functionals discussed before fail to produce the correct r^{-1} decay of the Coulomb operator.[224] This breakdown results in errors in the estimation of ionization potentials (IP), non-linear optical properties, polarizabilities of large molecules, and charge-transfer states, to name a few. Savin and coworkers proposed that partitioning the Coulomb operator into short-range (SR) and long-range (LR) operators could alleviate the problem.[225-227] Using the standard error function (erf) and its complement (erfc), the partitioned Coulomb operator is represented as

$$\frac{1}{r} = \frac{\mathrm{erf}(\omega r)}{r} + \frac{\mathrm{erfc}(\omega r)}{r}$$

where ω is the range separation operator. Savin and coworkers treated the LR with wavefunction methods such as configuration interactions and the SR with DFT. Iikura et al. further simplified the scheme using the Hartree–Fock theory for SR, significantly reducing the computational time.[228]

For the application of the LR correction, the unknown ω must be evaluated. Of the methods developed for this aim,[229-232] optimizing the range separation parameter for each system of interest is widely used.[233-236] In this approach, the parameter is tuned by enforcing the DFT analog of Koopmans' theorem,[237-239], which states that the HOMO is equal and opposite to IP:

$$\varepsilon_H = -IP$$

The optimized ω can be obtained by minimizing the target parameter Δ_{IP}:

$$\Delta_{IP}(\omega) = \left|\varepsilon_H^{\omega} + E_{gs}(\omega, N-1) - E_{gs}(\omega, N)\right|$$

This process is called IP tuning of long-range corrected (LRC) functionals. Brédas and coworkers demonstrated that the tuned value of ω is dependent on the π-conjugation length in organic π-conjugated systems, and ω^{-1} grows with increasing π conjugation.[240] Using the tuning scheme has provided more accurate results for polarizability and fundamental gap, as Figure 4 demonstrates.[240-242] As shown by Baer and coworkers,[233] the IP for PTCDA is heavily underestimated to be 6.10 eV and 6.67 eV by PBE and B3LYP, respectively, when compared to the experimental value of 8.20 eV. But when the tuned BNL functional is used, the estimated value is 8.08 eV, thus yielding better accuracy.

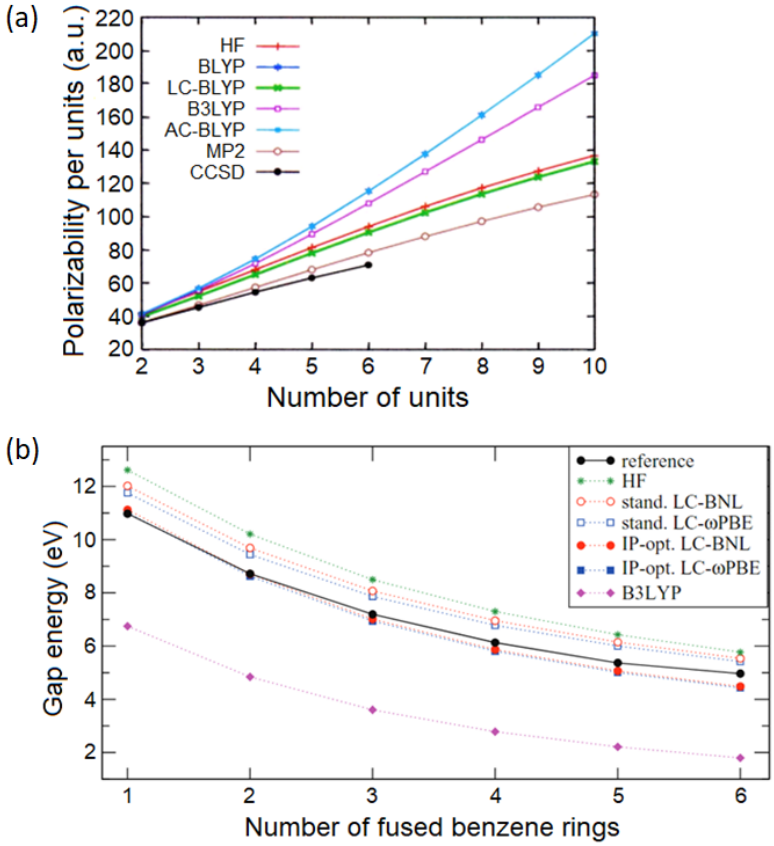

Figure 4. (a) Longitudinal polarizabilities of polyacetylene (in a.u): The number along the horizontal axis is the number of –C=C– unit. Adapted with permission from Ref.[241] Copyright 2007 AIP Publishing. (b) Difference between highest occupied molecular orbital (HOMO)and lowest unoccupied molecular orbital (LUMO) eigenvalues from Hartree–Fock, standard- and IP-optimized LRC-hybrids, and B3LYP for oligoacenes from benzene (n = 1) to hexacene (n = 6) using a cc-pVTZ basis. The reference gap corresponds to differences between the vertical IP and vertical EA from CCSD(T)/cc-pv∞Z calculations.[243, 244] Adapted with permission from Ref.[240] Copyright 2011 AIP Publishing.

LR corrections can also be extended to TDDFT. Baer and coworkers showed that charge-transfer excitations are more accurately determined with LRC functionals.[245, 246] In contrast to IP tuning, the EA must also be tuned for charge-transfer excitations; this approach is termed gap tuning.[236, 247, 248] Electron–hole pairs predicted with tuned-LRC hybrid shows more localization than standard hybrid functional, as shown in Figure 5. To investigate charge transfer in a system with multiple components like bulk-heterojunction solar cells, Brédas and coworkers showed that using a screened range-separated hybrid functional (SRSH) is more effective, as the SRSH functional has a weak dependence on ω.[249] Tozer and coworkers observed that singlet energies improved on increasing the amount of the exchange, but that the triplet energies were too low in energy.[223] These authors proposed stability analysis with Hartree–Fock (HF)

methods to detect the instability. Furthermore, this investigation showed that using TDA could significantly alleviate the problem with triplet instabilities in TDDFT calculations, as demonstrated earlier in Figure 3.

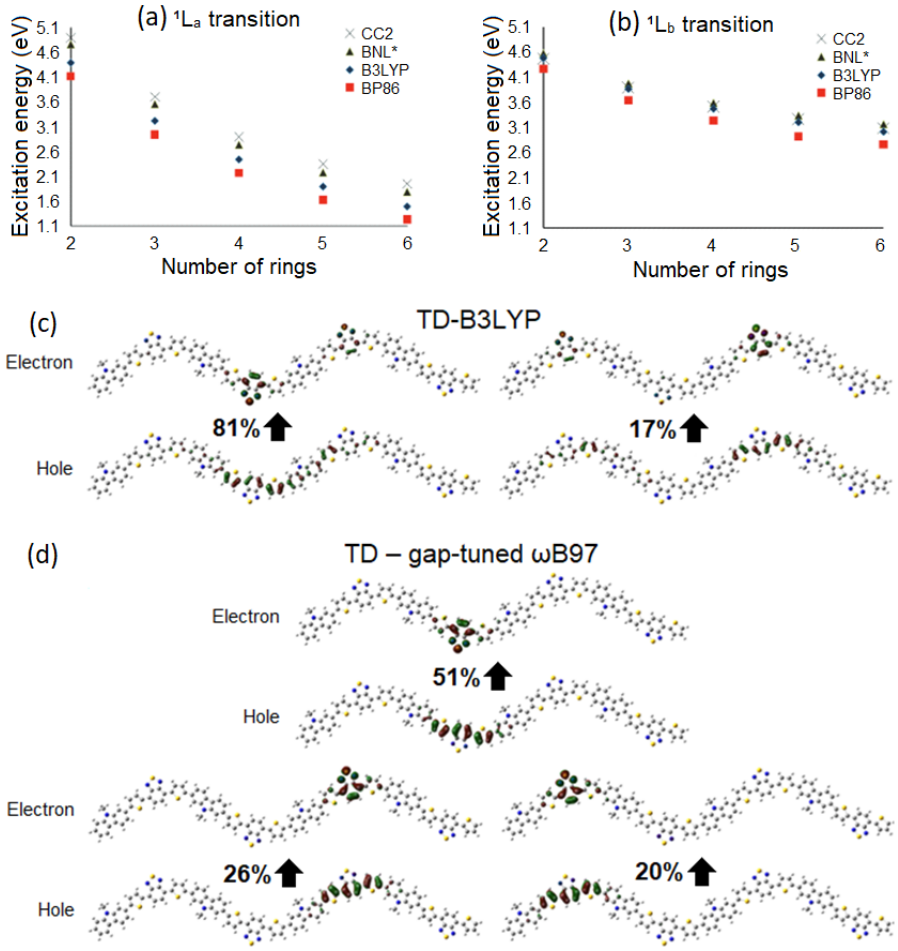

Figure 5. Excitation energies of the (a) ^1L_a and (b) ^1L_b transitions in the $C_{2+4n}H_{4+2n}$ oligoacene series (n = 2 to n = 6). TDDFT data obtained with the BP86 GGA functional (red squares), the B3LYP standard hybrid functional (blue diamonds), and the optimally tuned BNL range-separated hybrid functional (green triangles) are compared to reference CC2 values, taken from Ref.[250] (black X markers). Adapted with permission from Ref.[251] Copyright 2011 American Chemical Society. TDDFT natural transition orbitals for the S_0−S_1 transition in the tetramer of the low-band-gap polymer PCDTBT (poly[N-alkyl-2,7-carbazole-alt-5,5-(40,70-di-2-thienyl-20,10,30-benzothiadiazole)]) determined with (c) B3LYP and (d) gap-tuned ωB97.[248] The numbers specify the weight of the respective particle–hole contributions. The electron−hole pairs predicted from the tuned LRC-hybrid are much more localized than those predicted by standard functionals such as B3LYP. Adapted with permission from Ref.[252] Copyright 2014 American Chemical Society.

2.2.4 Modeling solvent effects

The absorption spectrum of organic molecules can be highly dependent on the dielectric of the environment. Several efforts have been made to model solute-solvent interactions, with many early efforts either being

computationally expensive or lacking appropriate statistical treatment.[253-256] Tomasi and coworkers proposed the continuum solvation approach to alleviate these problems.[257, 258] This method determines the molecular electrostatic potential at a finite number of points on the molecular surface to evaluate the effects of a solvent on the properties. This method, commonly called the polarized continuum model (PCM), is widely used to model solvent effects.[259-262]

PCM/TDDFT[263] provides an approach to model photoexcitation processes for organic molecules that includes solvent effects, as the time scale for absorption is faster than nuclear motion.[264] In cases of fast solvation, Painelli and coworkers proposed an adiabatic approximation to model the system.[265] However, for analyzing processes on the timescale of nuclear relaxations (e.g., fluorescence and phosphorescence), linear response,[266] state-specific,[267, 268] and vertical excitation[269] PCM models have been proposed and yield better results than standard PCM. For instance, recent works of Krumland et al. used PCM/TDDFT to investigate the effect of solvent and alkyl chains in sexithiophene.[270] These authors observe that the torsion angles between the adjunct monomers are heavily affected by solvent and alkyl chain, which correlate with experimental findings. An alternative to PCM, the COSMO (COnductor-like Screening MOdel)[271] model for solvation, has also shown improved estimation of excited-state energies. The equilibrium approaches mentioned earlier are also available for the COSMO model.[272] Efforts are also being made to couple the LRC functional tuning procedure discussed in the previous subsection with the solvent model to improve the estimates of molecular properties.[235, 273, 274]

2.2.5 Real-time TDDFT

Excited-state dynamics can be investigated by evolving the time-dependent quantum electronic system in the time domain (see Figure 6). An in-depth discussion on the theory of RT-TDDFT can be found elsewhere,[275, 276] though we note its development and application here for completeness. The method was first proposed in 1999 by Yabana et al.[277] and later applied to π-conjugated molecules, namely polyenes, retinal, benzene, and C_{60}.[277] These authors observed good agreement with experimental results with an error

of a few tenths in transition energies and 20% in transition strengths. The works of Van Voorhis and coworkers and Lopata et al. improved the efficiency of the method.[278, 279] In addition to determining the optical spectrum, RT-TDDFT can be applied to study two-photon absorption, Raman scattering, and non-linear response.[280, 281] Recent work by Seiler et al. used RT-TDDFT to understand the structural dynamics accompanying the singlet fission process in pentacene crystal.[282]

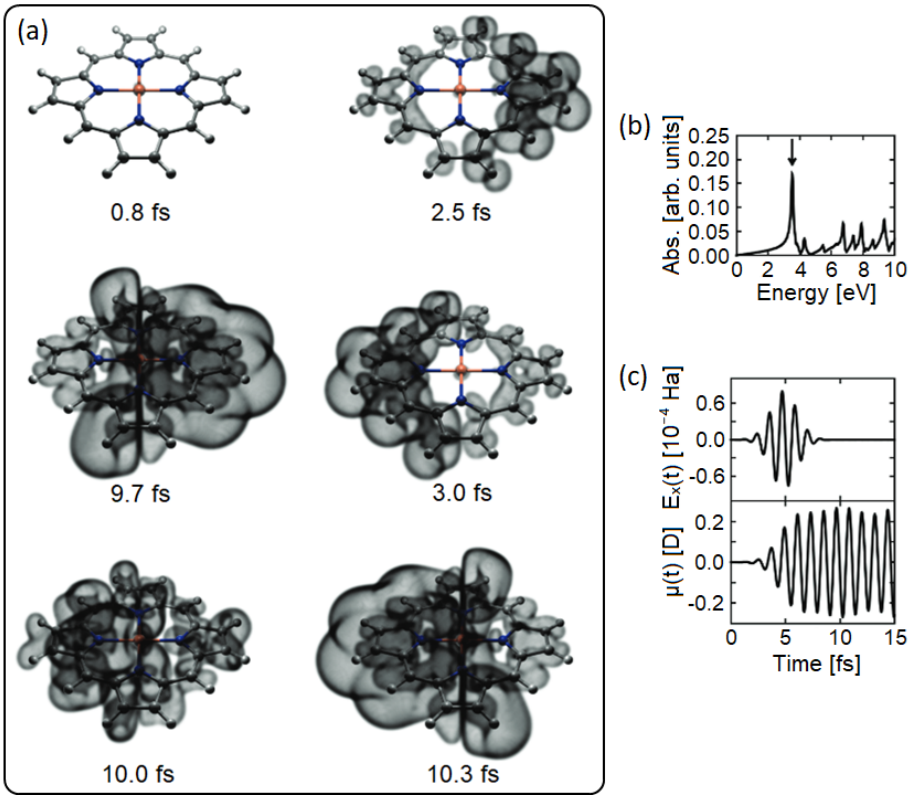

Figure 6. (a) Isosurface snapshots of the difference $\rho(\boldsymbol{r},t)$ - $\rho(\boldsymbol{r},0)$ between the excited- and ground-state charge densities for zinc porphyrin at the B3LYP/6-31G* level of theory (H, C, and N atoms), using the Stuttgart RSC 1997 effective core potential for Zn. (b) Using a transient cross-polarized laser pulse, the system was excited at its resonance of 3.53 eV. (c) The excitation results in charge oscillations along the π-conjugated backbone lasting ~1.2 fs each. Adapted with permission from Ref.[278] Copyright 2011 American Chemical Society.

2.2.6 Visualizing excitations

A direct method to visualize excited-state transitions is complicated, as multiple configurations often contribute to excitation amplitudes. In 2003, Martin applied the orbital transformation of Amos and Hall[283] to occupied and virtual orbitals to yield natural transition orbitals (NTO).[284] NTO have a maximal correspondence between the excited particle and the empty hole, with the parameter λ reflecting the

importance of a particular particle–hole transition. Analyses with NTO provide physical insights into the nature of excitations, as shown in Figure 7. Some example applications of NTO can be seen in the works of Tretiak and coworkers, wherein the authors used NTO analyses to understand the donor-acceptor strengths and conjugated bridge length impact in the two-photon absorption for dyes,[285] localization of excitations in conjugated polymers,[286] and excitation states in Y6.[287] Investigations involving excited triplet state phenomena like TADF also use NTO for analysis.[288-291]

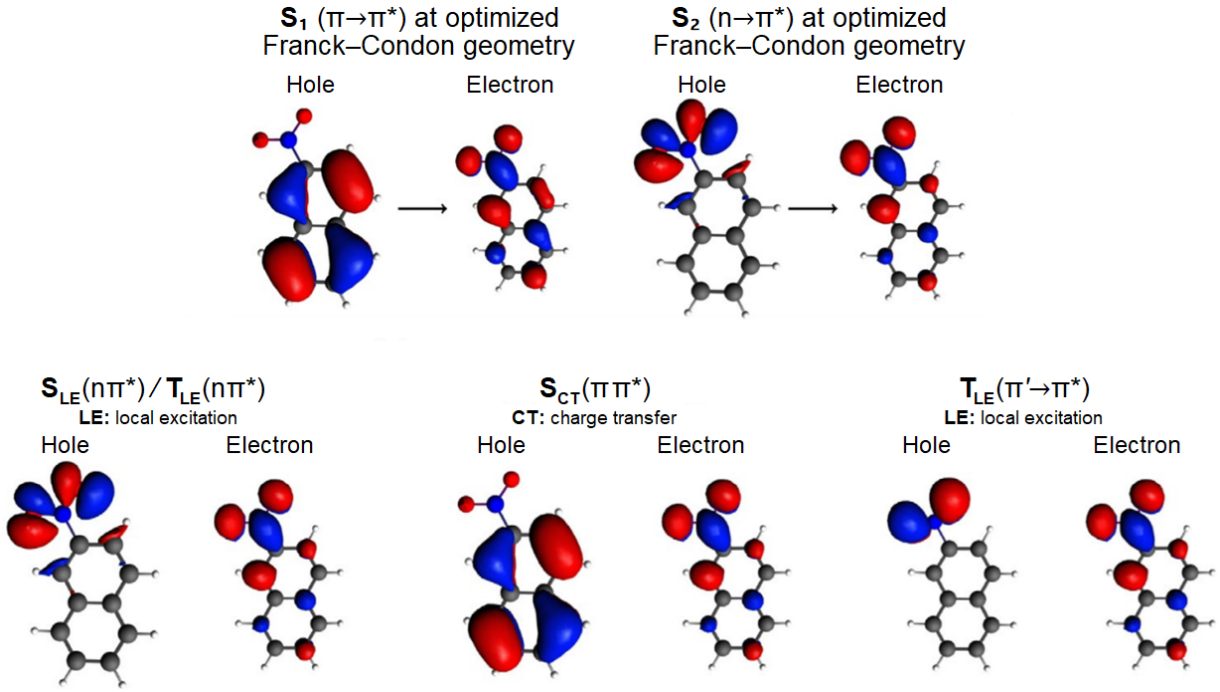

Figure 2. Natural transition orbitals describing the excited states of 2-nitronaphthalene. Adapted with permission from Ref.[292] Copyright 2018 John Wiley & Sons, Inc.

2.3 Beyond DFT: GW-BSE

The excited-state properties of solid-state materials can be evaluated with the TDDFT methods discussed earlier.[293-296] As demonstrated by Spano and coworkers,[297-300] as well as by Hoffmann and Soos,[301] excited states can also be investigated with the Holstein model.[302, 303] In this section, we focus our discussion on the application of Green's function formalism of many-body perturbation theory (MBPT) within the GW approximation to realize excited-states in crystalline organic π-conjugated materials.[304] A detailed overview of the theory of the GW method to obtain excited state properties is available in previous reviews.[305-308] In

brief, Dyson's equation is first solved with GW approximation to obtain the band structure. As shown in Figure 8, this is followed by solving the Bethe–Salpeter equation (BSE) for the two-particle Green's function, which yields the other excited state properties, including the optical spectra.[309, 310]

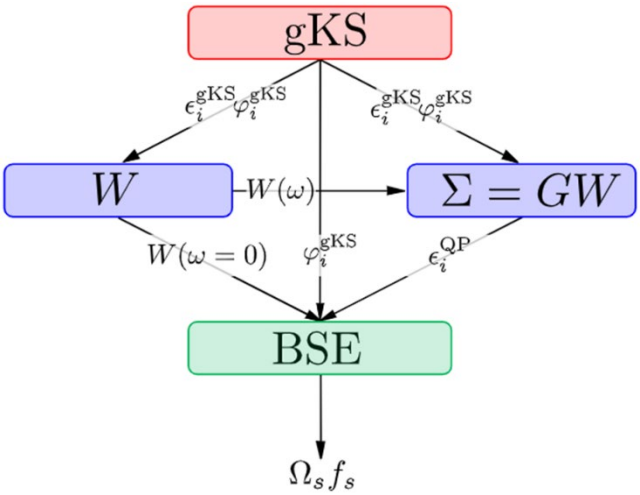

Figure 8. Standard workflow for a BSE calculation. Adapted with permission from Ref.[311] Copyright 2015 AIP Publishing.

In 2003, Tiago et al. first proposed using GW-BSE for organic π-conjugated systems.[312] The calculated optical excitations for pentacene were in good agreement with the experiment, as shown in Table 1. Using the GW-BSE approach, Hummer et al. analyzed the lowest absorption peaks in anthracene crystals.[313] The authors found that the peaks are generated by strongly bound excitons or free electron–hole pairs, which are dictated by the direction of the polarization with respect to the molecular axis. Sharifzadeh et al. later proposed the electron–hole correlation function to provide a measure of electron–hole distance and charge transfer character (Figure 9), which is beneficial for exploring exciton dissociation and singlet fission in organic materials with GW-BSE.[307, 314, 315]

Table 1. Comparison between measured and calculated energy position of the main features in the extinction coefficient of the vapor-phase crystallized pentacene structure.

	Energy (eV)			
Experimental[a]	1.82	1.94	2.11	2.25
Calculated[b]	1.73	1.86	2.13	2.27

[a]Based on ellipsometric spectra measured by Park et al.[316]
[b]Based on DFT calculations performed by Tiago et al.[312]

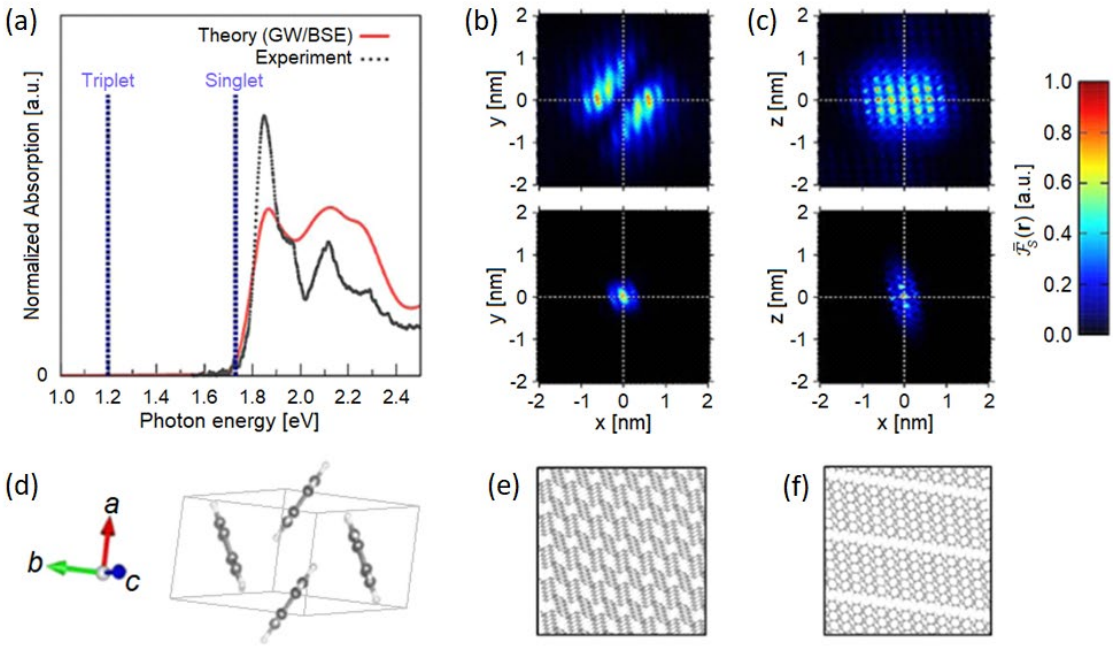

Figure 9. (a) Computed optical absorption spectrum of the pentacene crystal compared with experimental data. The computed spectrum was averaged along all three unit cell directions for incident polarizations. The computed energy of the first singlet and triplet is indicated by dashed vertical lines. (b,c) Two-dimensional electron–hole correlation function, $\mathcal{F}_S(r)$, in the *ab* plane (*left column)* and in the *ac* plane (*right column*) for the singlet (*top row*) and triplet (*bottom row*). (d) Bulk crystal structure of pentacene. (e) Projection of the atomic structure onto the *ab* (*left*) and *ac* (*right*) planes. Adapted with permission from Ref.[315] Copyright 2013 American Chemical Society.

2.4 Modeling charge-carrier transport

In 1960, experiments detailing the charge-carrier mobility in anthracene crystals by Kepler and Leblanc prompted the development of a theory for the underlying physical process.[317, 318] Within the band model, the T^{-1} temperature dependence with $1 < n < 2$ for the mobilities in anthracene was modeled with a TB approximation that assumed rigid, non-vibrating molecules and neglected molecular overlap.[122] Later works improved the method by including intermolecular electron exchange and molecular vibrations.[319, 320] DFT-based implementations for the systems were adapted after the success of the method in inorganic systems. Later, electron mobility experiments on anthracene showed that mobility increases with increasing temperature along the c-axis.[321-323] The hopping model was used to describe this behavior of charge-carrier hops within the Marcus–Hush model of charge transfer;[324-326] non-local electron-phonon couplings were neglected. When the thermal motions were included, large fluctuations in intermolecular electronic coupling are observed. The proposed transient localization model accounts for these thermal motions, which

can could lead to the localization of the charge carrier.[327] A generalized model to describe experimentally observed temperature dependence of charge-carrier transport (CCT) has not been fully resolved and continues to be under development. Hence, materials are usually modeled with one of the available models (band, hopping, and transient localization) to reproduce the experimental observations.[328] There are extensive reviews on the theory of CCT in organic π-conjugated systems;[329-337] hence, in this section, we provide an overview of the development of QC methods to describe charge-carrier transport within the purview of the models. The QC methods discussed here provide a static picture of CCT and need to be coupled the models of atomic motion. We describe such multiscale modeling approaches for CCT in Section 4 (*vide infra*).

2.4.1 Intermolecular electronic coupling

Irrespective of the model for describing CCT in OSC, the intermolecular electronic coupling (also called the transfer integral) is a critical parameter. Within the dimer approach, the intermolecular electronic coupling is obtained by evaluating the following equation for dimer-level splitting:

$$J_n = \frac{1}{2}\left|E_{n,1} - E_{n,2}\right|$$

where $E_{n,1}$ and $E_{n,2}$ are the energies for the nth molecular orbital (generally n = HOMO or LUMO) of the two molecules in the dimer, and J_n is the electronic coupling. The principal assumption is that the two molecules that make the dimer are equivalent. In cases where the molecules are not equivalent (e.g., the pentacene dimer), the difference in the site energy is incorporated, and the electronic coupling can be obtained using the following equation:

$$J_n = \frac{1}{2}\sqrt{\left(E_{n,1} - E_{n,2}\right)^2 - \left(\alpha_{n,1} - \alpha_{n,2}\right)^2}$$

Here, $\alpha_{n,1}$ and $\alpha_{n,2}$ correspond to site energies for a given pair of molecules. Huang and Kertesz observed that the intermolecular electronic couplings from semiempirical calculations largely differed from ab initio

methods However, the results were consistent for a variety of DFT functionals;[338] this work showed a dependence on the basis set that can lead to an error >20% for a minimal basis set and <4% for split valence basis set like 6-31G*.[339] Sutton et al. explored the dependence on HF exchange and observed a twofold linear increase in the electronic coupling from 0 to 100% HF exchange.[340] Correction to the dimer level splitting method was proposed by Valeev et al., wherein polarization effects to the electronic couplings were considered.[341] This quantum-mechanical electrostatic-based method involved using an orthonormal basis that preserved the local character of the monomer orbitals and, thereby, the polarization effects, as shown in Figure 10. A more in-depth discussion on the electronic coupling is reviewed elsewhere.[342-346]

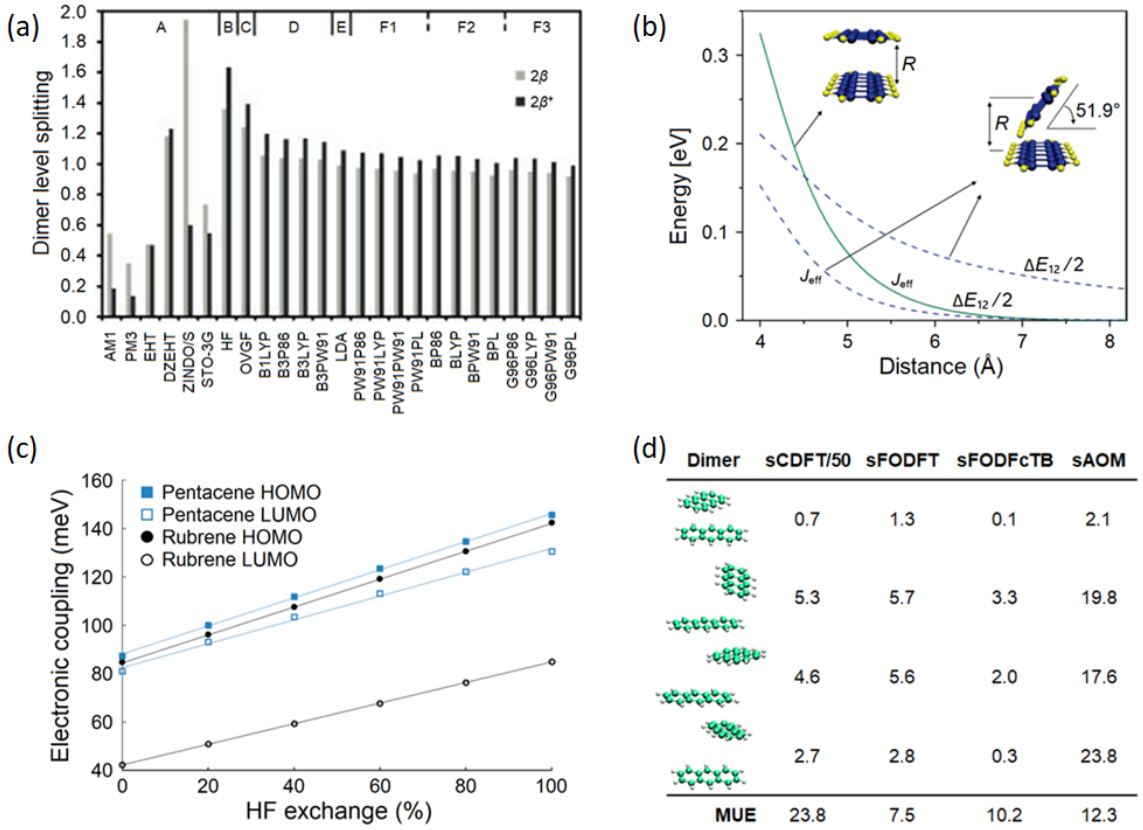

Figure 10. (a) Ethylene π-dimer level splittings (2β and $2\beta*$) calculated at various levels of theory. Adapted with permission from Ref.[338] Copyright 2005 AIP Publishing. (b) Evolution of the effective electronic coupling (J_{eff}) the dimer energy splitting approach ($\Delta E_{12}/2$) as a function of intermolecular center-to-center distance (R) of the cofacial and tilted dimers. Adapted with permission from Ref.[347] Copyright 2006 American Chemical Society. (c) Evolution of the tABH (filled symbols) and tABL (open symbols) values for rubrene (black circles) and pentacene (blue squares) with BαLYP as a function of varying amount of HF exchange. Adapted with permission from Ref.[340] Copyright 2013 American Chemical Society. (d) Electronic coupling matrix elements calculated for six randomly oriented anthracene dimers (in meV). For each molecule the closes contact is given. Unscaled $|H_{ab}|$ values are given in brackets. Adapted with permission from Ref.[344] Copyright 2015 Royal Society of Chemistry.

2.4.2 Reorganization energy

The reorganization energy is required for modeling CCT using the Marcus–Hush equation. The reorganization energy contributes to inner-sphere (intramolecular vibrational relaxations) and outer-sphere (solvent reorganization) modes. In general, the inner-sphere reorganization energy can be determined from single-point QC calculations using the four-point method.[348] Engels and coworkers observed that the reorganization has a correlation with the IP of the organic system and can show a strong dependence on the DFT functional, as demonstrated in Figure 11. As a result, IP-tuned functionals tend to yield reliable reorganization energies. From a molecular design perspective, the reorganization energy can be analyzed as a sum of contributions from the vibrational modes of the molecule, as shown by Malagoli et al.[349] Later methods developed by Uejima et al.[350] and Lin et al.[351] are based on atomic vibronic coupling constants and local fragment modes respectively.[352]

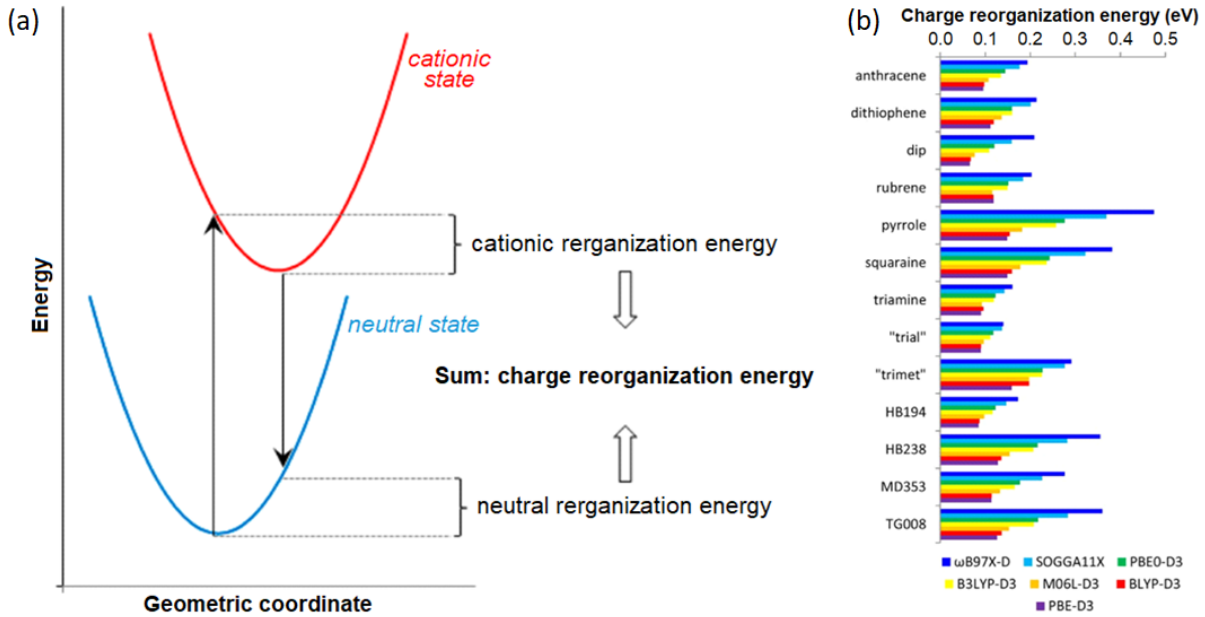

Figure 11. (a) Charge reorganization energy and its decomposition into the neutral reorganization energy and the cationic reorganization energy Adapted with permission from Ref.[353] Copyright 2015 American Chemical Society. (b) Charge reorganization energies in eV for molecular p-type semiconductors calculated with different functionals (without IP-tuning). Adapted with permission from Ref.[354] Copyright 2016 John Wiley & Sons, Inc.

2.4.3 Electronic band structures

Similar to the other descriptors discussed above, the electronic band structures of crystals derived for π-conjugated molecules can be evaluated with DFT.[355] Microscopic properties such as band gaps, band widths, and effective masses can be obtained from these calculations.[356-360] Fonari et al. investigated the impact of exact exchange on the evaluating band structures (Figure 12).[361] This work observed that in molecular crystals like pentacene, the bandgap and effective mass increase linearly with an increase in exchange. In contrast, for systems like TTF-TCNQ, the bandgap increases linearly, and the effective mass shows a marginal variation with an increase in non-local HF exchange.

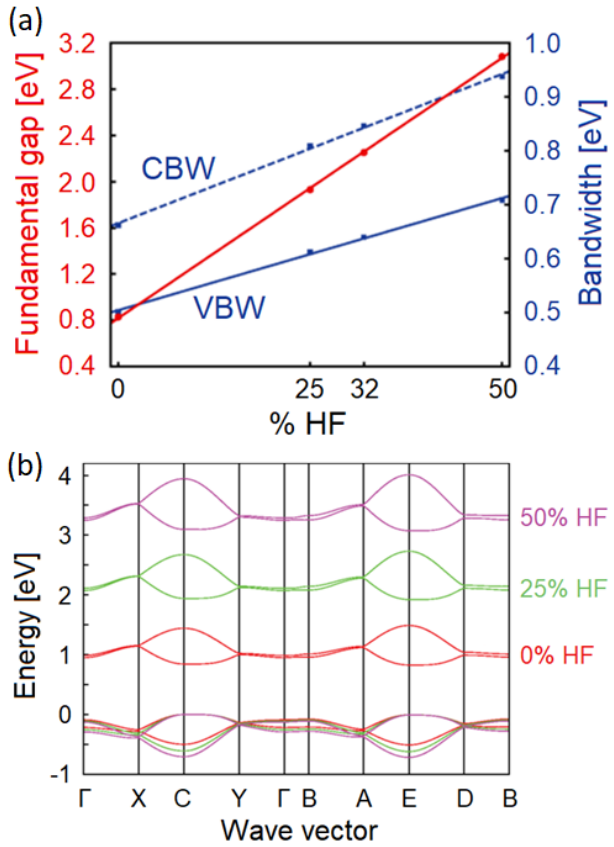

Figure 12 (a) *Left axis:* Dependence of the fundamental gap, valence, and conduction bandwidths on the percent HF exchange. *Right axis:* Dependence of the largest hole electronic coupling and smallest hole effective mass on percent HF exchange in the crystalline pentacene. (b) Valence and conduction bands of pentacene obtained using the αPBE functional with different percent HF. Adapted with permission from Ref.[361] Copyright 2014 American Physical Society.

Notably, DFT electronic band gaps are often underestimated with respect to experiment due to the inherent multi-electron self-interaction error (MESIE).[355] Improved agreement with experiments can be obtained

with first-principles many-body perturbation theory (MBPT).[304, 362] Sharifzadeh et al. demonstrated an improvement in estimating the electronic band gap using the GW approach.[363] The band gap for pentacene, for instance, was determined to be 0.75 eV for a DFT-based approach and 2.2 eV with the GW approach, which agreed well with experimental value of 2.2 eV. A similar agreement was seen for 3,4,9,10-perylene tetracarboxylic dianhydride (PTCDA).[362, 363]

2.5 Crystal structure–property relationships

OSC properties, here with a focus on crystalline materials though it is also true for amorphous materials and those of varying order (as discussed below), are dependent on the packing arrangements of the molecules in the solid state. As discussed in the Introduction, the interactions that govern this packing arrangement are non-covalent, making the prediction of solid-state structure from a single molecule a challenging and active area of research. This section provides a brief overview of methods that aim to predict crystal structures and understand the interactions between the π-conjugated molecules in a crystal.

2.5.1 Crystal structure prediction

Molecular crystal structure prediction (CSP) is still an overarching challenge.[364-366] Detailed reviews on the development of computational tools for CSP can be found elsewhere.[367-369] In brief, CSP involves three stages: (i) conformer exploration of a molecule, (ii) generation of a crystal packing arrangement, and (iii) structure ranking with a score or fitness function. In the early application of CSP to organic π-conjugated systems, Aspuru-Guzik and coworkers generated crystal structures of fused ring systems.[370, 371] Because the molecules were rigid, the authors omitted the first step of conformation exploration and used an experimental crystal structure template to generate crystal structures of similar molecular cores and crystal packing with force field-based MD simulations. The resulting structures were subjected to DFT calculations to account for atomic charges and van der Waals effects. This approach agreed reasonably well with experimental crystal structures and relative trends in estimated CCT properties. Day and coworkers improved the generation of crystal structures by employing a quasi-random search that considered the shape

of the molecule to evaluate its crystal packing preference. This quasi-random approach, implemented in Global Lattice Energy Explore software, also provides the lattice energy surface of the molecules.[372] Furthermore, to better access candidate molecules for discovery, the authors created molecular energy–structure–function maps by mapping the properties onto the crystal energy landscape from CSP.[373, 374] Another method to explore the lattice energy landscape was proposed by Marom and coworkers, which uses a genetic algorithm, as shown in Figure 13.[375, 376] The method was tested on four chemically diverse sets of molecules from the sixth blind test,[377] and the predicted structures were in agreement with the target structures.[375] The bottleneck for CSP is the final ranking of the generated crystal structures, which often uses DFT methods to estimate the lattice energies. Early lattice energy estimates were reliable to only 10 kJ/mol, and capturing polymorphs, which are often separated by energies of approximately 1 kJ/mol, was challenging. The problem was alleviated by Yang et al., who proposed a highly accurate method to evaluate lattice energy based on coupled cluster theory and DMRG.[378] With this method, the authors demonstrated that the lattice energy of crystalline benzene could be estimated with an error of <1 kJ/mol.

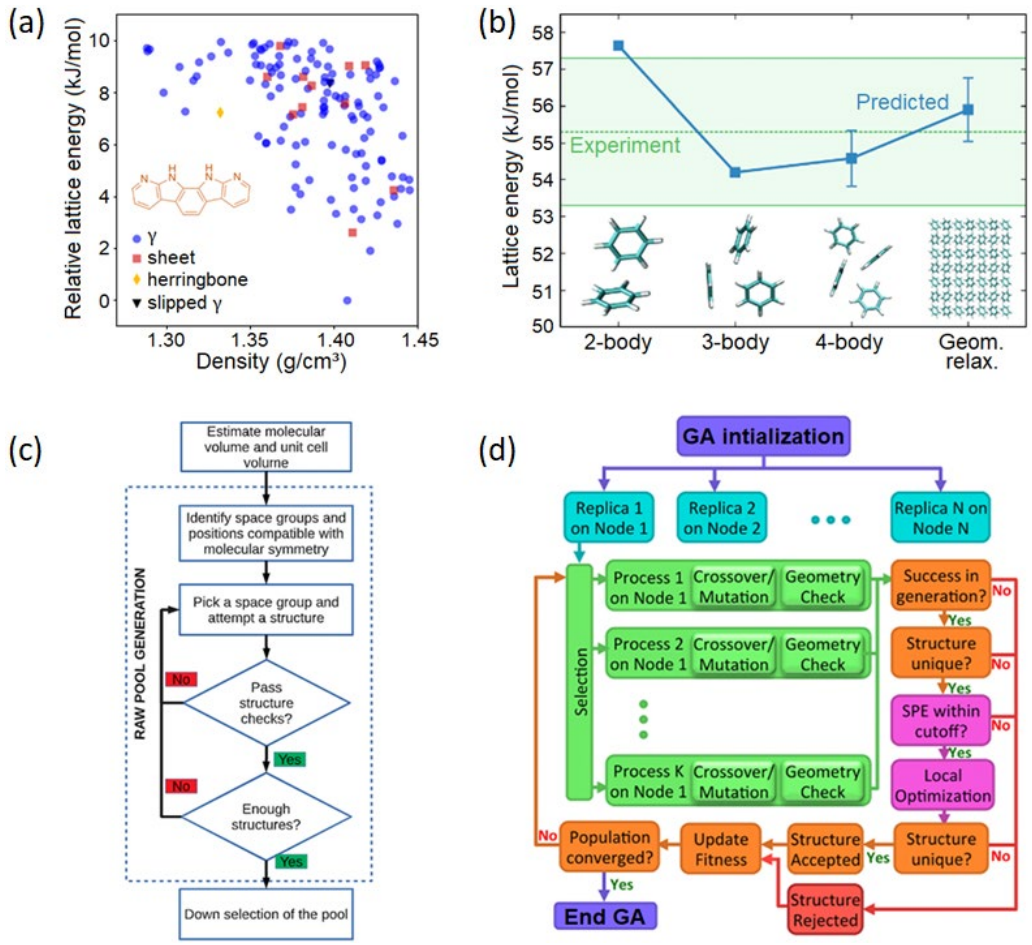

Figure 13. (a) Predicted energy–density landscape for the molecule inset. Each point on the landscape corresponds to a distinct predicted crystal structure and the predicted global minimum (red open circle) corresponds to the experimentally observed crystal structure. Structures on the landscape are color-coded according to their packing type. Adapted with permission from Ref.[374] Copyright 2018 American Chemical Society. (b) Convergence of the predicted benzene lattice energy as a function of the types of interactions included (dimers, trimers, etc.) and relaxation to the 0 K structure relative to the experimental value of (55.3±2.2) kJ mol^{-1}.[378] Adapted with permission from Ref.[379] Copyright 2014 John Wiley & Sons, Inc. (c) The workflow for Genarris 2.0 from Marom and coworkers. Adapted with permission from Ref.[376] Copyright 2020 Elsevier. (d) Schematic illustration of the workflow of GAtor on a high-performance computing cluster. In the diagram, N independent GA replicas run on N computing nodes, with K core processing units per node. Adapted with permission from Ref.[375] Copyright 2018 American Chemical Society.

2.5.2 Solid-state interactions

Noncovalent interactions dictate the packing arrangement of organic π-conjugated molecules in the crystal. Several methods have been developed to better understand the interplay of the noncovalent interactions on stability and packing of crystal structures.[380-383] Energy decomposition analysis (EDA) deconstructs the interaction energy into physically interpretable constituents. Kitaura and Morokuma proposed in 1967 a method that partitioned the Hartree–Fock interaction energy into electrostatic, exchange repulsion,

polarization, charge transfer, and unassigned interaction components using a variational approach.[383] Later methods included localized molecular orbitals,[384] absolutely localized molecular orbitals,[382] and block-localized,[385] to name a few. A more detailed review of EDA can be found elsewhere.[386] Lai et al. investigated the stacking principles involved in the close packing of naphthalenetetracarboxylic diimide (NTCDI) in crystals with EDA.[387] These authors used the ETS-NOCV[388] implementation of EDA and observed that the dispersion interactions played an important role in packing with a substantial contribution from NTCDI and alkyl chain interactions.

Unlike the variational EDA methods, symmetry-adapted perturbation theory (SAPT) computes the perturbative expansion of the interaction energy.[389, 390] SAPT includes terms describing: (i) electrostatic interactions, which arise from dipole-dipole interactions; (ii) dispersion, which accounts for van der Waals-like interactions; (ii) exchange interaction, which is quantum mechanical in nature and arises as a result of Pauli's exclusion rule; and, (iv) Coulomb interaction due to electron-electron repulsions.[391] Of the many SAPT variants, SAPT(0) neglects the intermolecular correlation potentials and is often used for π-conjugated systems. Sherrill and coworkers used SAPT to test the competing hypotheses of Hunter–Sanders[380, 392] and Wheeler–Houk,[393] which aim to understand substituent effects of varied stacking interactions in benzene dimers.[394] The results indicated that both frameworks contributed to the interaction energy, but the Wheeler–Houk is more dominant. This was followed by Ryno et al. who used SAPT(0) to understand the variation in electrostatic effects in pentacene and TIPS-pentacene that are responsible for experimentally observed shifts in ionization energy.[168, 395] Several works use SAPT analysis to investigate dimer and side chain interactions in experimentally observed polymorphic solid-state structures of organic π-conjugated molecules.[396-398] The use of SAPT for material design has also been demonstrated by Brédas and coworkers.[29, 399, 400] In one of the works, these authors explored the effect of chemical substituent on the planarity of tetracene core in rubrene.[399] The SAPT analysis indicated that the planarity of the tetracene core in rubrene is due to the minimization of the Pauli repulsion between the neighboring phenyl cores, which can be tuned via chemical modification of the substituents, as shown in Figure 14.

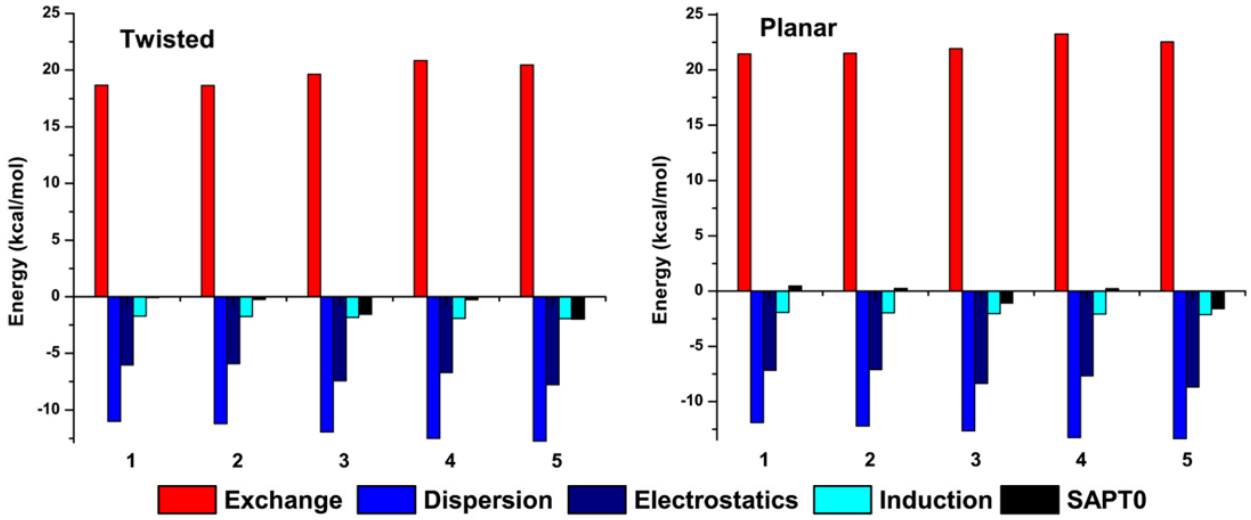

Figure 14. SAPT0/jun-cc-pVDZ computed exchange (red), dispersion (royal blue), electrostatic (navy blue), and induction (light blue) components for phenyl dimers extracted from fully relaxed twisted and constrained-planar geometries of rubrene at the IP-tuned ωB97/cc-pVDZ level of theory. The total SAPT0 interaction energy (black) is also shown. Adapted with permission from Ref.[399] Copyright 2015 American Chemical Society.

3 Classical simulations

3.1 Theory of fundamental approaches

3.1.1 Force field-based atomistic simulations

Just as QC methods describe the electronic state of a molecular system via an approximate solution to the Schrödinger equation, molecular dynamics (MD) describe the time evolution of a collection of molecules according to the classical equations of motion. However, the two families of techniques fundamentally differ in resolution. QC techniques capture electronic degrees of freedom and thus allow the calculation of optoelectronic properties. By contrast, MD simulations and time-independent molecular mechanics (MM) calculations usually represent electrons implicitly by assigning fractional charges to individual atoms (e.g., through DFT or other QC methods). By sacrificing resolution, MM/MD approaches can access significantly larger time and length scales for significantly larger collections of atoms. It is not uncommon in recent literature to find MD simulations of hundreds of thousands of atoms for dozens (if not hundreds) of nanoseconds, with this performance made possible through nearly seven decades of algorithmic improvements in cutting-edge simulation packages and computing power.

The earliest implementations of MD simulations arose in the mid-twentieth century, with Alder and Wainwright's 1957 demonstration of simulated phase transitions for hard sphere systems and Rahman's 1964 simulations of liquid argon standing as foundational testaments to the potential of the approach.[401, 402] In 1967, Verlet introduced a stable numerical integration scheme for calculating the time dynamics of a collection of particles, along with an algorithm for keeping track of the nearby neighbors of a given particle,[403] both of which are still commonly used today. Indeed, modern atomistic MD simulations broadly share the same underpinning conceit as these early works. Through iterative calculations of the classical equations of motion, the dynamics of a collection of atoms or molecules are simulated over time, subject to a set of constraints defined by the designer of the simulation.

Almost all modern implementations of MD simulations incorporate a handful of core mechanistic features. A set of system-specific input files describe the atomic positions and velocities at a given time, as well as the equilibrium geometric features (e.g., bond lengths, bond angles, dihedral angles, etc.) of the species in the system. To manage atomic interactions, a force field (FF) selected or designed by the user comprises a collection of simple functions that approximately capture the complex shape of a multidimensional potential energy surface (PES) defined by contributions from bond stretching, angle bending, dihedral torsion, electrostatic, and van der Waals interactions. Finally, system controls defined by the user manage the bookkeeping of the simulation; for example, an integrator algorithm calculates atomic trajectories by iteratively propagating the interdependent system of atomic positions, velocities, and net forces at each time step, while thermostats and barostats maintain a prescribed system temperature or pressure. This simple toolkit, which can be augmented with specialized terms to capture more complex interactions, offers a means to rationalize the relationships among chemical structure, solution-phase and solid-state ordering, and device performance.

Today, MD simulation packages are sleek and scalable, designed to exploit advances in computing capabilities. Through spatial decomposition of the simulation system into a series of subsystems, each managed by a different processor, time evolution within the subsystems can be simulated in parallel for

greater efficiency. In addition, calculations for nonbonded (and/or bonded) interactions can be offloaded to graphical processing units whose architectures are well suited for the calculation of many calculations at once.[404-406] In 2011, Larsson et al. reviewed some of these advancements, as well as others in software and hardware.[407] Owing to two-thirds of a century of progress, MD simulations are now a powerful and accessible avenue for the intelligent prediction of the properties of OSC materials based on chemical and structural insights.

3.1.2 MD simulations of OSC: Practical considerations

The many contributions comprising MD's long history have been well documented in 2011 by Beljonne et al.[408] and in 2022 by Ciccotti et al.,[409] with a 2011 review of the fundamental theory and practice presented by González et al.[410] A review of MD simulations applied to small-molecule OSC thin-film growth phenomena was also presented in 2011 by Clancy et al.[411] Given the importance of the FF in capturing interactions between atoms in the simulation system, considerable attention has been paid to the accuracy of the FF itself. Most MD works adapt an initial set of bonded and nonbonded parameters from the OPLS-AA,[412, 413] GAFF,[414] GROMOS,[415, 416] CHARMM,[417, 418] AMBER,[419, 420] or MM3 FFs,[421-423] often with dihedral torsion potentials and partial atomic charges reparameterized according to DFT results.[424-426] Tsourtou et al. recently compared seven atomistic FFs derived from some of these FFs listed above to examine the effect of molecular model parameterization on the predicted properties.[427] In a similar vein, Wolf et al. demonstrated the importance of accurately capturing the functional form of the dihedral torsion potentials between repeat units in MD simulations of OSC polymers.[428, 429] In their 2021 work, these authors weighed the relative merits of a variety of popular FFs for OSCs with a focus on polythiophenes and discussed future directions for more efficient parameterization of new species.[429] For a comparison of specific adaptations of these FFs to OSC systems across roughly two decades (some of which overlap with the work of Tsourtou et al.), the reader is directed to Table 1 of that work.

Because many relevant optoelectronic, mechanical, and thermomechanical properties for OSC show some dependence on polymer molecular weight, the decision of polymer chain length to use in MD simulations is of high importance. Several sources offer guidance on this question, but the answer is not clear-cut. Rissler's 2004 work on the effective conjugation length of π-conjugated systems discusses in detail the dependence of excitation energy and electron–hole distances on polymer size (i.e., number of repeat units).[430] Literature suggests that the electronic properties saturate at about 10-20 double bonds along the conjugation pathway,[431] but longer lengths (up to 24 – 30 double bonds or even more) may be necessary to mitigate spurious end effects on the electronic and optical properties.[432] The lower bound of the number of repeat units to use in simulation is thus evident; chains should be sufficiently longer than the effective molecular weight to appropriately capture the semiflexible chain dynamics of OSC polymers.

Estimating the upper bound is trickier. A 2022 work by Jiang et al. demonstrated for the DPP-based polymer PDPPTT-T-10 that chains with only 20 repeat units showed a nearly identical density variation with time to those with 40 repeat units.[433] In particular, a 2012 study of P3HT by Bhatta et al. suggests that the torsional potentials between repeat units and within side chains may even converge by 8 repeat units.[434] On the other hand, Tsourtou et al. paint a more complicated picture in their 2020 work exploring the effects of FF choice and P3HT chain length.[427] Comparing chains with 20, 40, 90, and 150 repeat units, the authors observe that while density and persistence length is approximately constant beyond 40 repeat units, the effective conjugation length increases monotonically with chain length. It is thus a good idea to probe the effects of chain molecular weight on a target property (e.g., density) for a given species to gauge the dependence of the property on molecular weight.

The physics of semiflexible OSC homopolymers and donor–acceptor copolymers may motivate the development of potential energy functions and FFs specifically designed for this class of materials. Additionally, it is common in literature to see reparameterization of dihedral angles that have already been parameterized (or calculation of partial atomic charges that have already been calculated) by previous authors. While a growing trend of including simulation input files with submissions helps to ameliorate

this, the time and effort spent on this task in even recent works underscore a need for better understanding across the field of the recent progress in scientific understanding and in methodology.

3.1.3 Coarse-grained MD simulations

While MD simulations with atomistic resolution can provide valuable insights into OSC morphology, sometimes the target system scale is realistically inaccessible due to the computing power available for simulations. One strategy for approaching this hurdle is reducing the granularity of the simulation via coarse graining (CG). In coarse-grained MD (CGMD) simulations, a mapping is introduced in which groups of atoms are combined into new fictitious particle types. The properties of these particles are tuned to reproduce features calculated from atomistic MD simulations or measured experimentally, with greater CG (lower resolution) indicating a higher number of atoms encoded into a single CG particle. For example, three species – P3HT, $PC_{61}BM$, and chlorobenzene – are shown in Figure 15 at two levels of CG.[435] At the all-atom level, each species is represented at the full atomistic resolution, with every pair of atoms contributing interactions that must be calculated at each time step.

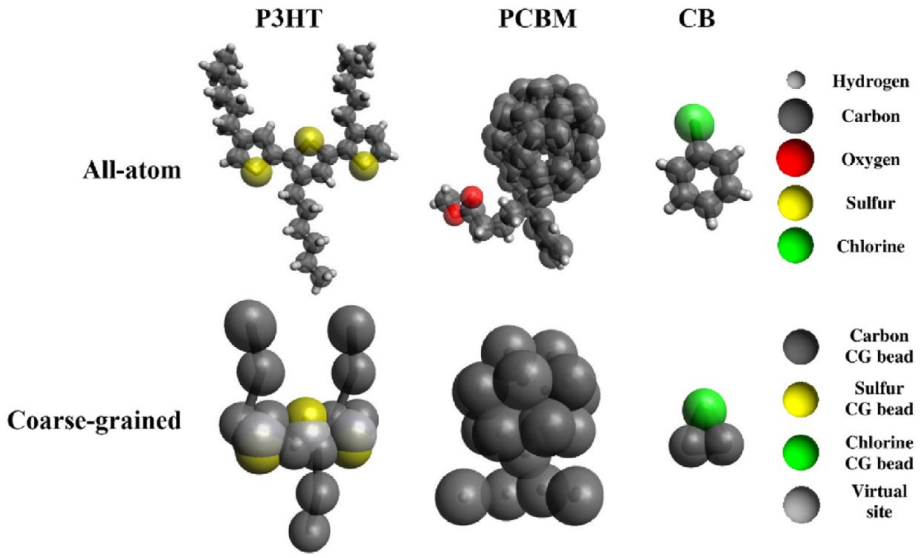

Figure 15. Coarse-grained MD models for P3HT, $PC_{61}BM$, and chlorobenzene. Adapted with permission from Ref.[435] Copyright 2018 Elsevier.

Consider just the chlorobenzene (CB) molecule shown here; one all-atom CB molecule contributes twelve atoms. These twelve atoms, in turn, contribute twelve bond stretching interactions, eighteen angle bending interactions, and thirty (proper and improper) dihedral torsion interactions. These sixty interactions must be calculated for each CB molecule in the system (which could be hundreds or thousands) at each time step (which could be hundreds of thousands or millions)! The CG representation, by contrast, has only three "bond" stretching interactions and three "angle" bending interactions. By reducing the number of particles in the mapping, CG also reduces the number of necessary calculations and greatly increases the accessible time and/or length scales.

CG mappings also fundamentally alter the connectivity of the molecular model. Due to these alterations, the FF parameterization must be fully redesigned; since CG particles do not represent individual atoms but rather groups of atoms, these particles must possess properties that capture the identity of the group they represent. Despite this difference, however, the functional forms of the FF potentials in CG models are often similar to those found at the atomistic level, with stretching, bending, and twisting potentials available to give individual chemical identities to different particle types. Many implementations of CGMD also include potentials like stochastic thermal impetuses and viscous drag-like potentials to satisfy the fluctuation–dissipation theorem.[436-438]

The fidelity of CG mapping is thus highly important in CGMD simulation design. It can, to some extent, be tuned to achieve a balance between accurate recreation of results extracted from atomistic trajectories and performance improvement by reducing resolution. This is a careful balance, however; as shown in 2016 by both Gross et al. and Root et al.,[439, 440] CG models of P3HT that map each entire repeat unit to a single particle yield worse predictive capabilities of thermomechanical properties than a three-particle model in which the side chains are mapped to two particles. Still, the computational savings from reducing the P3HT repeat unit from twenty-five atoms to only three particles offer exceptional savings in computational cost. In the literature, CG mappings are often chosen manually and through chemical intuition of distinct moieties. Nonetheless, in a recent review of applications of CGMD to OSC,[441] Jackson discussed modern

advancements in the systematic generation of CG mappings based on graph representations of molecules,[442-447] machine learning,[444] and spectral matching of dynamical modes.[448]

In addition to the mapping, a CG model requires a set of potentials (i.e., a FF) that characterize the interactions between particles, including both "bonded" and "nonbonded" interactions. While these terms are perhaps strictly inapplicable to CG methods, practically, they are still convenient shorthand. Many methods exist to generate these potentials,[449, 450] with the most popular today being Boltzmann inversion (BI),[451] iterative Boltzmann inversion (IBI),[452] inverse Monte Carlo,[453, 454] force matching (FM),[455-457] and relative entropy.[458] As noted by Jackson,[441] these methods are based on the goal of reproducing specific properties of the ensemble – namely, structural correlation functions for BI, IBI, and inverse Monte Carlo; potentials of mean force for FM; and the Kullback–Leibler divergence between the atomistic and CG representations for relative entropy.[459] Each approach has situationally dependent relative merits and demerits.[441, 449, 450] In 2016, Scherer and Andrienko explored combinations of BI, IBI, and FM applied to a three-particle CG mapping to capture bonded and nonbonded interactions;[460] in this case, a combination of BI for bonded interactions and IBI with pressure correction for nonbonded interactions led to a CG model with the best predictive capabilities.

Owing to the lower computational cost of CG approaches, many works have leveraged these methods for accelerated modeling of OSC morphology,[280, 435, 443, 461-480] donor/acceptor/solvent miscibility and blend ratio,[435, 461-464, 466-469, 473, 475, 476, 478, 481] phase transitions and solvent evaporation,[435, 440, 466, 468-470, 473-476, 478-480] diffusion,[461, 467, 470, 474] and mechanical properties.[440, 478] In a series of 2010-2014 works, Lee et al. developed and applied CG models for P3HT:$PC_{61}BM$ mixtures,[462, 469] PBTTT:$PC_{61}BM$,[464] and MEH-PPV.[280, 463, 465, 466] Based on these models, they characterized a wide range of properties, including the average domain sizes, interface-to-volume ratios, and percolation ratios of P3HT:$PC_{61}BM$ blends at different weight ratios;[462] bulk heterojunction morphologies, chain conformations, and π-π stacking;[280, 462-466, 469] and phase transitions and solubility.[464, 466, 469] Likewise, in a series of recent publications that focused on the P3HT:$PC_{61}BM$ system, Munshi et al. explored the morphological ramifications of preheating and

annealing, P3HT molecular weight, blend ratio, and polydispersity.[435, 476, 477] In a later work, they also used this model to examine the thermal and mechanical properties of P3HT:$PC_{61}BM$ active layers under uniaxial tension, demonstrating an anti-plasticizing effect of the $PC_{61}BM$ molecules.[478]

3.2 Conformational diversity

3.2.1 Enhanced sampling techniques

The central role of polymeric materials in organic electronic devices has motivated the development of simulation techniques to describe chain conformations accurately. In addition to approaches designed to capture the conformational diversity and its contribution to entropy and free energy (discussed in the following two sections), a wealth of enhanced sampling techniques exists to accelerate the exploration of the system's energetic landscape. In a comprehensive 2019 perspective, Yang et al. discuss and sort these methods depending on their use of collective variables (CV), also called reaction coordinates, to parameterize and guide the system evolution.[482] A 2020 protein-focused publication by Liao provides additional discussion of these two classes of techniques.[483] Today, the most widely used CV-based methods include metadynamics (MetaD),[484, 485] variationally enhanced sampling (VES),[486] umbrella sampling,[487] Markov state models (MSMs),[488] local elevation,[489] and steered MD,[490] while the most popular CV-free methods include parallel tempering (PT),[491] the closely related replica exchange MD (REMD),[492] integrated tempering sampling (ITS),[493] and accelerated and temperature-accelerated MD, [494-496] and multicanonical simulations.[497]

The general conceit of these methods is to incentivize the system to visit sites on the PES that are otherwise unlikely to be sampled (e.g., due to energetic barriers). CV-based methods typically feature a bias potential added to the other interatomic potentials, with the bias potential at a given CV based on visitation history (local elevation, MetaD),[484, 485, 489, 498, 499] potential energy (umbrella sampling),[487, 500, 501] Kullback–Leiber divergence (VES),[459, 486, 502] or an arbitrary CV trajectory (steered MD).[490, 503, 504] An exception is the MSM approach, in which the system is partitioned into states with fast intrastate transitions but slow interstate

transitions, allowing the transition probability between one state and another is dependent only on the first state.[488, 505-507] These probabilities may then be propagated to model dynamics on longer timescales.[508]

CV-free methods are more varied. Like many CV-based methods, the hyperdynamics variant of accelerated MD relies on introducing a bias potential to modify the PES and encourage the system to overcome potential barriers.[509, 510] Temperature-accelerated MD instead elevates the temperature of the system to facilitate transitions between states.[494, 511] The PT and REMD approaches involve multiple simultaneous low- and high-temperature replica simulations, accelerating the exploration of conformational space by periodic molecular swap attempts between replicas.[491, 492] The ITS method is similar, with Boltzmann-weighted contributions to an effective bias potential coming from multiple temperatures and an effectively infinite swap attempt frequency;[493, 512, 513] however, by avoiding the use of multiple parallel calculations, ITS offers higher efficiency than PT and REMD.[513] The sampling distribution of the multicanonical method is based on the inverse of the density of states, yielding a high sampling efficiency; the canonical ensemble properties can then be recovered through reweighting.[497, 514-516] Although the multicanonical method nominally requires foreknowledge of the density of states, the Wang–Landau algorithm allows the density of states to be calculated during the sampling convergence.[517] Finally, the simulated annealing approach uses an artificial system "temperature" as a parameter to determine the acceptance probability of a new system state;[518, 519] at lower temperatures, higher-temperatures states become harder to access, so while it is possible to access higher-energy states from a given state, the system gradually "cools" as the simulation progresses. This makes simulated annealing an efficient technique for guiding a system to a global minimum but less effective for thorough exploration of the conformational landscape.

Despite the computational cost and sophistication of enhanced sampling techniques, works throughout the past two decades have studied aggregational order and achieved improved torsional conformation space sampling in π-conjugated systems through PT and REMD,[439, 479, 520-528] umbrella sampling,[280, 465, 529-536] MetaD,[537-539] and MSMs.[540, 541] For example, several publications by Janke and coworkers apply PT methods to P3HT systems with atomistic MD and CGMD,[439, 524] revealing detailed insights into polymer

conformations and adsorption onto textured substrates.[525, 526] Likewise, de Pablo and coworkers conducted a detailed atomistic MD and CGMD investigation of the conformations and morphologies of BDT and PTB7 polymer systems through PT and umbrella sampling.[479, 530, 532]

3.2.2 Conformational analysis

The versatility of MD simulations makes them excellent tools for elucidating the roles played by backbone and side-chain chemistries in regulating chain conformations and, consequently, in modulating CCT. Most MD-based conformational analyses follow one or both of two primary approaches: (i) visual characterization, categorization of common conformation types, and discussion of the implications of these types on CCT;[425, 427, 433, 463, 479, 519-521, 542-546] and (ii) dihedral angle probability distributions and variation of selected properties with dihedral angle.[433, 547-554] However, other approaches to rationalizing conformational diversity have also been employed with success.[555-557] It is important to note that the predictive capacity of the MD simulation is directly and highly influenced by the accuracy of the dihedral angle parameterization defined within the FF. For this reason, the torsional potential parameters for dihedral angle rotation between repeat units along the main backbone must be carefully validated (e.g., via a dihedral angle scan).

Polymer chain conformation plays an influential role in modulating CCT, as it affects the tendency of the chains toward ordered π-π stacking, effective charge delocalization, and charge carrier mobilities throughout the OSC active layer. Atomistic MD and CGMD simulations offer a means to directly observe the conformational diversity of polymer chains in vacuum, solution, and bulk phases. Simulations of sufficiently large solvated and bulk systems may contain enough individual molecules to sample conformational space to a satisfactory extent, but in all three cases, enhanced sampling techniques may be employed to accelerate the sampling process. Conformational analyses performed in these fashions have been applied to OSC materials extensively in the literature, revealing a wealth of information about the effects of monomer chemistry, side chain density, regioregularity, chemical environment, and temperature on the predominant chain conformations.[425, 427, 433, 463, 479, 519-521, 542-546] Khoshkhoo et al., for instance,

presented images of representative conformations of MEH-PPV chains, demonstrating a more extended conformation in chloroform than in methanol.[544] More recently, Jackson et al. identified archetypical conformational classes adopted by a range of fifteen π-conjugated monomer chemistries, using contact maps to represent these conformations clearly and effectively.[545]

Aside from providing molecular-scale visualization of individual chain conformations, MD simulations are also effective tools for quantifying the conformational diversity of an entire ensemble. One popular approach is analyzing histograms or population distributions of specified dihedral angles, generally between monomer units. For example, Lemaur et al. extensively characterized the populations of PBTTT and IDTBT dihedral angles in crystalline (with both interdigitated and non-interdigitated side chains) and amorphous phases.[552] This idea can also be extended to quantify another measurable property as a function of the dihedral angle distributions. Batagin-Neto et al. investigated the variation of the heat of formation of MEH-PPV and DM-PPV dimers with intermonomer dihedral angle,[549] while Karunasena et al. examined the bond ellipticity and intermonomer bond length as a function of the intermonomer dihedral angle.[554] Finally, using the elegant folding and nonplanarity parameters devised by Qin and Troisi,[550] Jiang et al. quantitatively characterize the conformations of DPP-based donor–acceptor copolymers.[433] After extracting sample conformations from the bulk phase, they perform TDDFT calculations on 20-mer chains and analyze the NTOs of the excited states, demonstrating that while low-energy excitons tend to localize in relatively planar and unfolded regions, some excitons can delocalize across conjugation defects.

3.2.3 Entropy and free energy calculations

It is often desirable to obtain the free energy of a system to calculate an assortment of ensemble properties. However, while the enthalpy of an MD simulation system can be readily calculated from the total energy, pressure, and volume at a given time, the entropy is significantly more complicated to estimate due to the number of microstates increasing sharply with conformational diversity (and thus with the degree of polymerization). While enhanced sampling techniques can accelerate the exploration of the PES, enabling

the use of microstate counting methods for entropy estimation, there is no guarantee that all regions of the conformational landscape will be visited efficiently (or at all). Fortunately, other approaches exist to tackle this challenge; these methods can be categorized into those aimed at calculating relative free energy differences and those aimed at estimating absolute free energy. As a note, here we regard free energy and entropy as interconvertible based on fundamental thermodynamic relations and other system properties calculated during the MD simulation.

Here, we present a high-level overview of free energy calculation techniques; for a more detailed theoretical discussion, the reader is directed to a series of publications by Meirovitch.[558-560] Methods of calculating the system free energy can be categorized based on the goal of estimating relative free energy differences between states or absolute free energies. Popular approaches within the former category include microstate counting with enhanced sampling,[559] the weighted histogram analysis method (WHAM),[501, 561] thermodynamic integration (TI),[562-564] free energy perturbation (FEP),[565, 566] the adaptive integration method,[567] energy decomposition based on Jarzynski's equality,[503, 568] and Bennett's method.[569] Each of these techniques requires a way of capturing both of the states of comparison. Microstate counting methods involve a MD simulation capable of accessing both microstates, hence the utility of enhanced sampling methods. The other techniques generally rely on integration along a path that maps the path between the two states to a reaction coordinate, such as potential energy or temperature.

Whereas relative free energy difference calculation methods generally follow an integration path between states, absolute free energy calculation methods generally begin with a MD simulation to generate a sample morphology. This category of techniques includes the harmonic approximation,[570, 571] the quasi-harmonic (QH) approximation,[572-574] and step-by-step reconstruction approaches (e.g., the local states and hypothetical scanning methods).[558, 575-577] In the harmonic method, the free energy is calculated based on the Hessian matrix of second derivatives of the energy with respect to the atomic coordinates. The QH approximation instead uses the covariance of the coordinates, which can be expressed as internal coordinates for improved accuracy and higher computational efficiency. However, as the conversion to

internal coordinates is not always straightforward, the approximation introduced by Schlitter expresses the covariance in Cartesian coordinates.[578] By contrast, the step-by-step reconstruction scan conformational space by summing or integrating the conformational contributions from a probability function constructed from transition probabilities of partial chain reconstructions.

While techniques to calculate free energy (and entropy) through classical simulations have not been extensively applied to OSC, recent works have nonetheless demonstrated their feasibility in studying these materials. Guilbert et al. performed MD simulations to generate a BHJ morphology for the P3HT:$PC_{61}BM$ system, then built and diagonalized the covariance matrix of the atomic fluctuations.[579] Using Schlitter's approximation, they then determined the conformational entropy of the two species, showing that the blending-induced vitrification of P3HT and plasticization of $PC_{61}BM$ arise due to entropic changes in the two species. In another vein, several works have used MD simulations to decompose the calculated Gibbs free energy into contributions from Coulombic interactions, van der Waals interactions, enthalpy, and entropy.[532, 580-582] Using this method, Reid et al. demonstrated improved π-π stacking in PTB7 chains with linear side chains (as opposed to branched).[532] Using a similar decomposition strategy, Qian et al. identified the role of vibrational and conformational entropy changes in weakening polythiophene substrate adhesion.[580] Finally, Wu et al. leverage thermodynamic integration and Gibbs free energy decomposition to calculate the enthalpies and entropies of the integer charge transfer and partial charge-transfer complex polymorphs of doped P3HT, showing that the dominance of the integer charge transfer polymorph observed in prior literature can be attributed to its small critical nucleus and the modest activation barrier for converting to it from the partial charge-transfer complex polymorph.[582]

3.3 Estimation of bulk properties

3.3.1 Aggregation and ordering

MD simulation methods access length scales on the order of 10^1-10^2 nm, making them well-suited to characterizing the solvated and bulk-phase morphologies of OSC active layers. Indeed, they have been

exploited extensively throughout the past two decades to study the bulk ordering of π-conjugated molecules and polymers.[426, 433, 468, 470, 471, 474, 582-612] Given the crucial role played by ordered π-π and lamellar stacking in modulating CCT in organic electronic devices, it is hardly surprising that the aggregation tendencies of π-conjugated species have been widely studied.[426, 474, 583, 585, 589-595, 597, 598, 601-607, 609, 611, 612] Poelking et al., for example, simulated PBTTT morphology during heating to link changes in the chain stacking distances to the evolution of nematic and dynamic order parameters, side chain melting, paracrystallinity, variation in site energies, and interchain electronic coupling.[594] Likewise, Alberga et al. simulated the bulk morphologies of P3HT and PBTTT to examine the relationships between microstructural features such as nematic order, π-π stacking stability, and side-chain interdigitation and electronic characteristics such as hole mobilities and electronic coupling.[598] In a different vein, by varying the donor species in a series of DPP-based donor–acceptor copolymers, Reisjalali et al. probed the influence of polymer chemistry on aggregation and the stacking of the π-conjugated backbones.[609] As shown in Figure 16, the generated morphologies highlighted the effects of repeat unit chemistry and side chain density in regulating chain rigidity and average aggregate sizes.

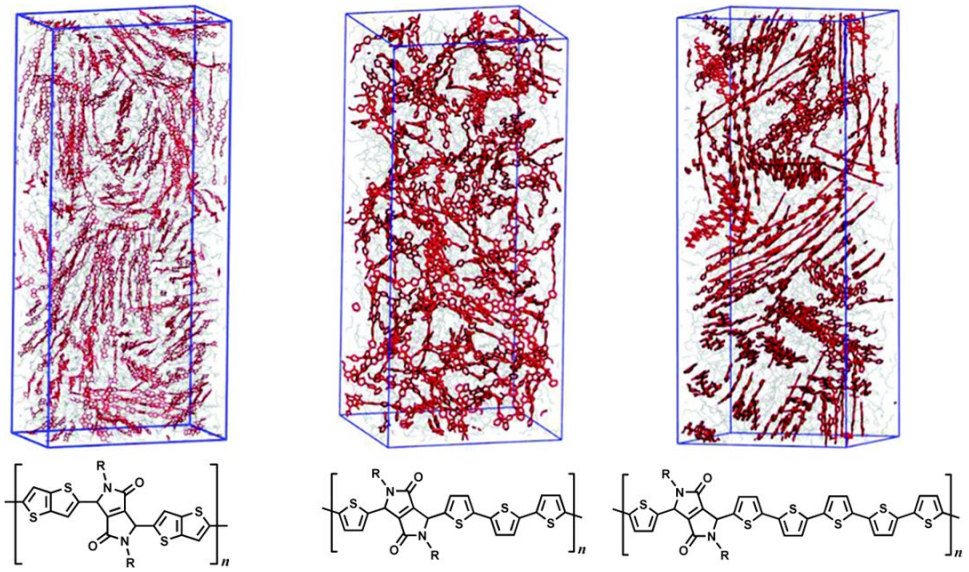

Figure 16. Atomistic MD simulation models of three similar DPP-based donor–acceptor copolymer, illustrating effects of donor moiety on π-π stacking characteristics. Adapted with permission from Ref.[609] Copyright 2021 Royal Society of Chemistry.

In addition to stacking of the π-conjugated backbones, computational efforts to rationalize the influential role of the chemical structure have explored the effects of regioregularity and polymorphism on supramolecular order.[591, 593, 595] Obata and Shimoi modeled regioregular and regiorandom P3HT systems via MD simulations, showing that regioregular chains arrange into ordered lamellae.[591] In regiorandom P3HT, however, the disordered PES of the alkyl side chains leads to increased disorder in the resultant morphology. Likewise, polymorphism in crystalline OSC polymers affects the ability to control device morphology with precision. Because the archetypical π-conjugated homopolymer, P3HT, exhibits two well-known structural polymorphs, several works explore features of these polymorphs through MD simulations.[426, 582, 595, 605, 606] Poelking et al. examined the transition from the metastable form I′ polymorph to the stable form I, linking polymorphism and regioregularity to electronic coupling and charge-carrier mobility.[595] Casalegno et al. also studied the phase transition between the two polymorphs, identifying three main steps: (i) loss of side chain interdigitation, (ii) interruption of stacking order, and (iii) polymer reorganization into tighter stacks and larger periodicities.[605] These authors also recently revisited the polymorphism of the P3HT system in a study comparing the performance of three FFs specifically adapted for poly(3-alkylthiophenes).[426] Meanwhile, in an investigation of the crystalline polymorphs of P3HT, Zhugayevych et al. perform a comprehensive conformational search for two-dimensional π-stacks, identifying multiple polymorphs with energy levels below those of both room-temperature amorphous structures and optimized experimental models.[606] Figure 17 shows a representation of supramolecular ordering in P3HT, as well as the energies of a collection of identified polymorphs. The authors observe that P3HT is a statistically frustrated system in which microstructural control is limited by the presence of multiple competing interactions.[606]

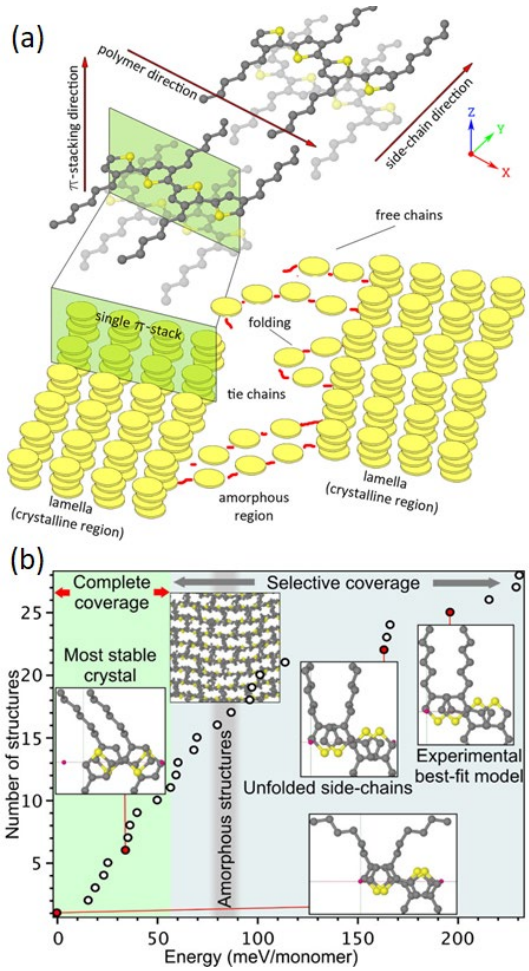

Figure 17. (a) Stacking and ordering features in P3HT. (b) As evidenced by the number of low-energy structures in P3HT, enabling precise morphological control requires a complete understanding of its significant polymorphism. Adapted with permission from Ref.[606] Copyright 2018 American Chemical Society.

Although the solid-state morphologies of OSC materials have been explored in many simulation studies, fewer works have explored the kinetic implications of solvent evaporation on the resultant active-layer microstructure. Nonetheless, several works demonstrate the feasibility of investigating this process through MD simulations.[474, 476, 607, 608] We highlight in Figure 18 images of the morphological evolution during solvent evaporation occurring on microsecond time scales from three of these computational studies. The first, shown in Figure 18(a), depicts snapshots from a CGMD simulation of a P3HT:$PC_{61}BM$ blend in chlorobenzene for approximately 14 μs generated using an assisted solvent evaporation model (i.e., a proportion of randomly selected solvent molecules are periodically deleted from the system);[474] in this

study, Alessandri et al. examined the effects of drying rate, P3HT molecular weight, and annealing on the BHJ microstructure, obtaining atomistic resolution from the CGMD model through back-mapping. A similar assisted evaporation approach was adopted by Gertsen et al. in an atomistic MD simulation protocol, wherein the authors studied IDTBR film drying during chloroform evaporation, as shown in Figure 18(b). These works are impressive technological demonstrations of the capability of simulation methods to capture evaporative phenomena. However, Alessandri et al. noted that the assisted evaporation scheme leads to an artificially uniform distribution of species throughout the system, whereas realistic evaporation occurs at the surface of the blend.[474] In the third work we highlight, Lee et al. employed an *unassisted* evaporation scheme to examine the evolution of an archetypical blended emissive layer for OLED devices.[608] As shown in Figure 18(c), the authors observed that solute aggregation initiated near the interface resulting in an inhomogeneous distribution of solvent throughout the system, in turn leading to preferential molecular alignment and solvent molecules remaining trapped within the film.

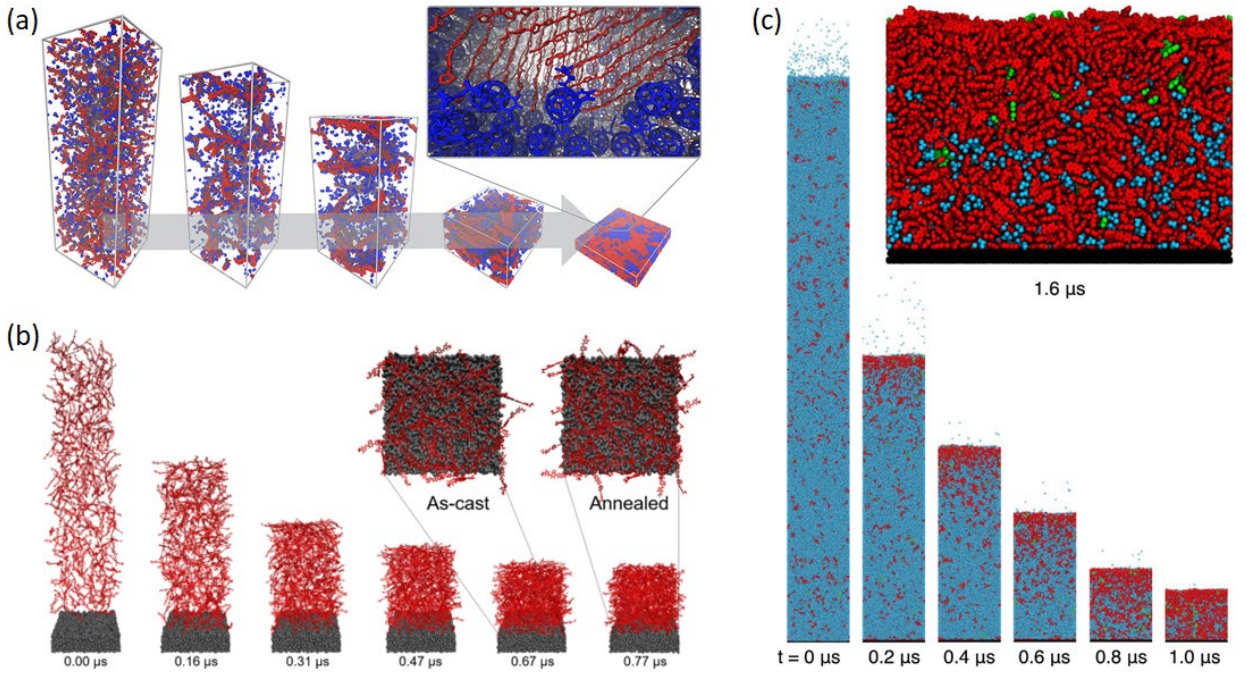

Figure 18. (a,b) Assisted simulated evaporation schemes, in which solvent molecules are randomly selected for deletion, are common approaches of modeling the evaporation of solvent species from OSC thin film morphologies. Reproduced from Ref.[474, 607, 608] Copyright 2017 American Chemical Society. Adapted with permission from Ref.[474, 607, 608] Copyright 2020 American Physical Society. (c) However, modern computing power also permits the simulation of unassisted simulated evaporation schemes. Adapted with permission from Refs.[474, 607, 608] Copyright 2020 American Chemical Society.

In addition to solvent evaporation, several works have investigated OSC adsorption on both inorganic substrates (e.g., silica) and organic substrates of the same or other species. [580, 584, 587, 590, 592, 597, 607, 613] Meredig et al., for example, investigated the orientation of P3HT nanocrystallites as a function of the packing density, packing order, and end-group functionalization of alkyl-trichlorosilane self-assembled monolayer substrates.[587] MD simulation results revealed that the edge-on P3HT orientation is encouraged by the smoothly varying PES of disordered substrates but hindered by potential energy wells in highly ordered substrates; these energetic traps are caused by favorable interactions between the substrate and the side chains of the P3HT chains. Similarly, Alberga et al. emphasized the importance of polymer–substrate interactions in modulating the ordering in the resultant film, demonstrating that P3HT and PBTTT chains display a stronger tendency to aggregate in the proximity of silica substrates, with this tendency enhanced after the annealing process.[597]

3.3.2 Mechanical and thermomechanical properties

A wide range of device-relevant mechanical and thermomechanical properties can be obtained by analyzing the morphologies generated from MD simulations. For example, the thermal stability of BHJ microstructures can be examined by analyzing the diffusivity of species at room temperature or elevated temperatures,[593, 610, 614] while simulated annealing procedures allow the calculation of some phase transitions like melting and glass transition temperatures (T_g).[440, 478, 602, 604, 609, 610, 615-617] Simulation trajectories also readily offer insights into mechanical characteristics like density and elastic modulus.[440, 476, 478, 604, 610, 611, 615-618] Further, developments in computational power have enabled atomistic MD and CGMD simulations of polymers with molecular weights large enough to capture entanglement.[427, 440, 466, 474, 476, 599, 604, 611, 614, 615, 618-621]

The thermal characteristics of OSC may be calculated in a relatively straightforward manner from simulation trajectories. Analysis of mean squared displacement during isothermal MD simulations gives estimates of the diffusivities of individual species; for example, Pani et al. studied the diffusion of C_{60} and

$PC_{61}BM$ through the P3HT morphology as a function of crystallinity and regioregularity.[593] They observed that while $PC_{61}BM$ aggregates in regioregular P3HT, it intercalates between the side chains of regiorandom P3HT, in turn suppressing $PC_{61}BM$ diffusion.

Thermal transitions may be estimated by instead varying the temperature over the course of an MD simulation. For instance, the coefficient of thermal expansion of amorphous polymers varies linearly at temperatures sufficiently above or below T_g. A simulated cooling procedure that spans this range thus enables estimation of T_g by applying linear fits to the high- and low-temperature regimes of a plot of density (or specific volume) vs. temperature.[440, 478, 602, 604, 609, 610, 615-617] This technique was applied to donor–acceptor copolymer systems in works by Root et al.,[604] Reisjalali et al.,[609] and Callaway et al.,[610] yielding predicted T_g values in good agreement with experimental measurements. In a similar fashion, Li et al. demonstrated the capability of MD simulations to accurately predict the melting temperatures of anthradithiophene-based OSC using slab models separated by vacuum gaps.[616]

Mechanical properties such as the elastic modulus are also accessible through MD simulations. The system is first extended in one direction at a fixed rate. A moving average of the virial stress tensor is then evaluated throughout this window,[440, 604] with the elastic modulus computed from the resulting stress–strain curve as normal. Many works have successfully modeled the stress–strain behavior of both neat and blended OSC active layer morphologies using both atomistic MD and CGMD simulations.[440, 478, 599, 604, 617-620] However, simulation methods are not limited to the elastic deformation regime. Indeed, several of these works additionally investigate the bulk morphology at the onset of fracture at high tensile strain;[478, 599, 619, 620] representative stress–strain curves and high-strain sample morphologies from three of these works are shown in Figure 19. In two 2015 publications, for example, Tummala et al. investigated the effects of P3HT degree of polymerization and fullerene adduct functionality on the fracture mechanics and amount of chain entanglement of neat and BHJ morphologies, as shown in Figure 19(a) and Figure 19(b), respectively.[599, 619] Similarly, Rodriquez et al. observed that while fracture occurred in systems of low molecular-weight P3HT 50-mers ($N \approx N_e$), as shown in Figure 19(c), the crack formation did not occur in the high molecular-

weight 300-mer systems ($N \approx 6N_e$), with stress instead concentrating within relatively few entangled chains.[620]

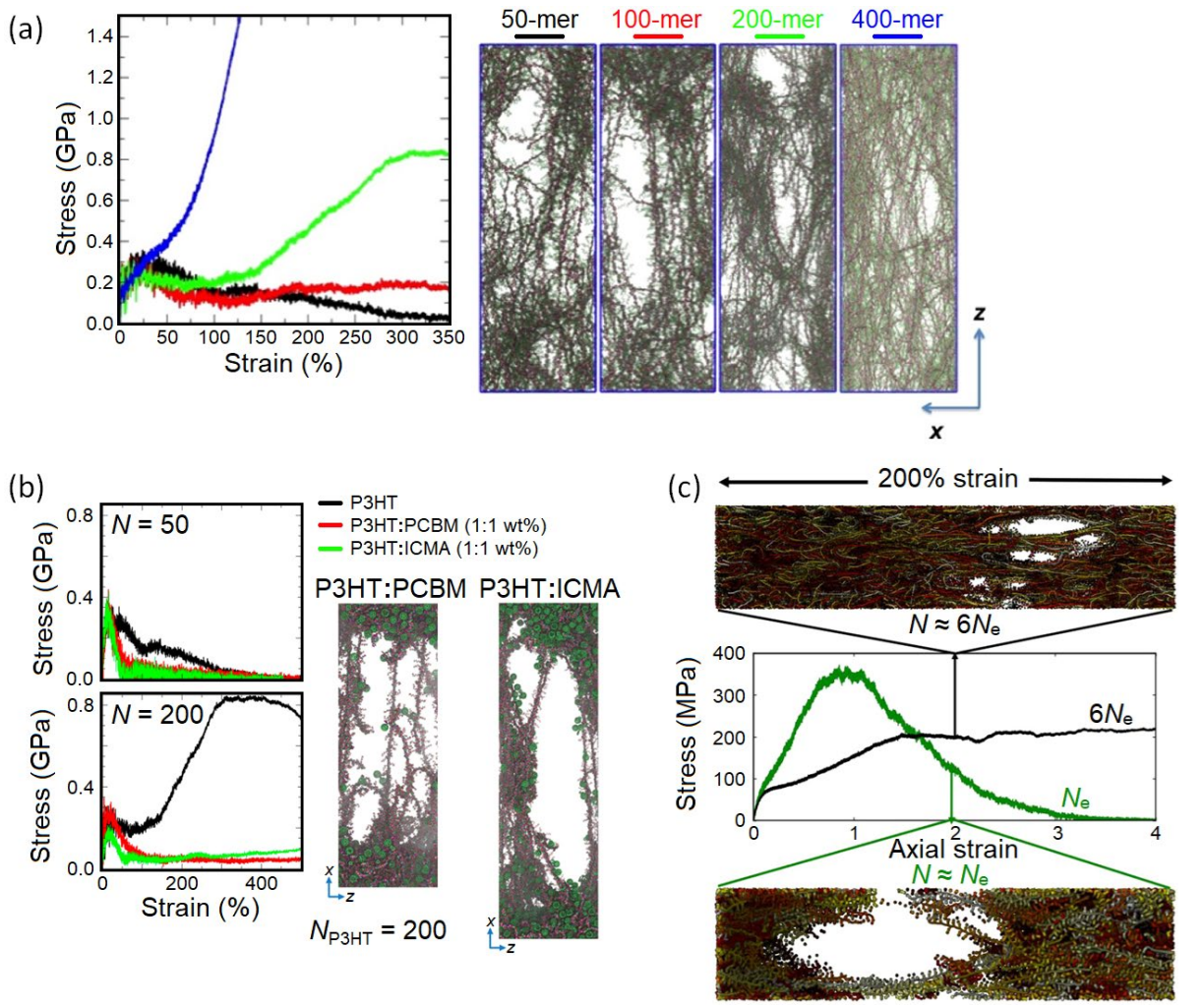

Figure 19. (a) Stress–strain curves and representative snapshots of P3HT when deformed at 0.1 nm/ps along the *z*-direction via atomistic MD. Adapted with permission from Ref.[599] Copyright 2015 John Wiley & Sons, Inc. (b) Stress–strain curves of P3HT, P3HT:PCBM, and P3HT:ICMA and representative snapshots of P3HT:acceptor blends at approximately 300% strain using atomistic MD. Adapted with permission from Ref.[619] Copyright 2015 American Chemical Society. (c) Stress–strain curves of disentangled ($N \approx N_e$) and highly entangled ($N \approx 6N_e$) P3HT and representative snapshots at approximately 200% strain. Adapted with permission from Ref.[620] Copyright 2017 American Chemical Society.

Finally, as suggested above, chain entanglement is an influential factor in diffusion, fracture toughness, and ductility. Atomistic MD and CGMD simulations can help clarify the ways in which chemical structure, backbone rigidity, and degree of polymerization affect chain entanglement (in turn, modulating diffusion rates and mechanical properties).[427, 466, 474, 476, 599, 611, 614, 615, 618, 619, 621] Characterization of the entanglement

properties of the system is often performed with primitive path analysis,[599, 618, 619] for which the Z1 code package is a popular choice.[622-625] This approach was demonstrated by Yoshimoto et al., for instance, the authors performed stress–strain simulations on P3HT:C_{60} blends with varying degrees of polymerization and blend ratios. Results from the simulations indicated that the elastic modulus is relatively insensitive to the amount of chain entanglement, whereas the ultimate tensile strength scales with the number of kinks per chain (a metric of chain entanglement).[618]

3.3.3 Phonon transport and thermal conductivity

As discussed by Wang et al. in a recent perspective of thermal transport in OSC,[626] the bulk transport of phonons (i.e., collective atomic vibrations) is of practical interest both to OSC materials, wherein phonon transport is a vector of heat transfer and a reflection of thermal stability, and to organic thermoelectric materials. As low-frequency acoustic modes are thought to make the most important contribution to thermal transport,[627] phonon transport is thus often captured through the thermal conductivity (κ) and/or the figure of merit ZT for thermoelectrics. Many older exact ab initio and approximate semiclassical techniques model κ through the Boltzmann transport equation;[628-638] however, these methods require calculating interatomic force constants, a computationally expensive task. Other approaches extract the bulk lattice thermal conductivity directly from quantities calculated during the course of MD simulation.[639-646] In the GK relations, κ is calculated from the autocorrelation of microscopic heat currents at equilibrium (i.e., the decay rate of thermal fluctuations).[639-641] While the slow convergence of the heat current autocorrelation functions (ACFs) limited the initial GK formulation, several averaging schemes have been proposed to accelerate convergence.[647-649] Importantly, κ values show distinct dependence on the heat flux formulation used in the GK calculation.[650-654]

NEMD and AEMD simulations directly probe the system's thermal response to applied heat currents, avoiding the problem of slow ACF convergence.[642, 643, 651] In NEMD, a heat flux is established by increasing and decreasing the atomic velocities within hot and cold regions at opposing ends of the system; κ is then

extracted from Fourier's law of conduction based on the thermal gradient arising in response to the imposed heat flux.[655-658] It is worth noting that long simulation times are often necessary to establish a steady-state linear thermal gradient.[645, 646, 651] Further, this method exhibits pronounced finite-size effects; however, the corrected κ can be extrapolated through a Matthiessen-like equation.[646, 651, 659] The limitations of GK and NEMD motivated the development of AEMD, wherein the thermal response is measured by establishing a stepwise temperature differential between the left and right halves of the system and then observing the decay of the thermal gradient (occurring on a timescale ~10^2 ps) after the boundary is released.[644, 645] More recently, the first-principles sinusoidal AEMD (SAEMD) variant introduced by Puligheddu et al. imposes a sinusoidal thermal profile that varies continuously with position;[646] a detailed comparison of the computational performance of the GK, NEMD, and SAEMD approaches in that work revealed that the equilibrium time in SAEMD was approximately two orders of magnitude faster than the convergence of the heat current ACFs in GK or of the thermal gradient in NEMD.

Several authors have used these methods to explore the effects of chain length, crystallinity, polydispersity, and doping level on phonon transport and heat conduction in PEDOT systems.[660-665] A 2017 work by Shi et al. applied NEMD to model phonon transport in PEDOT fibers, highlighting chain length and crystallinity as avenues to control κ.[660] In order to improve thermal stability, they showed that rationally designed chain-oriented PEDOT fibers can exhibit significantly reduced κ and enhanced ZT. Similarly, Genovese et al. used GK and AEMD to study the effect of morphology on thermal transport, demonstrating a decrease in κ of over two orders of magnitude in nearly amorphous PEDOT compared to the purely crystalline phase.[661] In addition to the degree of crystallinity, κ depends strongly on chain length, as shown by these works and by Maeno et al.; in their 2018 NEMD work, they demonstrated that adsorption of toluene sulfonic acid on PEDOT reduces κ, with more pronounced effects at longer chain lengths.[663] Later, Yu et al. simulated thermal transport at different tosylate dopant concentrations with GK, with heavily doped systems demonstrating a roughly 50% reduction in κ.[664] Thermal transport in this system was demonstrated to occur

via a combination of PEDOT:dopant interfacial conduction, PEDOT lattice conduction, and dopant convection.

In a 2014 work, Shi et al. proposed a model to estimate the optimal doping level and peak *ZT* value based on intrinsic carrier mobility, lattice κ, and effective density of states.[666] Using NEMD to calculate κ for a series of BTBT derivatives, the species were shown to have high charge carrier mobilities, low κ, and high Seebeck coefficients. Recently, Gueye et al. studied thermal conduction in two of these BTBT derivatives via scanning thermal microscopy, with results supported by AEMD.[667] In contrast to the two-dimensional CCT characteristics, AEMD simulations revealed appreciable thermal transport along all three crystal axes.

Finally, these techniques have also been used to study thermal conduction in the archetypical family of polythiophenes. Lv et al. performed MD simulations and GK modal analysis to rationalize the contributions of individual phonon modes to κ in individual polythiophene chains.[668] Results of their approach suggested that anomalous divergent thermal conductivity is possible for chains of specific lengths due to low-frequency transverse vibrations in the plane of the thiophene rings, supporting earlier hypotheses that attributed divergent κ values to correlated phonon–phonon scattering. Later, Zheng et al. synthesized a series of poly(3-alkylthiophene) copolymers and copolymers of 3-butylthiophene and 3-butoxythiophene, comparing experimental characterization against NEMD simulations.[669] In the second family of species, the authors show that κ is enhanced by reducing steric hindrance and enhancing p-π conjugation.

4 Multiscale modeling approaches

4.1 Connecting optoelectronics to morphology

As the preceding sections demonstrate, the predictive scope of QC methods and classical simulation approaches includes a wide range of phenomena relevant to organic electronic device performance. However, each technique has optimal temporal and spatial scales of applicability; while QC methods can resolve electronic phenomena, the lower cost of classical simulation methods is more amenable to modeling the evolution of bulk microstructure on nanosecond time scales. At the same time, the distinguishing

characteristics of π-conjugated materials rely on the rich interplay between electronic and nuclear dynamics, with different relevant processes occurring on time scales of femtoseconds, picoseconds, and nanoseconds. A natural conclusion of these observations is that capturing these phenomena accurately requires using a multiscale modeling approach leveraging the strengths of each constituent method to capture phenomena within its scope of applicability.

Modern computing allows multiple length scales to be resolved in tandem via combined quantum and classical dynamics approaches. These approaches enable the effects of electronic structure to be captured explicitly while atomic motion is still propagated classically via integration of the equations of motion; for example, this is the basic premise of ab initio MD and the Car–Parrinello MD scheme.[670] However, multiscale simulation design is more often piecemeal, applying the techniques discussed previously at their respective length scales to develop a holistic understanding of the relationships among optoelectronic processes, self-assembly, bulk morphology, and (thermo)mechanical properties. For example, after FF parameterization, a sample morphology can be generated through classical simulations, optionally using coarse-grained MD or enhanced sampling techniques to accelerate the exploration of conformational space. After sampling molecular conformations from this morphology, QC methods can be used to calculate electronic structure and intermolecular electronic coupling. Additionally, kinetic Monte Carlo (KMC) simulations can be performed on the MD-generated morphology to calculate charge carrier mobilities. For a theoretical discussion of Monte Carlo and KMC methods, the reader is directed to a comprehensive theoretical treatment by Kratzer,[671] as well as to MC and KMC reviews by Andersen et al. and Cheimarios et al.[672, 673] Of particular interest to this work, several works have reviewed KMC simulations of OSC materials for modeling CCT, exciton diffusion lengths, charge recombination, and Seebeck coefficients.[333, 674-679] We also highlight a handful of additional works that used KMC methods to characterize a variety of phenomena in OSC materials.[542, 613, 680-684]

Combining results from these approaches into an aggregate picture thus offers insights into the relationships among repeat unit chemistry, exciton delocalization, electronic coupling (and electron–phonon coupling,

as discussed below), chain conformations, morphological (dis)order, and CCT. Many works demonstrate the utility of this type of piecemeal modeling paradigm in connecting the optical, electronic, thermomechanical, and morphological characteristics across length scales in a diverse variety of OSC molecules and polymers.[327, 370, 439, 471, 472, 543, 547, 548, 550, 553, 554, 586, 589, 590, 600, 685-703] For example, D'Avino et al. used a combination of MD simulations, QC calculations, and classical microelectrostatic calculations to explore electron–hole separation processes occurring at a prototypical P3HT:$PC_{61}BM$ interface.[692] The authors demonstrated the energetic favorability of charge separation of about 50% of the interfacial electron–hole pairs, which they explain by connecting electronic polarization, the electrostatic landscape, and interfacially induced torsional disorder in P3HT chains. Similarly, Olivier et al. leveraged MM/MD simulations and QC calculations to examine the supramolecular organization and subsequent charge-carrier mobilities of three families of polymers based on P3HT, CDT-BTZ, and P(NDI2OD-T2).[695] Through a combination of QC and MD methods, the authors succeeded in linking the chemistry, dimensions, and side-chain density of the monomers comprising the conjugated backbone to the supramolecular organization and subsequent charge-carrier mobilities of these species.

Böckmann et al. demonstrated the effectiveness of interconnected multiscale simulations in a study comparing simulated optical absorption spectra of P3HT in solution, thin films, and bulk crystals with those obtained from UV/Vis spectroscopy experiments.[471] After modeling the thin-film morphology via CGMD, the authors used the CG definitions to backmap the resultant morphology to atomistic resolution; statistically averaged TDDFT calculations performed on an ensemble of molecules selected from the generated morphology yielded optical absorption spectra in good agreement with the experimental spectra. From these results, the authors observed that torsion between adjacent thiophene rings dominated intermolecular effects in determining the position of the main absorption peak. Most recently, a 2022 multiscale simulation study from Mombrú et al. combined DFT calculations, MD simulations, and ab initio MD simulations to examine mixed ionic–electronic transport in a P3HT crystalline supercell with explicitly represented lithium-based dopants and additives,[703] a notably rare feature in simulation works. The reported

ionic and electronic conductivity values agreed well with experimental values, allowing further exploration of the static and dynamic disorder effects arising from the explicit Li dopants. These works highlight the many ways that quantum and classical simulation methods complement each other to yield deeper insights into the multiscale phenomena governing the performance of these materials in OSC devices.

4.2 Adding charge-carrier transport

To supplement the techniques discussed above, charge-carrier mobilities can be calculated via Marcus theory,[704] Miller–Abrahams theory,[705] KMC simulations, or charge patching methods. As highlighted in several high-level reviews of CCT modeling approaches, this pipeline allows for thorough characterization of the CCT characteristics of OSC materials.[337, 675, 677, 706-710] For example, a 2009 Account by Nelson et al. illustrated a variety of key computational approaches to model molecular packing, charge transfer rates, and charge carrier transport.[707] The same year, Rühle et al. introduced the versatile object-oriented toolkit for coarse-graining applications (VOTCA),[709] now a popular modeling package in multiscale studies of CCT. The workflow of the interrelated approaches on which the VOTCA package is based is depicted in Figure 20.[337, 710]

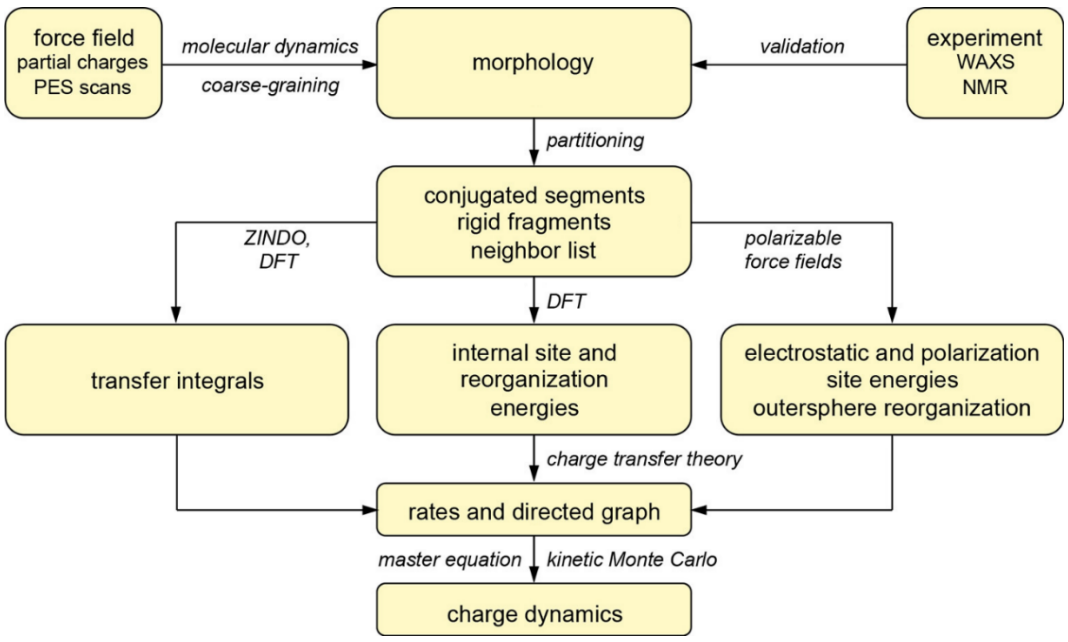

Figure 20. A flowchart of multiscale approaches connecting relevant optoelectronic properties to computational modeling methods. Reproduced from Ref.[337, 710] Copyright 2018 American Chemical Society.

In a 2014 review, Shuai et al. discussed a multiscale approach to modeling charge-carrier mobility in OSC by combining quantum charge transfer theory, MD simulations, and KMC simulations;[675] their work extends past the semiclassical Marcus theory by highlighting the quantum nuclear tunneling effect in charge transfer. More recently, a 2018 perspective by Gryn'ova et al. distilled insights from these and other works into a set of design principles for effective quantum, classical, and multiscale simulations enhanced with data-driven analysis. These studies offer extensive insights into the underlying framework of KMC as applied to OSC materials.

Many works have leveraged KMC techniques to extract charge-carrier mobilities from a morphology generated through MD approaches.[546, 556, 588, 613, 675, 689, 707, 708, 711-721] As early as 2009, Vukmirović and Wang developed a multiscale ab initio simulation method combining QC calculation of electronic states, classical FF simulations, and KMC simulations.[588] Using this method, the authors estimated the mobility of disordered P3HT, yielding good agreement with experimental values. Later, a 2017 work by Li and Brédas demonstrated that charge-carrier self-interaction errors could result in significant inaccuracies in KMC simulations of OSC materials. They proposed two approaches to overcome these errors. The first, the "exact" method, takes into account the evolution of the electric potential between the initial and final configurations; in the second, the "exclusion" method, the electric potential difference in the absence of the hopping carrier is considered in order to evaluate the site-energy difference. By reducing finite-size effects, the authors show that improved accuracy can be delivered in KMC simulations at a lower computational cost. In 2018, Kaiser et al. developed a generalized KMC framework based on Voronoi tessellation.[684] Their approach models excitonic processes (including triplet exciton dynamics) in crystalline and amorphous domains of OSC materials by performing a weighted average over a set of interaction sites at predefined locations around each species.

A 2021 publication by Paterson et al. used a swath of experimental characterization techniques in conjunction with DFT, MD, and KMC approaches to examine the effects of molecular *n*-doping on CCT in the popular non-fullerene acceptor species O-IDTBR.[720] In these explorations, the authors identified a previously unreported dopant-induced packing orientation resulting in high electron mobilities in excess of 1 cm^2 V^{-1} s^{-1}, which was confirmed through computational simulations to be the result of the synergy between the *n*-type doping and morphological changes. More recently, a 2022 multiscale study by Dilmurat et al. exploited atomistic MD simulations, QC calculations, and KMC simulations to show that the density and quality of close-contact points between donor–acceptor copolymers modulate the charge-carrier mobilities in the amorphous phase.[721] Further, the donor block size and the alkyl side-chain density are shown to be important factors in determining the quality of close-contact points between chains; the elongated and bulky dithiopheneindenofluorene promote a larger number of higher-quality close contacts, which subsequently yields improved charge-carrier mobilities. Finally, in 2022, Giannini and Blumberger presented a detailed overview of computational techniques, which include multiscale and mixed QC-MD techniques like nonadiabatic MD (NAMD) for modeling CCT in OSC materials.[330] Figure 21 shows their fragment orbital-based surface hopping approach for direct charge propagation in a NAMD framework in the context of other theories of charge transport with corresponding ranges of applicability.

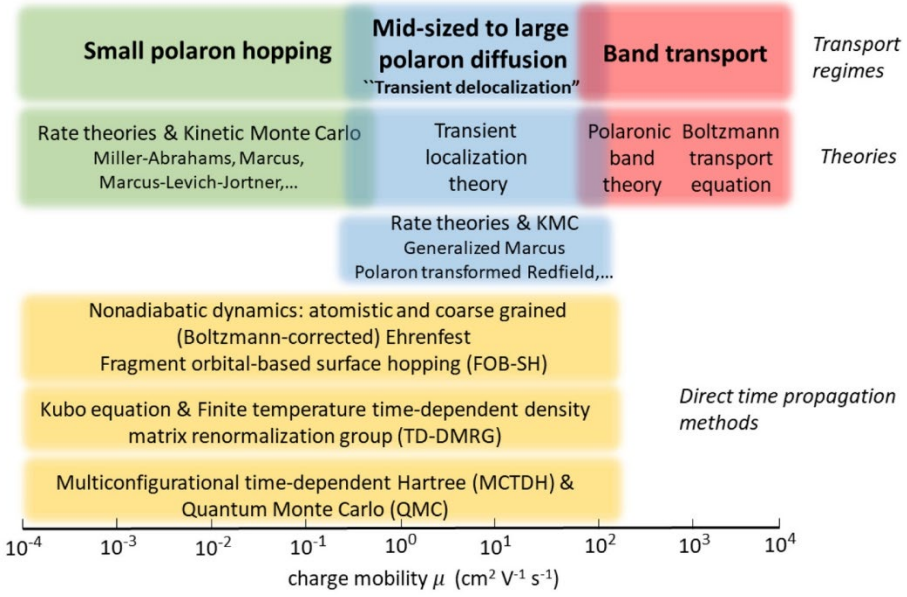

Figure 21. A complex multiscale framework of CCT regimes in OSC materials. Reproduced from Ref.[330] Copyright 2022 American Chemical Society.

4.3 Modeling electron–phonon coupling

As the Franck–Condon principle demonstrates, the electronic and nuclear dynamics are fundamentally intertwined; the motion of the nuclei over time can cause electronic transitions, while the relaxation of excited electronic states can likewise induce vibrational motion in nearby atoms.[722-725] Moreover, phonons can couple to charge carriers, resulting in energy and momentum transfer, in turn lowering charge-carrier mobility and degrading overall device performance. Reflecting the different scales of electronic and nuclear dynamics, accurate description of electron–phonon coupling often motivates specific multiscale approaches designed to model both electronic and nuclear processes.

In discussing these approaches, it is useful to break the larger picture of electron–phonon (e-ph) coupling into local and nonlocal coupling, which can be understood in the context of the Holstein–Peierls model.[302, 303, 629, 726, 727] The local Holstein-type coupling, also known as diagonal dynamic disorder, represents the fluctuation of on-site electronic energies (i.e., Coulomb integrals, corresponding to the EA and IP of the site for mobile holes and electrons, respectively[728, 729]) with the phonon normal modes. The local e-ph coupling can be quantified via the polaron binding energy;[302, 303] in the framework of Marcus–Hush theory, it has been shown that the reorganization energy is approximately twice the polaron binding energy.[333, 728, 729] The Huang–Rhys factor, which can be used to calculate the interchain charge transfer rate, also quantifies the strength of the local e-ph coupling. The nonlocal Peierls-type coupling, also known as off-diagonal dynamic disorder, represents the fluctuations in intermolecular electronic couplings (often called transfer integrals) as a function of the vibrational modes.

The local and nonlocal e-ph coupling can be determined based on three essential quantities: (i) site energies, (ii) electronic couplings, and (iii) phonon normal modes. The site energies and electronic couplings can be calculated through QC methods like DFT or the semiempirical valence bond/Hartree–Fock (VB/HF) formalism, as discussed in Section 2.4.1 (*vide supra*). On the other hand, the normal modes can be obtained

via QC or classical FF-based methods; although classical simulations naturally allow larger systems to be modeled at equal or lower computational cost, thereby reducing finite-size effects, it is important to note that QC-based approaches often offer greater flexibility and accuracy in going beyond the Γ-point approximation (i.e., including other points within the first Brillouin zone).[730-733] Phonon normal-mode analysis is generally performed using a software package such as DUSHIN[734] or Phonopy.[735]

Using these techniques, local and nonlocal e-ph coupling have been extensively investigated in a variety of OSC species.[704, 736-740] For example, as early as 2006, Troisi and Orlandi presented a mixed quantum–classical approach in which QC calculations and MD simulations were used to examine the nonlocal coupling in pentacene and anthracene, showing that the perturbative treatment of the e-ph coupling is invalid due to the large fluctuations in the electronic couplings.[327] Their results suggested the dynamic electronic disorder as a key factor in limiting the charge mobility of crystalline OSC. In a similar vein, Sánchez-Carrera et al. explored the oligoacene crystal series from naphthalene to pentacene.[730] Their results demonstrated that neither the weak nor the strong electronic coupling limit were adequate for naphthalene and anthracene due to the comparable strength of nonlocal e-ph couplings and electronic couplings, although the electronic couplings were shown to dominate in tetracene and pentacene. Further, they observed a decrease in the nonlocal relaxation energies *w*ith increasing molecular size.

The validity of the Γ-point approximation in calculating the nonlocal e-ph coupling has been explored by Yi and coworkers in 2012 and again in 2018; in both cases, they demonstrate that the overall nonlocal e-ph couplings are underestimated by considering only the Γ-point approximation.[731, 732] These authors observe in the latter of these works that, in order to describe the force constants accurately, sufficiently large simulation supercells are needed to eliminate the imaginary phonon modes. More recently, Xie et al. explored the rigid-body approximation commonly used in the evaluation of the nonlocal e-ph coupling.[138] By allowing the mixing of intra- and intermolecular modes, they revealed moderate to strong contributions to the nonlocal coupling from low-frequency modes (i.e., acoustic modes and librations), certain out-of-

plane modes, and a combination of some C–C stretching modes. The low-frequency (<200 cm^{-1}) acoustic modes are shown to be the strongest contributors to the nonlocal coupling.

5 Data-driven methods

5.1 High-throughput virtual screening

While the chemical space of OSC is large, recent advancements in computational hardware and optimized computational codes have enabled the computational screening of large OSC libraries to discover candidates with desired properties for experimental investigations. In this process, termed high-throughput virtual screening (HTVS), a computational funnel approach is used wherein each level yields progressively more accurate property estimation at increased computational cost, as shown in Figure 22(a). The HTVS approach, which is routinely used in drug discovery,[741-743] is growing in popularity in accelerating the discovery of new materials.[744-747]

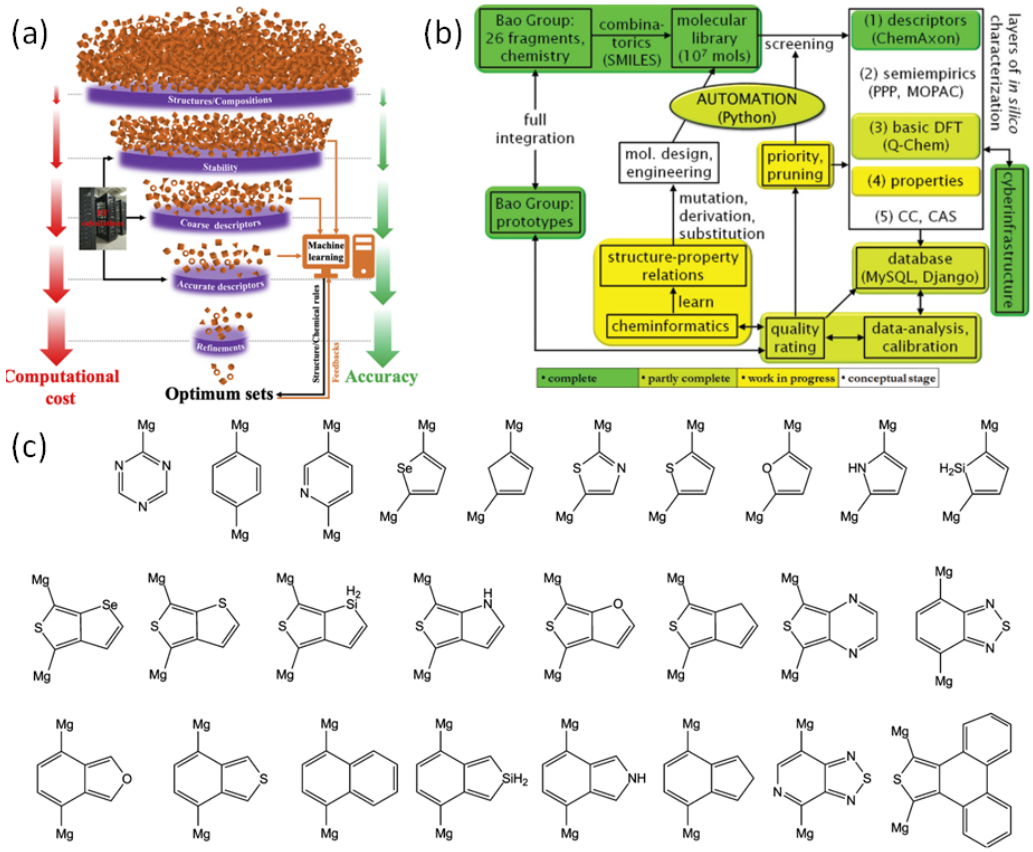

Figure 22. (a) A computational funnel scheme. The increasingly strict filtering criterion eliminates many molecules that are not of interest and identifies the top-performing candidates in a virtual library. Adapted with permission from

Ref.[748] Copyright 2020 John Wiley & Sons, Inc. (b) Structure and workflow of the Clean Energy Project (CEP). (c) The 26 building blocks used for generating the CEP molecular library. The Mg atoms represent chemical handles, i.e., the reactive sites in the generation process. We introduce simple links between two moieties (by means of substituting two Mg for a single C–C bond) as well as the fusion of two rings. Adapted from Ref.[749] Copyright 2011 American Chemical Society.

In 2011, Aspuru-Guzik and coworkers presented an approach to discover organic π-conjugated materials for application in solar cells using high-throughput screening.[749] 2.4 million combinatorially generated molecules were screened by HTVS workflow, as shown in Figure 22(b). In the initial screening, low computational cost cheminformatics descriptors were used, which was followed by semiempirical calculations. The molecular geometry of each screened molecule from semiempirical calculation was optimized at the BP86/def2-SVP level of theory. Further, 14 DFT single-point calculations were performed on the optimized geometry, which provided the eigenvalues of molecular orbitals and other properties, including Mülliken populations and bond order analyses. The computational results were correlated to experimental observations to provide insights into structure-property relationships and thereby lead candidates for organic photovoltaic applications.[750] Wilbraham et al. created a library of π-conjugated polymers and used a combination of tight binding and DFT methods for HTVS of optoelectronic properties.[751] The authors then used the data to calibrate a linear model, which provided DFT-level accuracy from tight binding data thus reducing the computational cost for further polymer screening. In the works of Oberhofer and coworkers,[752] Troisi and coworkers,[753, 754] and Ai et al.,[755] the authors used HTVS on the experimental crystal structures from the Cambridge Structural Database, which contains over 1 million structures.[756] Their workflows used reorganization energy, electronic coupling, and optical excitation energy as properties for screening and proposed few candidate crystals for semiconducting applications.

5.2 Machine learning

The HTVS approach provides sets of potential target materials with desired properties but the computational cost to accurately estimate property for new structure is high. The use of machine learning (ML) algorithms aids the computer in learning the relationship between the input (structure) and output

(property), thereby predicting the output from new inputs. ML algorithms, including ridge regression,[757] support vector machines,[758] decision trees,[759] and artificial neural networks,[760] provide estimates of output in a few seconds. While some of the ML models are black boxes, the implementation of ML in organic π-conjugated materials is still sought as ML models rapidly predict electronic, redox, and optical properties, thereby accelerating discovery.[761-763] The data to train the ML model is generally from high-throughput calculations or data infrastructures like the Clean Energy Project (CEP),[749] OMDB,[764] and OCELOT.[755] An in-depth review of ML can be found elsewhere.[765, 766] In this section, we will discuss some notable contributions of ML in organic π-conjugated systems.

5.2.1 Property prediction

The property prediction for organic π-conjugated systems is performed with ML algorithms, including support vector machines, random forests, ridge regression, and artificial neural networks. For predicting properties like molecular orbitals and low-lying excited states, various methods were explored to transform the chemical information into the necessary fixed-size vector input for the ML models.[767] Some of the vector inputs consist of extended circular fingerprints (ECFP)[768], molecular access system (MACCS)[769] fingerprints that are abundantly used in medicinal chemistry or human selected set of descriptors like number of rings, number of rotatable bonds. The ML predictions of Pyzer-Knapp et al. on the CEP dataset achieved a mean absolute error of 28 meV for HOMO and 32 meV for LUMO.[770] In 2015, Duvenaud et al.[771] proposed using graph fingerprints of a molecule as the input for ML models, as shown in Figure 23. These neural graph fingerprints do not require a set of descriptors of fixed-size and are more interpretable than the cheminformatics fingerprints discussed earlier.

With the development of ML model architecture, more sophisticated models are available. The ML models usually depend on learning the input representation and reduce the need for a human selection of input features.[772] The use of SMILES[773] string to generate the learned representation from variational autoencoders (VAE)[774] was proposed by Gómez-Bombarelli et al.[775] The HOMO, LUMO, and gap

prediction with the VAE for the QM9[776] dataset yield similar performance as the graph fingerprints discussed earlier but could be improved by hyperparameter tuning. Models like SchNet,[777, 778] message passing neural networks (MPNN)[779], and graph neural networks[780-784] are also applied in property prediction tasks. The input for these models is the molecular structure with information on atoms and bonds. Lu et al. compared the performance of some of these models in predicting molecular orbital energies and gaps and singlet excited-state energies and observed that SchNet outperforms other models, as shown in Figure 23(c).[785]

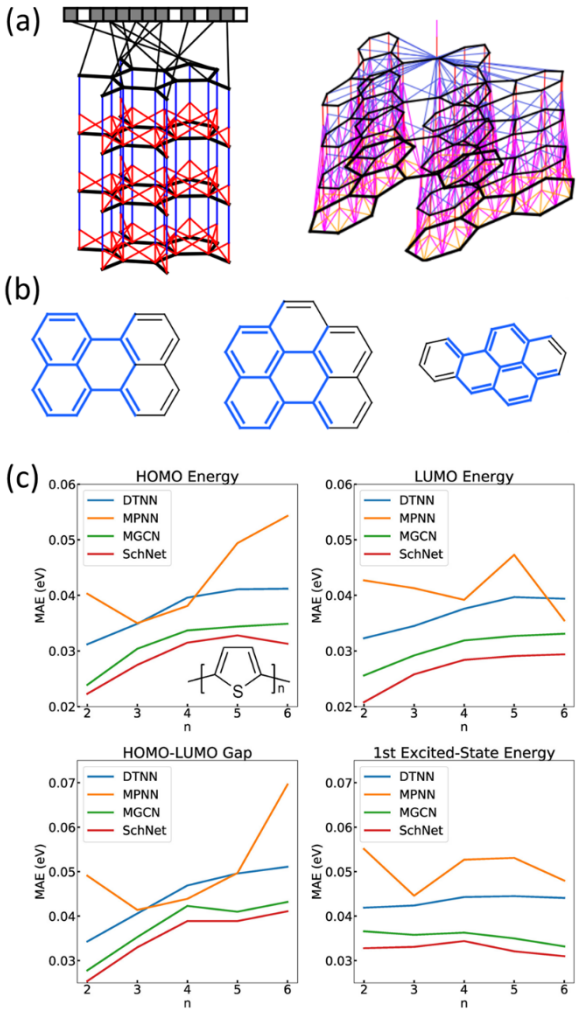

Figure 23. (a) A visual representation of the computational graph of both standard circular fingerprints and neural graph fingerprints. First, a graph is constructed matching the topology of the molecule being fingerprinted, in which nodes represent atoms, and edges represent bonds. At each layer, information flows between neighbors in the graph. Finally, each node in the graph turns on one bit in the fixed-length fingerprint vector. A more detailed sketch including the bond information used in each operation is shown on right. Adapted from Ref.[771] (b) Examining fingerprints optimized for predicting insolubility. Shown here are representative examples of molecular fragments (highlighted in

blue) which most activate different features of the fingerprint. Adapted from Ref.[771] (right panel) Lu et al.[785] use oligothiophenes (OTs) of varying lengths to test the performance of four state-of-the-art DNNs in predicting various optoelectronic properties. Plotted above are the test set mean average errors (MAEs) as a function of the length of OTs, and the optoelectronic properties considered here are (c) HOMO energy, (d) LUMO energy, (e) HOMO–LUMO gap, and (f) first excited-state energy. Reproduced from Ref.[785] Copyright 2020 American Chemical Society.

Materials properties like PCE, crystal packing arrangement, and reorganization energy can be predicted from molecular representation. For instance, Ito et al. used neural graph fingerprints of molecules to predict molecular packing with an accuracy of 64% for organic crystals.[786] Sun et al. developed a model capable of predicting PCE with an accuracy of 91%,[787] based on chemical structure images input into convolutional neural networks (CNN). [788] Atahan-Evrenk et al. trained ML models with kernel ridge regression and deep neural networks to predict reorganization energy and observed that deep neural networks yield mean-absolute as low as 6.5 meV.[789] Recent ML models for bandgap[790] and electronic coupling[791] predictions use representation like SOAP kernel[792, 793] or Coulomb matrix[793] coupled with an artificial neural network or SchNet.[778]

5.2.2 Inverse design

As in the case of property prediction, SMILES can be used as input to generative models that output a molecule with desired target property. Jorgensen et al. developed a grammar VAE that uses SMILES representation for monomeric donor-acceptor units of a polymer to learn the mapping to a continuous vector representation that is then used to generate new molecules.[794] The model generates molecules within the 61% target range of HOMO, LUMO, and optical gap values. Kim et al. used a recurrent neural network[795] for an inverse design approach to discover blue phosphorescent OLED molecules.[796] They employed a target condition of T1 > 3.0 eV with SMILES as input to the model. The model generated a distribution of molecules with a mean T1 of 3.02 eV, with over 58% of molecules satisfying the target condition, as shown in Figure 24. Recent generative models[797, 798] are using SELFIES[799] instead of SMILES, as the validity of SELFIES is always guaranteed but not SMILES. Generative models based on flow,[800-802] diffusion,[803,] and

generative adversarial networks (GAN)[804-807] are used in molecular design, but their application in the discovery of OSC materials is currently limited.

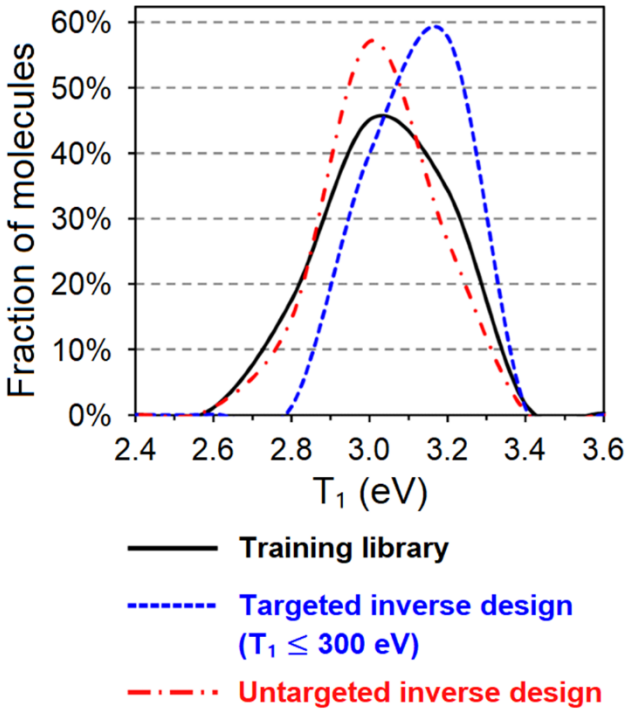

Figure 24. Distribution of simulated T1 (eV) energy levels for blue phosphorescent OLED hosts for the training library, the targeted (T1 ≥ 3.00 eV) inverse-designed molecules, and the untargeted inverse-designed molecules. The fractions of hosts possessing T1 values greater than 3.00 eV were 36.2%, 58.7%, and 26.9%, respectively. Adapted with permission from Ref.[796] Copyright 2020 American Chemical Society.

5.2.3 Active learning

Sampling the whole chemical space of organic π-conjugated systems is unfeasible; hence there is a need to sample this space effectively. Active learning (AL) provides the tools necessary for such investigations.[808, 809] The approach generally consists of a Bayesian optimization algorithm that acts as a surrogate model for exploring the chemical space. The works of Reuter and coworkers demonstrate the application of AL to organic π-conjugated systems.[810] From the chemical space of over 65,000 computationally generated molecules, these authors optimized the charge-conduction fitness, consisting of the reorganization energy and the energy-level alignment of the molecular HOMO and Au work function. The authors observed that the AL approach outperformed the convectional computational funnel discussed previously. The AL approach is not only limited to the virtual screening of molecules but could be used to generate the data for

training the ML models. Smith et al. used an automated AL workflow, shown in Figure 25, to generate new samples for training where the ANI ML potential fails to predict the energy accurately.[811]

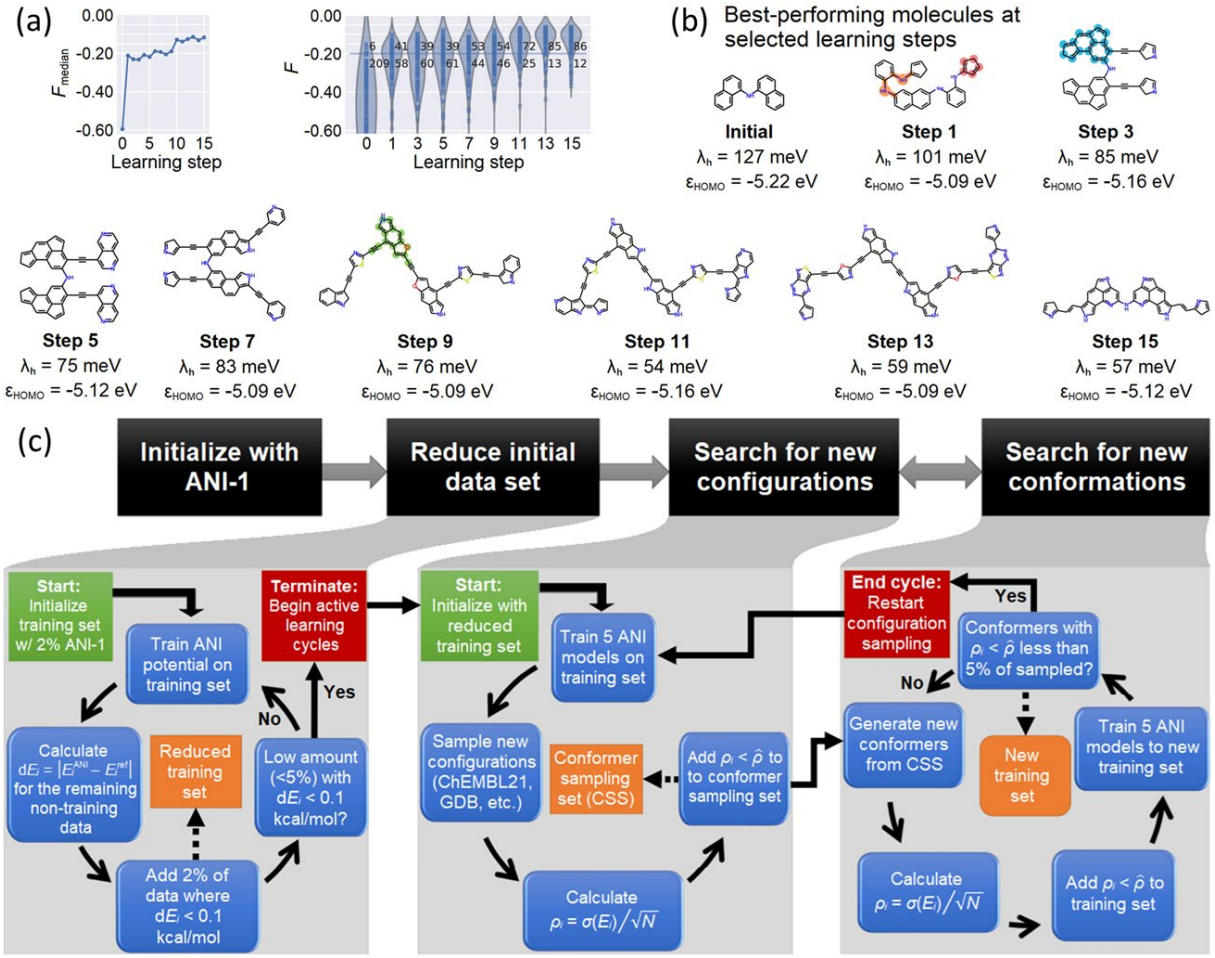

Figure 25. (a) Median values F_{median} of molecular fitness F over the prioritized molecules at different learning steps; step 0 shows the initial population median. (b) Kernel-density estimated distribution of F over the batch of molecules. The number of queries leading to favorable and unfavorable molecules is indicated next to each violin. Examples of high-performing molecules at various learning steps. Adapted from Ref.[810] (c) Fully automated active learning workflow for data generation comprising three main steps of reduction of existing dataset, configurational search, and conformational search. Adapted with permission from Ref.[811] Copyright 2018 AIP Publishing.

5.2.4 ML potentials

As discussed in Section 3.1.2, parametrizing the FF for OSC is challenging and time-consuming. ML potentials can alleviate many of these problems, providing accurate atomic potential energy surfaces and reaction pathways with reduced computational costs. ML potentials are classified as being dedicated or transferable. Dedicated ML potentials need quantum-chemical data and can be applied only to a small set

of systems, while the transferable ML potentials require no prior quantum-chemical calculations and can be applied to many systems. Detailed reviews on ML potentials are provided by Manzhos and Carrington[812] and by Müller and coworkers.[813] ANI, an example of transferable ML potentials for small organic molecules, was introduced by Roitberg and coworkers.[814] The initial ANI model, ANI-1, was trained on molecules up to 8 heavy atoms, including four atom types (C, H, N, and O), with subsequent potentials ANI-2x including S, F, and Cl.[814, 815] The AIMNet[816] model, which is based on Bader's theory of atoms in molecules[817] and shares some similarities with ANI models, is capable of predicting not only energies but also molecular charges and spin multiplicity with error in the range of 2-3 kcal/mol, as shown in Figure 26.[818] While these ML potentials enable rapid exploration of the lowest-energy conformer of small organic molecules,[819] the application to extended organic π-conjugated molecules/polymers remains less explored.

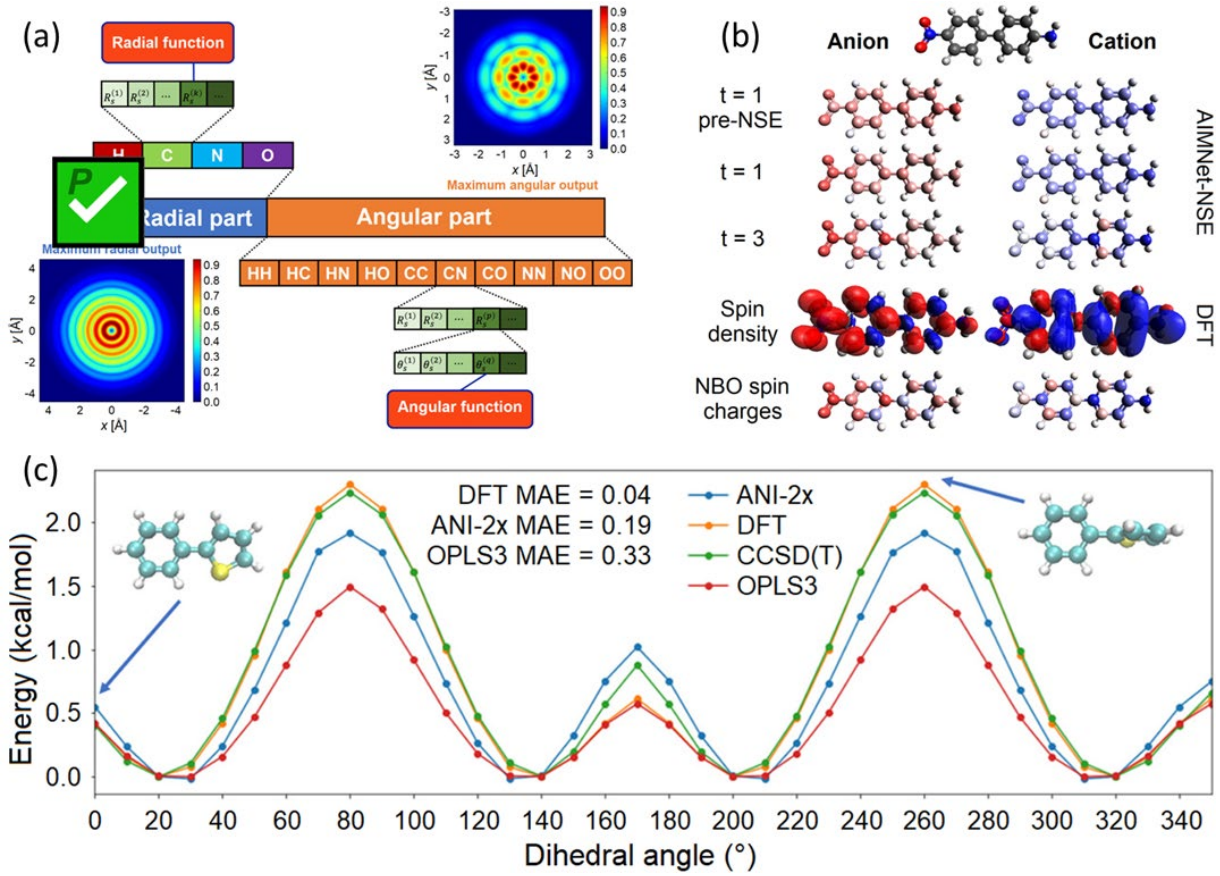

Figure 26. (a) Structure of the ANI AEVs. The sum of j and k is on all neighbor atoms of selected species/pair of species. R and θ are hyperparameters called radial/angular shifts. f_c is the cutoff cosine function, defined as for $R \leq R_c$ and 0 otherwise, where R_c is the cutoff radius, a hyperparameter that defines how far to reach when investigating chemical environments. Reproduced from Ref.[820] Copyright 2020 American Chemical Society. (b) For the anion, colors correspond to spin electron atomic charges or density ($\alpha - \beta$), while for cation to spin hole density ($\beta - \alpha$), with red color corresponding to negative spin-charge. The parameter t

corresponds to AIMNet iterative passes. For comparison, DFT (PBE0/ma-def2-SVP) spin-density and charges are also depicted. Adapted from Ref.[818] (c) Comparison of dihedral potentials computed via the ANI-2x ML potential and via other methods. Reproduced from Ref.[815] Copyright 2020 American Chemical Society.

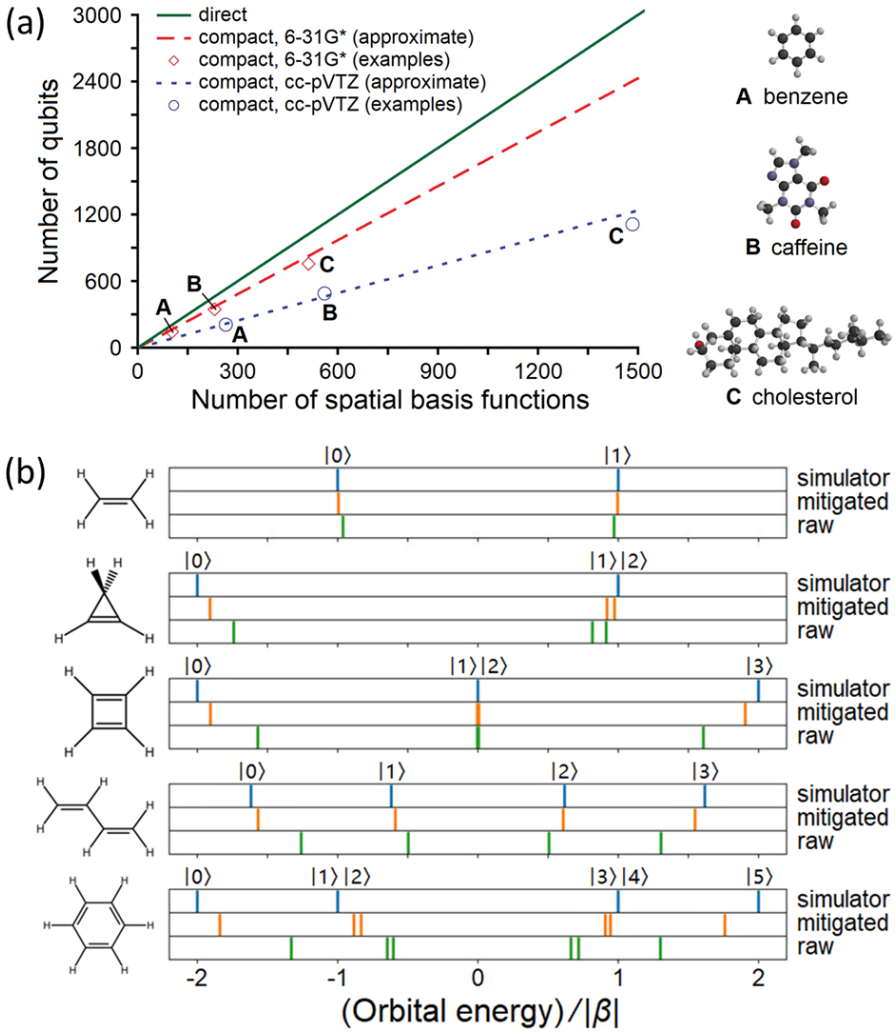

Figure 27. (a) The number of qubits required to store the wave function of a molecule is shown as a function of the number of basis functions for different mappings. For the compact mapping, the qubit requirement also depends on the ratio of the number of electrons to basis functions, which is relatively constant for a given basis set; although the higher quality cc-pVTZ basis is more economical per basis function, a molecule in this basis uses substantially more functions than with the 6-31G* basis. The qubits required for specific molecules and basis sets are also shown. Adapted with permission from Ref.[821] Copyright 2005 The American Association for the Advancement of Science. (b) The Hückel MO energies of the five π-bonding molecular systems obtained by the state vector simulator (simulator), the ibm_kawasaki machine with error mitigations (mitigated), and the ibm_kawasaki machine without error mitigation (raw). The orbital energy specified by |i⟩ just above the respective subfigures represents the orbital energy of the ith excited MO. Adapted with permission from Ref.[822] Copyright 2022 AIP Publishing.

6 Outlook

In this Review, we examined several decades of advances in computational materials modeling techniques and their application to develop physicochemical insights into π-conjugated molecules and polymers and OSC. These systems provide particular challenges for computational study given their size – pushing the limits of quantum and classical mechanical techniques – chemical diversity, and disparate properties that are highly dependent on the environment in which they are studied or operate. With the advent of exascale computing, and the continued development of computational algorithms and mathematical and physical frameworks, ever more complex systems are being investigated in silico with increased accuracy.[823] However, we note that many of the methods that are now a few decades old still find wide use given their simple nature and capability to provide distinct physical understanding; for instance, a recent work used the Hückel MO method to simulate an organic system on emerging quantum computing hardware, as shown in Figure 27.[822] Further, the emergence of more complex computational workflows will necessitate the need to adapt open-source tools (e.g., SEAMM[824]) to promote easy workflow implementation and reproducibility, and the continued democratization of data and computational method utility; for example, making it easier to find, access, and implement standardized FF parameterizations for OSC, especially π-conjugated polymers, would streamline the process of initializing MD simulation systems.

Computational methods will continue to play critical roles as OSC materials design and discovery evolve from Edisonian trial-and-error approaches toward machine-informed and machine-driven design and discovery. Advances in ML and artificial intelligence (AI) to drive (semi)autonomous robotic platforms require data sets of immense size. Although a wide variety of OSC are regularly explored with computational methods, open access to this data abiding by FAIR principles[825] is limited. While recent efforts have curated small datasets, a dataset for OSC with extensive muti-fidelity data is needed to produce reliable ML models. Furthermore, the trained ML models should provide the uncertainty associated with predictions and be made accessible to the OSC community, leveraging infrastructure like OCELOT ML.[761] Currently, OSC molecular property prediction methods are being adapted from drug design, while ML

models for material properties prediction from the solid-state structure are still scarce. Such a situation calls for future method development focused on the data-driven design of next-generation OSC materials.

Acknowledgments

This work was funded in part by the National Science Foundation through award numbers DMR 1627428 and DMR 1922174 and by the Office of Naval Research through award number N00014-22-1-2179.

Author Biography

Vinayak Bhat is a Ph.D. candidate in the Department of Chemistry at the University of Kentucky under the supervision of Dr. Chad Risko. Vinayak received a B.S.–M.S. degree in Chemistry from the Indian Institute of Science Education and Research, Thiruvananthapuram, India. Vinayak's research focuses on creating data architectures and implementing data-driven methods to accelerate the design of organic □-conjugated systems.

Connor P. Callaway is a postdoctoral scholar in the Department of Chemistry at the University of Kentucky working under the mentorship of Dr. Chad Risko. Connor received his B.S. in Materials Science and Engineering from the University of Kentucky and his Ph.D. from the Georgia Institute of Technology under the mentorship of Dr. Seung Soon Jang. Connor's research focuses on molecular dynamics simulations of organic semiconductors with a focus on adapting simulation methodologies for π-conjugated polymers.

Chad Risko is an Associate Professor in the Department of Chemistry and an affiliated faculty member of the Center for Applied Energy Research (CAER) at the University of Kentucky. Chad received his B.S. in Chemistry at Baker University and his Ph.D. from the Georgia Institute of Technology under the mentorship of Dr. Jean-Luc Brédas. Chad was then a postdoctoral researcher with Dr. Mark Ratner and Dr. Tobin

Marks at Northwestern University. Chad's research centers on developing and deploying computational and machine-based methods to investigate and predict materials properties.

Author Information

Corresponding author: Chad Risko, chad.risko@uky.edu

†V.B. and C.P.C. contributed equally to this work.

Notes

The authors declare no competing financial interest.

References

(1) Chen, M.; Yan, L.; Zhao, Y.; Murtaza, I.; Meng, H.; Huang, W. Anthracene-based semiconductors for organic field-effect transistors. *J. Mater. Chem. C Mater* **2018**, *6* (28), 7416-7444

(2) Anthony, J. E. The Larger Acenes: Versatile Organic Semiconductors. *Angew. Chem. Int. Ed.* **2008**, *47* (3), 452-483

(3) Figueira-Duarte, T. M.; Müllen, K. Pyrene-Based Materials for Organic Electronics. *Chem. Rev.* **2011**, *111* (11), 7260-7314

(4) Sun, Y.; Guo, Y.; Liu, Y. Design and synthesis of high performance π-conjugated materials through antiaromaticity and quinoid strategy for organic field-effect transistors. *Mater. Sci. Eng. R Rep.* **2019**, *136*, 13-26

(5) Huang, Y.; Egap, E. Open-shell organic semiconductors: an emerging class of materials with novel properties. *Polym. J.* **2018**, *50* (8), 603-614

(6) Zeng, Z.; Shi, X.; Chi, C.; López Navarrete, J. T.; Casado, J.; Wu, J. Pro-aromatic and anti-aromatic π-conjugated molecules: an irresistible wish to be diradicals. *Chem. Soc. Rev.* **2015**, *44* (18), 6578-6596

(7) Frederickson, C. K.; Rose, B. D.; Haley, M. M. Explorations of the Indenofluorenes and Expanded Quinoidal Analogues. *Acc. Chem. Res.* **2017**, *50* (4), 977-987

(8) Takimiya, K.; Shinamura, S.; Osaka, I.; Miyazaki, E. Thienoacene-Based Organic Semiconductors. *Adv. Mater.* **2011**, *23* (38), 4347-4370

(9) Jiang, W.; Li, Y.; Wang, Z. Heteroarenes as high performance organic semiconductors. *Chem. Soc. Rev.* **2013**, *42* (14), 6113

(10) Miao, Q. Ten Years of N-Heteropentacenes as Semiconductors for Organic Thin-Film Transistors. *Adv. Mater.* **2014**, *26* (31), 5541-5549

(11) Liu, Z.; Zhang, G.; Zhang, D. Modification of Side Chains of Conjugated Molecules and Polymers for Charge Mobility Enhancement and Sensing Functionality. *Acc. Chem. Res.* **2018**, *51* (6), 1422-1432

(12) Mishima, K.; Yamashita, K. Importance of Side-Chains on Molecular Characteristics of Interacting Organic Molecules. *ACS Omega* **2019**, *4* (6), 10396-10404

(13) Zhang, F.; Hu, Y.; Schuettfort, T.; Di, C.-A.; Gao, X.; Mcneill, C. R.; Thomsen, L.; Mannsfeld, S. C. B.; Yuan, W.; Sirringhaus, H.; et al. Critical Role of Alkyl Chain Branching of Organic Semiconductors in Enabling Solution-Processed N-Channel Organic Thin-Film Transistors with Mobility of up to 3.50 cm2 V-1 s-1. *J. Am. Chem. Soc.* **2013**, *135* (6), 2338-2349

(14) Alessandri, R.; Sami, S.; Barnoud, J.; Vries, A. H.; Marrink, S. J.; Havenith, R. W. A. Resolving Donor–Acceptor Interfaces and Charge Carrier Energy Levels of Organic Semiconductors with Polar Side Chains. *Adv. Funct. Mater.* **2020**, *30* (46), 2004799

(15) Thorley, K. J.; Benford, M.; Song, Y.; Parkin, S. R.; Risko, C.; Anthony, J. E. What is special about silicon in functionalised organic semiconductors? *Mater. Adv.* **2021**, *2* (16), 5415-5421

(16) Anthony, J. E. Functionalized Acenes and Heteroacenes for Organic Electronics. *Chem. Rev.* **2006**, *106* (12), 5028-5048

(17) Takimiya, K.; Osaka, I.; Mori, T.; Nakano, M. Organic Semiconductors Based on [1]Benzothieno[3,2-b][1]benzothiophene Substructure. *Acc. Chem. Res.* **2014**, *47* (5), 1493-1502

(18) Gsänger, M.; Bialas, D.; Huang, L.; Stolte, M.; Würthner, F. Organic Semiconductors based on Dyes and Color Pigments. *Adv. Mater.* **2016**, *28* (19), 3615-3645

(19) Zhang, X.; Jie, J.; Deng, W.; Shang, Q.; Wang, J.; Wang, H.; Chen, X.; Zhang, X. Alignment and Patterning of Ordered Small-Molecule Organic Semiconductor Micro-/Nanocrystals for Device Applications. *Adv. Mater.* **2016**, *28* (13), 2475-2503

(20) Liu, S.; Wang, W. M.; Briseno, A. L.; Mannsfeld, S. C. B.; Bao, Z. Controlled Deposition of Crystalline Organic Semiconductors for Field-Effect-Transistor Applications. *Adv. Mater.* **2009**, *21* (12), 1217-1232

(21) Chen, S.; Li, Z.; Qiao, Y.; Song, Y. Solution-processed organic semiconductor crystals for field-effect transistors: from crystallization mechanism towards morphology control. *J. Mater. Chem. C Mater* **2021**, *9* (4), 1126-1149
(22) Peng, B.; Wang, Z.; Chan, P. K. L. A simulation-assisted solution-processing method for a large-area, high-performance C10-DNTT organic semiconductor crystal. *J. Mater. Chem. C Mater* **2016**, *4* (37), 8628-8633
(23) Murphy, A. R.; Fréchet, J. M. J. Organic Semiconducting Oligomers for Use in Thin Film Transistors. *Chem. Rev.* **2007**, *107* (4), 1066-1096
(24) Gu, X.; Shaw, L.; Gu, K.; Toney, M. F.; Bao, Z. The meniscus-guided deposition of semiconducting polymers. *Nat. Commun.* **2018**, *9* (1), 534
(25) Hiszpanski, A. M.; Loo, Y.-L. Directing the film structure of organic semiconductors via post-deposition processing for transistor and solar cell applications. *Energy Environ. Sci.* **2014**, *7* (2), 592-608
(26) De Luca, G.; Pisula, W.; Credgington, D.; Treossi, E.; Fenwick, O.; Lazzerini, G. M.; Dabirian, R.; Orgiu, E.; Liscio, A.; Palermo, V.; et al. Non-conventional Processing and Post-processing Methods for the Nanostructuring of Conjugated Materials for Organic Electronics. *Adv. Funct. Mater.* **2011**, *21* (7), 1279-1295
(27) Wang, S.; Peng, L.; Sun, H.; Huang, W. The future of solution processing toward organic semiconductor devices: a substrate and integration perspective. *J. Mater. Chem. C Mater* **2022**, *10* (35), 12468-12486
(28) Peng, X.; Hu, L.; Qin, F.; Zhou, Y.; Chu, P. K. Low Work Function Surface Modifiers for Solution-Processed Electronics: A Review. *Adv. Mater. Interfaces.* **2018**, *5* (10), 1701404
(29) Sutton, C.; Risko, C.; Brédas, J.-L. Noncovalent Intermolecular Interactions in Organic Electronic Materials: Implications for the Molecular Packing vs Electronic Properties of Acenes. *Chem. Mater.* **2016**, *28* (1), 3-16
(30) Ravva, M. K.; Risko, C.; Brédas, J.-L. Chapter 9 - Noncovalent Interactions in Organic Electronic Materials. In *Non-Covalent Interactions in Quantum Chemistry and Physics*, Otero de la Roza, A., DiLabio, G. A. Eds.; Elsevier, 2017; pp 277-302.
(31) Bredas, J.-L.; Chen, X.; Körzdörfer, T.; Li, H.; Risko, C.; Ryno, S.; Wang, T. Recent Advances in the Computational Characterization of π-Conjugated Organic Semiconductors. In *Conjugated Polymers*, 2019; pp 37-106.
(32) Bhaskaran-Nair, K.; Kowalski, K.; Jarrell, M.; Moreno, J.; Shelton, W. A. Equation of motion coupled cluster methods for electron attachment and ionization potential in polyacenes. *Chem. Phys. Lett.* **2015**, *641*, 146-152
(33) Borges, I.; Aquino, A. J. A.; Köhn, A.; Nieman, R.; Hase, W. L.; Chen, L. X.; Lischka, H. Ab initio modeling of excitonic and charge-transfer states in organic semiconductors: the PTB1/PCBM low band gap system. *J. Am. Chem. Soc.* **2013**, *135* (49), 18252-18255
(34) Settels, V.; Schubert, A.; Tafipolski, M.; Liu, W.; Stehr, V.; Topczak, A. K.; Pflaum, J.; Deibel, C.; Fink, R. F.; Engel, V.; et al. Identification of Ultrafast Relaxation Processes As a Major Reason for Inefficient Exciton Diffusion in Perylene-Based Organic Semiconductors. *J. Am. Chem. Soc.* **2014**, *136* (26), 9327-9337
(35) Risko, C.; Brédas, J.-L. Small Optical Gap Molecules and Polymers: Using Theory to Design More Efficient Materials for Organic Photovoltaics. In *Multiscale Modelling of Organic and Hybrid Photovoltaics*, Beljonne, D., Cornil, J. Eds.; Springer Berlin Heidelberg, 2014; pp 1-38.
(36) Brédas, J.-L.; Coropceanu, V.; Doiron, C.; Fu, Y.-T.; Körzdörfer, T.; Pandey, L.; Risko, C.; Sears, J.; Yang, B.; Yi, Y.; et al. Modeling the Electronic and Optical Processes in Organic Solar Cells: Density Functional Theory and Beyond. In *Organic Solar Cells*, 2014; pp 537-588.
(37) Schrödinger, E. Quantisierung als Eigenwertproblem. *Ann. Phys.* **1926**, *384* (4), 361-376
(38) Pople, J. A.; Beveridge, D. L. *Approximate Molecular Orbital Theory*; 1970.
(39) Thiel, W. Perspectives on Semiempirical Molecular Orbital Theory. In *Advances in Chemical Physics*, 1996; pp 703-757.

(40) Hückel, E. Quantentheoretische Beiträge zum Benzolproblem. *Z. Phys.* **1931**, *70*, 204-286
(41) Heitler, W.; London, F. Wechselwirkung neutraler Atome und homöopolare Bindung nach der Quantenmechanik. *Z. Phys.* **1927**, *44*, 455-472
(42) Heisenberg, W. Zur Theorie des Ferromagnetismus. *Z. Phys.* **1928**, *49* (9-10), 619-636
(43) Slater, J. C. Cohesion in Monovalent Metals. *Phys. Rev.* **1930**, *35* (5), 509-529
(44) Slater, J. C. Molecular Energy Levels and Valence Bonds. *Phys. Rev.* **1931**, *38* (6), 1109-1144
(45) Slater, J. C. Directed Valence in Polyatomic Molecules. *Phys. Rev.* **1931**, *37* (5), 481-489
(46) Bloch, F. Über die Quantenmechanik der Elektronen in Kristallgittern. *Z. Phys.* **1929**, *52*, 555-600
(47) Bloch, F. Zur Theorie des Ferromagnetismus. *Z. Phys.* **1930**, *61*, 206-219
(48) Hartree, D. R. The Wave Mechanics of an Atom with a Non-Coulomb Central Field. Part I. Theory and Methods. *Math. Proc. Cambridge Philos.* **1928**, *24* (1), 89-110
(49) Frenking, G. Perspective on "Quantentheoretische Beiträge zum Benzolproblem. I. Die Elektronenkonfiguration des Benzols und verwandter Beziehungen". *Theor. Chem. Acc.* **2000**, *103*, 187-189
(50) Pauling, L.; Wheland, G. W. The Nature of the Chemical Bond. V. The Quantum-Mechanical Calculation of the Resonance Energy of Benzene and Naphthalene and the Hydrocarbon Free Radicals. *J. Chem. Phys.* **1933**, *1* (6), 362-374
(51) Pauling, L.; Sherman, J. The Nature of the Chemical Bond. VII. The Calculation of Resonance Energy in Conjugated Systems. *J. Chem. Phys.* **1933**, *1* (10), 679-686
(52) Kekulé, A. Sur la Constitution des substances aromatiques. *Bull. Soc. chim. Fr.* **1865**, *3* (2), 98-111
(53) Hückel, E. Die freien Radikale der organischen Chemie. *Z. Phys.* **1933**, *83* (9), 632-668
(54) Hückel, E. Theory of free radicals of organic chemistry. *Trans. Faraday Soc.* **1934**, *30* (0), 40-52
(55) Van Vleck, J. H. On the Theory of the Structure of CH4 and Related Molecules: Part II. *J. Chem. Phys.* **1933**, *1* (4), 219-238
(56) Van Vleck, J. H. On the Theory of the Structure of CH4 and Related Molecules: Part III. *J. Chem. Phys.* **1934**, *2* (1), 20-30
(57) Wheland, G. W. The Quantum Mechanics of Unsaturated and Aromatic Molecules: A Comparison of Two Methods of Treatment. *J. Chem. Phys.* **1934**, *2* (8), 474-481
(58) Mulliken, R. S.; Rieke, C. A. Journal of the Chemical Society, Perkin Transactions 2. *J. Am. Chem. Soc.* **1941**, *63* (6), 1770-1771
(59) Mulliken, R. S.; Rieke, C. A.; Brown, W. G. Hyperconjugation. *J. Am. Chem. Soc.* **1941**, *63* (1), 41-56
(60) Sklar, A. L. Theory of Color of Organic Compounds. *J. Chem. Phys.* **1937**, *5* (9), 669-681
(61) Goeppert-Mayer, M.; Sklar, A. L. Calculations of the Lower Excited Levels of Benzene. *J. Chem. Phys.* **1938**, *6* (10), 645-652
(62) Mulliken, R. S. Intensities of Electronic Transitions in Molecular Spectra III. Organic Molecules with Double Bonds. Conjugated Dienes. *J. Chem. Phys.* **1939**, *7* (2), 121-135
(63) Coulson, C. A.; Longuet-Higgins, H. C. The electronic structure of conjugated systems I. General theory. *Proc. R. Soc. Lond. A Math. Phys. Sci.* **1947**, *191* (1024), 39-60
(64) Pariser, R.; Parr, R. G. A Semi-Empirical Theory of the Electronic Spectra and Electronic Structure of Complex Unsaturated Molecules. I. *J. Chem. Phys.* **1953**, *21* (3), 466-471
(65) Pople, J. A. Electron interaction in unsaturated hydrocarbons. *Trans. Faraday Soc.* **1953**, *49*, 1375-1385
(66) Nishimoto, K.; Mataga, N. Electronic structure and spectra of some nitrogen heterocycles. *Z Phys Chem (N F)* **1957**, *12*, 335-338
(67) Nishimoto, K. A MO theoretical study of organic dyes I. Effect of chemical softness on the electronic spectra. *Bull. Chem. Soc. Jpn.* **1993**, *66* (7), 1876-1880
(68) Hiruta, K.; Tokita, S.; Nishimoto, K. Precise PPP molecular orbital calculations of excitation energies of polycyclic aromatic hydrocarbons. Part 1. On the correlation between the chemical softness and the absolute hardness. *J. Chem. Soc., Perkin Trans. 2* **1995**, (7), 1443

(69) Hiruta, K.; Tokita, S.; Tachikawa, T.; Noguchi, F.; Nishimoto, K. Precise PPP molecular orbital calculations of excitation energies of polycyclic aromatic hydrocarbons. Part 6. Spectrochemical atomic softness parameter†. *J. Chem. Soc., Perkin Trans. 2* **2001**, (6), 975-980
(70) Aryanpour, K.; Shukla, A.; Mazumdar, S. Theory of Singlet Fission in Polyenes, Acene Crystals, and Covalently Linked Acene Dimers. *J. Phys. Chem. C.* **2015**, *119* (13), 6966-6979
(71) Parenti, K. R.; Chesler, R.; He, G.; Bhattacharyya, P.; Xiao, B.; Huang, H.; Malinowski, D.; Zhang, J.; Yin, X.; Shukla, A.; et al. Quantum interference effects elucidate triplet-pair formation dynamics in intramolecular singlet-fission molecules. *Nature Chemistry* **2022**,
(72) Bhattacharyya, P.; Rai, D. K.; Shukla, A. Pariser–Parr–Pople Model Based Configuration-Interaction Study of Linear Optical Absorption in Lower-Symmetry Polycyclic Aromatic Hydrocarbon Molecules. *J. Phys. Chem. C.* **2020**, *124* (26), 14297-14305
(73) Raghu, C.; Pati, Y. A.; Ramasesha, S. Structural and electronic instabilities in polyacenes: Density-matrix renormalization group study of a long-range interacting model. *Phys. Rev. B.* **2002**, *65* (15), 155204
(74) White, S. R. Density matrix formulation for quantum renormalization groups. *Phys. Rev. Lett.* **1992**, *69* (19), 2863-2866
(75) Anusooya, Y.; Pati, S. K.; Ramasesha, S. Symmetrized density matrix renormalization group studies of the properties of low-lying states of the poly-para-phenylene system. *J. Chem. Phys.* **1997**, *106* (24), 10230-10237
(76) Shuai, Z.; Brédas, J. L.; Pati, S. K.; Ramasesha, S. Quantum-confinement effects on the ordering of the lowest-lying excited states in conjugated chains. *Phys. Rev. B.* **1997**, *56* (15), 9298-9301
(77) Ramasesha, S.; Pati, S. K.; Krishnamurthy, H. R.; Shuai, Z.; Brédas, J. L. Symmetrized density-matrix renormalization-group method for excited states of Hubbard models. *Phys. Rev. B.* **1996**, *54* (11), 7598-7601
(78) Barford, W.; Bursill, R. J.; Lavrentiev, M. Y. Density-matrix renormalization-group calculations of excited states of linear polyenes. *Phys. Rev. B.* **2001**, *63* (19),
(79) Raghu, C.; Anusooya Pati, Y.; Ramasesha, S. Density-matrix renormalization-group study of low-lying excitations of polyacene within a Pariser-Parr-Pople model. *Phys. Rev. B.* **2002**, *66* (3),
(80) Yaron, D.; Moore, E. E.; Shuai, Z.; Brédas, J. L. Comparison of density matrix renormalization group calculations with electron-hole models of exciton binding in conjugated polymers. *J. Chem. Phys.* **1998**, *108* (17), 7451-7458
(81) Fano, G.; Ortolani, F.; Ziosi, L. The density matrix renormalization group method: Application to the PPP model of a cyclic polyene chain. *J. Chem. Phys.* **1998**, *108* (22), 9246-9252
(82) Barford, W. Theory of the dark state of polyenes and carotenoids. *Phys. Rev. B.* **2022**, *106* (3),
(83) Manawadu, D.; Georges, T. N.; Barford, W. Photoexcited state dynamics and singlet fission in carotenoids. *arXiv preprint arXiv:2211.02267* **2022**,
(84) Hoffmann, R. An Extended Hückel Theory. I. Hydrocarbons. *J. Chem. Phys.* **1963**, *39* (6), 1397-1412
(85) Pople, J. A.; Santry, D. P.; Segal, G. A. Approximate Self-Consistent Molecular Orbital Theory. I. Invariant Procedures. *J. Chem. Phys.* **1965**, *43* (10), S129-S135
(86) Pople, J. A.; Segal, G. A. Approximate Self-Consistent Molecular Orbital Theory. II. Calculations with Complete Neglect of Differential Overlap. *J. Chem. Phys.* **1965**, *43* (10), S136-S151
(87) Pople, J. A.; Segal, G. A. Approximate Self-Consistent Molecular Orbital Theory. III. CNDO Results for AB2 and AB3 Systems. *J. Chem. Phys.* **1966**, *44* (9), 3289-3296
(88) Pople, J. A.; Beveridge, D. L.; Dobosh, P. A. Approximate Self-Consistent Molecular-Orbital Theory. V. Intermediate Neglect of Differential Overlap. *J. Chem. Phys.* **1967**, *47* (6), 2026-2033
(89) Beveridge, D. L.; Dobosh, P. A.; Pople, J. A. Molecular-Orbital Theory of Geometry and Hyperfine Coupling Constants of Fluorinated Methyl Radicals. *J. Chem. Phys.* **1968**, *48* (10), 4802-4803
(90) Ridley, J.; Zerner, M. An intermediate neglect of differential overlap technique for spectroscopy: Pyrrole and the azines. *Theor. Chim. Acta.* **1973**, *32* (2), 111-134

(91) Bingham, R. C.; Dewar, M. J. S.; Lo, D. H. Ground states of molecules. XXV. MINDO/3. Improved version of the MINDO semiempirical SCF-MO method. *J. Am. Chem. Soc.* **1975**, *97* (6), 1285-1293
(92) Dewar, M. J. S.; Thiel, W. Ground states of molecules. 38. The MNDO method. Approximations and parameters. *J. Am. Chem. Soc.* **1977**, *99* (15), 4899-4907
(93) Clark, T. Quo Vadis semiempirical MO-theory? *Theochem* **2000**, *530* (1), 1-10
(94) Thiel, W. Semiempirical methods: current status and perspectives. *Tetrahedron* **1988**, *44* (24), 7393-7408
(95) Stewart, J. J. P. MOPAC: A semiempirical molecular orbital program. *J. Comput. Aided Mol. Des.* **1990**, *4* (1), 1-103
(96) Dewar, M. J. S.; Zoebisch, E. G.; Healy, E. F.; Stewart, J. J. P. Development and use of quantum mechanical molecular models. 76. AM1: a new general purpose quantum mechanical molecular model. *J. Am. Chem. Soc.* **1985**, *107* (13), 3902-3909
(97) Stewart, J. J. P. Optimization of parameters for semiempirical methods I. Method. *J. Comput. Chem.* **1989**, *10* (2), 209-220
(98) Stewart, J. J. P. Optimization of parameters for semiempirical methods II. Applications. *J. Comput. Chem.* **1989**, *10* (2), 221-264
(99) Stewart, J. J. P. Optimization of parameters for semiempirical methods V: Modification of NDDO approximations and application to 70 elements. *J. Mol. Model.* **2007**, *13* (12), 1173-1213
(100) Stewart, J. J. P. Optimization of parameters for semiempirical methods VI: more modifications to the NDDO approximations and re-optimization of parameters. *J. Mol. Model.* **2013**, *19* (1), 1-32
(101) Kolb, M.; Thiel, W. Beyond the MNDO Model: Methodical Considerations and Numerical Results. *J. Comput. Chem.* **1993**, *14*, 775
(102) Weber, W.; Thiel, W. Orthogonalization Corrections for Semiempirical Methods. *Theor. Chem. Acc.* **2000**, *103*, 495
(103) Scholten, M. Semiempirische verfahren mit orthogonalisierungskorrekturen: Die OM3 Methode. *Heinrich-Heine-Universität Düsseldorf* **2003**,
(104) Cornil, J.; Beljonne, D.; dos Santos, D. A.; Shuai, Z.; Brédas, J. L. Towards a better understanding of polymer-based light-emitting diodes: a theoretical insight into the basic phenomena. *Synthetic Metals* **1996**, *78* (3), 209-217
(105) Lögdlund, M.; Brédas, J. L. Theoretical analysis of the charge-storage states in diphenylpolyenes with one to seven double bonds. *J. Chem. Phys.* **1994**, *100* (9), 6543-6549
(106) Lögdlund, M.; Brédas, J. L. Theoretical analysis of conjugated polymers with a degenerate ground state: Type-I and type-II soliton charge storage states in poly(1,6-heptadiyne) and derivatives. *J. Chem. Phys.* **1995**, *103* (10), 4201-4210
(107) Tretiak, S.; Saxena, A.; Martin, R. L.; Bishop, A. R. Collective electronic oscillator/semiempirical calculations of static nonlinear polarizabilities in conjugated molecules. *J. Chem. Phys.* **2001**, *115* (2), 699-707
(108) Sifain, A. E.; Bjorgaard, J. A.; Nelson, T. R.; Nebgen, B. T.; White, A. J.; Gifford, B. J.; Gao, D. W.; Prezhdo, O. V.; Fernandez-Alberti, S.; Roitberg, A. E.; et al. Photoexcited Nonadiabatic Dynamics of Solvated Push–Pull π-Conjugated Oligomers with the NEXMD Software. *J. Chem. Theory. Comput.* **2018**, *14* (8), 3955-3966
(109) Coheur, P.-F.; Cornil, J.; Dos Santos, D. A.; Birkett, P. R.; Liévin, J.; Brédas, J. L.; Walton, D. R. M.; Taylor, R.; Kroto, H. W.; Colin, R. Photophysical properties of hexa-functionalized C60 derivatives: Spectroscopic and quantum-chemical investigations. *J. Chem. Phys.* **2000**, *112* (19), 8555-8566
(110) Dick, B. AM1 and INDO/S calculations on electronic singlet and triplet states involved in excited-state intramolecular proton transfer of 3-hydroxyflavone. *J. Phys. Chem.* **1990**, *94* (15), 5752-5756
(111) Konovalov, V. V.; Kispert, L. D. AM1, INDO/S and optical studies of carbocations of carotenoid molecules. Acid induced isomerization. *J. Chem. Soc., Perkin Trans. 2* **1999**, (4), 901-910

(112) Cornil, J.; Beljonne, D.; Calbert, J.-P.; Brédas, J.-L. Interchain Interactions in Organic π-Conjugated Materials: Impact on Electronic Structure, Optical Response, and Charge Transport. *Adv. Mater.* **2001**, *13* (14), 1053-1067
(113) Silva-Junior, M. R.; Thiel, W. Benchmark of Electronically Excited States for Semiempirical Methods: MNDO, AM1, PM3, OM1, OM2, OM3, INDO/S, and INDO/S2. *J. Chem. Theory. Comput.* **2010**, *6* (5), 1546-1564
(114) Gieseking, R. L. M. A new release of MOPAC incorporating the INDO/S semiempirical model with CI excited states. *J. Comput. Chem.* **2021**, *42* (5), 365-378
(115) Cui, G.; Lu, Y.; Thiel, W. Electronic Excitation Energies, Three-State Intersections, and Photodissociation Mechanisms of Benzaldehyde and Acetophenone. *Chem. Phys. Lett.* **2012**, *537*, 21-26
(116) Xie, B. B.; Xia, S. H.; Chang, X. P.; Cui, G. Photophysics of Auramine-O: Electronic Structure Calculations and Nonadiabatic Dynamics Simulations. *Phys. Chem. Chem. Phys.* **2016**, *18*, 403
(117) Cui, G.; Thiel, W. Nonadiabatic Dynamics of a Truncated Indigo Model. *Phys. Chem. Chem. Phys.* **2012**, *14*, 12378-12384
(118) Sporkel, L.; Cui, G.; Thiel, W. Photodynamics of Schiff base salicylideneaniline: trajectory surface-hopping simulations. *J. Phys. Chem. A* **2013**, *117* (22), 4574-4583
(119) Hu, D.; Huang, J.; Xie, Y.; Yue, L.; Zhuang, X.; Lan, Z. Nonadiabatic Dynamics and Photoisomerization of Biomimetic Photoswitches. *Chem. Phys.* **2015**, *463*, 95-105
(120) Brückner, C.; Engels, B. Benchmarking Ground-State Geometries and Vertical Excitation Energies of a Selection of P-Type Semiconducting Molecules with Different Polarity. *J. Phys. Chem. A.* **2015**, *119* (51), 12876-12891
(121) Slater, J. C.; Koster, G. F. Simplified LCAO Method for the Periodic Potential Problem. *Phys. Rev.* **1954**, *94* (6), 1498-1524
(122) Leblanc, O. H. Band Structure and Transport of Holes and Electrons in Anthracene. *J. Chem. Phys.* **1961**, *35* (4), 1275-1280
(123) André, J. M.; Burke, L. A.; Delhalle, J.; Nicolas, G.; Durand, P. H. A nonempirical model potential technique for calculations of band structures of polymers. *Int. J. Quantum Chem* **1979**, *16*, 283-291
(124) Brédas, J. L.; Chance, R. R.; Baughman, R. H.; Silbey, R. Ab initio effective Hamiltonian study of the electronic properties of conjugated polymers. *J. Chem. Phys.* **1982**, *76* (7), 3673-3678
(125) Brédas, J. L.; Scott, J. C.; Yakushi, K.; Street, G. B. Polarons and bipolarons in polypyrrole: Evolution of the band structure and optical spectrum upon doing. *Phys. Rev. B.* **1984**, *30* (2), 1023-1025
(126) Brédas, J. L.; Heeger, A. J.; Wudl, F. Towards organic polymers with very small intrinsic band gaps. I. Electronic structure of polyisothianaphthene and derivatives. *J. Chem. Phys.* **1986**, *85* (8), 4673-4678
(127) Toussaint, J. M.; Brédas, J. L. Towards organic polymers with small intrinsic band gaps. III. Geometric and electronic structures of the base and salt forms of polypyrrylenemethine. *J. Chem. Phys.* **1991**, *94* (12), 8122-8128
(128) Meyers, F.; Heeger, A. J.; Brédas, J. L. Fine tuning of the band gap in conjugated polymers via control of block copolymer sequences. *J. Chem. Phys.* **1992**, *97* (4), 2750-2758
(129) Suzuki, Y. Y.; Beljonne, D.; Brédas, J. L. Two-band tight-binding model for push–pull polyenes. *J. Chem. Phys.* **1996**, *104* (18), 7270-7283
(130) Cornil, J.; Calbert, J. P.; Brédas, J. L. Electronic structure of the pentacene single crystal: Relation to transport properties *J. Am. Chem. Soc.* **2001**, *123* (6), 1250-1251
(131) Seifert, G.; Eschrig, H. LCAO-Xα Calculations of Transition Metal Clusters. *Phys. Status Solidi B* **1985**, *127* (2), 573-585
(132) Seifert, G.; Joswig, J. O. Density-functional tight binding—an approximate density-functional theory method. *Wiley Interdiscip. Rev. Comput. Mol. Sci.* **2012**, *2* (3), 456-465
(133) Elstner, M.; Seifert, G. Density functional tight binding. *Philos. Trans. A Math. Phys. Eng. Sci.* **2014**, *372* (2011), 20120483

(134) Gaus, M.; Cui, Q.; Elstner, M. DFTB3: Extension of the Self-Consistent-Charge Density-Functional Tight-Binding Method (SCC-DFTB). *J. Chem. Theory. Comput.* **2011**, *7* (4), 931-948
(135) Elstner, M.; Porezag, D.; Jungnickel, G.; Elsner, J.; Haugk, M.; Frauenheim, T.; Suhai, S.; Seifert, G. Self-consistent-charge density-functional tight-binding method for simulations of complex materials properties. *Phys. Rev. B.* **1998**, *58* (11), 7260-7268
(136) Heck, A.; Kranz, J. J.; Kubař, T.; Elstner, M. Multi-Scale Approach to Non-Adiabatic Charge Transport in High-Mobility Organic Semiconductors. *J. Chem. Theory. Comput.* **2015**, *11* (11), 5068-5082
(137) Heck, A.; Kranz, J. J.; Elstner, M. Simulation of Temperature-Dependent Charge Transport in Organic Semiconductors with Various Degrees of Disorder. *J. Chem. Theory. Comput.* **2016**, *12* (7), 3087-3096
(138) Xie, X.; Santana-Bonilla, A.; Troisi, A. Nonlocal Electron–Phonon Coupling in Prototypical Molecular Semiconductors from First Principles. *J. Chem. Theory. Comput.* **2018**, *14* (7), 3752-3762
(139) Gallmetzer, J. M.; Kröll, S.; Werner, D.; Wielend, D.; Irimia-Vladu, M.; Portenkirchner, E.; Sariciftci, N. S.; Hofer, T. S. Anthraquinone and its derivatives as sustainable materials for electrochemical applications – a joint experimental and theoretical investigation of the redox potential in solution. *Phys. Chem. Chem. Phys.* **2022**, *24* (26), 16207-16219
(140) Gaus, M.; Goez, A.; Elstner, M. Parametrization and Benchmark of DFTB3 for Organic Molecules. *J. Chem. Theory. Comput.* **2013**, *9* (1), 338-354
(141) Hohenberg, P.; Kohn, W. Inhomogeneous Electron Gas. *Phys. Rev.* **1964**, *136* (3B), B864-B871
(142) Parr, R. G. Density Functional Theory. *Annu. Rev. Phys. Chem.* **1983**, *34* (1), 631-656
(143) Parr, R. G.; Yang, W. Density-Functional Theory of the Electronic Structure of Molecules. *Annu. Rev. Phys. Chem.* **1995**, *46* (1), 701-728
(144) Baerends, E. J.; Gritsenko, O. V. A Quantum Chemical View of Density Functional Theory. *J. Phys. Chem. A.* **1997**, *101* (30), 5383-5403
(145) Geerlings, P.; De Proft, F.; Langenaeker, W. Conceptual Density Functional Theory. *Chem. Rev.* **2003**, *103* (5), 1793-1874
(146) Verma, P.; Truhlar, D. G. Status and Challenges of Density Functional Theory. *Trends Chem.* **2020**, *2* (4), 302-318
(147) Kohn, W.; Sham, L. J. Self-consistent equations including exchange and correlation effects. *Phys. Rev.* **1965**, *140* (4A), A1133-A1138
(148) Perdew, J. P.; Zunger, A. Self-interaction correction to density-functional approximations for many-electron systems. *Phys. Rev. B.* **1981**, *23* (10), 5048-5079
(149) Albertazzi, E.; Zerbetto, F. Local density functional theory calculation of the in-plane force field and vibrational frequencies of conjugated molecules: benzene and octatetraene. *Chem. Phys.* **1992**, *164* (1), 91-97
(150) Bylaska, E. J.; Kawai, R.; Weare, J. H. From small to large behavior: The transition from the aromatic to the Peierls regime in carbon rings. *J. Chem. Phys.* **2000**, *113* (15), 6096-6106
(151) Langreth, D. C.; Perdew, J. P. Theory of nonuniform electronic systems. I. Analysis of the gradient approximation and a generalization that works. *Phys. Rev. B.* **1980**, *21* (12), 5469-5493
(152) Langreth, D. C.; Mehl, M. J. Beyond the local-density approximation in calculations of ground-state electronic properties. *Phys. Rev. B.* **1983**, *28* (4), 1809-1834
(153) Perdew, J. P.; Chevary, J. A.; Vosko, S. H.; Jackson, K. A.; Pederson, M. R. S., D. J.; Fiolhais, C. Atoms, molecules, solids, and surfaces: Applications of the generalized gradient approximation for exchange and correlation. *Phys. Rev. B.* **1992**, *46* (11), 6671-6687
(154) Perdew, J. P.; Burke, K.; Wang, Y. Generalized gradient approximation for the exchange-correlation hole of a many-electron system. *Phys. Rev. B.* **1996**, *54* (23), 16533-16539
(155) Perdew, J. P.; Burke, K.; Ernzerhof, M. Generalized Gradient Approximation Made Simple. *Phys. Rev. Lett.* **1996**, *77* (18), 3865-3868

(156) Becke, A. D. A new mixing of Hartree–Fock and local density-functional theories. *J. Chem. Phys.* **1993**, *98* (2), 1372-1377
(157) Becke, A. D. Density-functional thermochemistry. III. The role of exact exchange. *J. Chem. Phys.* **1993**, *98* (7), 5648-5652
(158) Lee, C.; Yang, W.; Parr, R. G. Development of the Colle-Salvetti correlation-energy formula into a functional of the electron density. *Phys. Rev. B.* **1988**, *37* (2), 785-789
(159) Pederson, M. R.; Quong, A. A. Polarizabilities, charge states, and vibrational modes of isolated fullerene molecules. *Phys. Rev. B.* **1992**, *46* (20), 13584-13591
(160) Pederson, M. R.; Jackson, K. A.; Pickett, W. E. Local-density-approximation-based simulations of hydrocarbon interactions with applications to diamond chemical vapor deposition. *Phys. Rev. B.* **1991**, *44* (8), 3891-3899
(161) Harris, J. Adiabatic-connection approach to Kohn-Sham theory. *Phys. Rev. A.* **1984**, *29* (4), 1648-1659
(162) Perdew, J. P.; Ernzerhof, M.; Burke, K. Rationale for mixing exact exchange with density functional approximations. *J. Chem. Phys.* **1996**, *105* (22), 9982-9985
(163) Adamo, C.; Barone, V. Toward reliable density functional methods without adjustable parameters: The PBE0 model. *J. Chem. Phys.* **1999**, *110* (13), 6158-6170
(164) Perdew, J. P.; Burke, K.; Wang, Y. Generalized gradient approximation for the exchange-correlation hole of a many-electron system. *Phys. Rev. B Condens. Matter* **1996**, *54* (23), 16533-16539
(165) Heyd, J.; Scuseria, G. E.; Ernzerhof, M. Hybrid functionals based on a screened Coulomb potential. *J. Chem. Phys.* **2003**, *118* (18), 8207-8215
(166) Bauschlicher, C. W. A comparison of the accuracy of different functionals. *Chem. Phys. Lett.* **1995**, *246*, 40-44
(167) Curtiss, L. A.; Raghavachari, K.; Redfern, P. C.; Pople, J. A. Assessment of Gaussian-2 and density functional theories for the computation of enthalpies of formation. *J. Chem. Phys.* **1997**, *106* (3), 1063-1079
(168) Griffith, O. L.; Anthony, J. E.; Jones, A. G.; Lichtenberger, D. L. Electronic Properties of Pentacene versus Triisopropylsilylethynyl-Substituted Pentacene: Environment-Dependent Effects of the Silyl Substituent. *J. Am. Chem. Soc.* **2010**, *132* (2), 580-586
(169) Sun, H.; Autschbach, J. Electronic Energy Gaps for π-Conjugated Oligomers and Polymers Calculated with Density Functional Theory. *J. Chem. Theory. Comput.* **2014**, *10* (3), 1035-1047
(170) Turan, H. T.; Kucur, O.; Kahraman, B.; Salman, S.; Aviyente, V. Design of donor–acceptor copolymers for organic photovoltaic materials: a computational study. *Phys. Chem. Chem. Phys.* **2018**, *20* (5), 3581-3591
(171) Peng, B.; Yang, S.; Li, L.; Cheng, F.; Chen, J. A density functional theory and time-dependent density functional theory investigation on the anchor comparison of triarylamine-based dyes. *J. Chem. Phys.* **2010**, *132* (3), 034305
(172) Tabor, D. P.; Gómez-Bombarelli, R.; Tong, L.; Gordon, R. G.; Aziz, M. J.; Aspuru-Guzik, A. Mapping the frontiers of quinone stability in aqueous media: implications for organic aqueous redox flow batteries. *J. Mater. Chem. A Mater* **2019**, *7* (20), 12833-12841
(173) Liu, L.; Miao, L.; Li, L.; Li, F.; Lu, Y.; Shang, Z.; Chen, J. Molecular Electrostatic Potential: A New Tool to Predict the Lithiation Process of Organic Battery Materials. *J. Phys. Chem. Lett.* **2018**, *9* (13), 3573-3579
(174) Hoja, J.; Tkatchenko, A. First-principles stability ranking of molecular crystal polymorphs with the DFT+MBD approach. *Faraday Discuss.* **2018**, *211*, 253-274
(175) Neumann, M. A.; Perrin, M.-A. Energy Ranking of Molecular Crystals Using Density Functional Theory Calculations and an Empirical van der Waals Correction. *J. Phys. Chem. B.* **2005**, *109* (32), 15531-15541
(176) Nabok, D.; Puschnig, P.; Ambrosch-Draxl, C. Cohesive and surface energies of π-conjugated organic molecular crystals: A first-principles study. *Phys. Rev. B.* **2008**, *77* (24), 245316

(177) Gruenewald, M.; Schirra, L. K.; Winget, P.; Kozlik, M.; Ndione, P. F.; Sigdel, A. K.; Berry, J. J.; Forker, R.; Brédas, J.-L.; Fritz, T.; et al. Integer Charge Transfer and Hybridization at an Organic Semiconductor/Conductive Oxide Interface. *J. Phys. Chem. C.* **2015**, *119* (9), 4865-4873
(178) Zhang, Y.; Qiao, J.; Gao, S.; Hu, F.; He, D.; Wu, B.; Yang, Z.; Xu, B.; Li, Y.; Shi, Y.; et al. Probing Carrier Transport and Structure-Property Relationship of Highly Ordered Organic Semiconductors at the Two-Dimensional Limit. *Phys. Rev. Lett.* **2016**, *116* (1), 016602
(179) Kalappattil, V.; Geng, R.; Das, R.; Pham, M.; Luong, H.; Nguyen, T.; Popescu, A.; Woods, L. M.; Kläui, M.; Srikanth, H.; et al. Giant spin Seebeck effect through an interface organic semiconductor. *Mater. Horiz.* **2020**, *7* (5), 1413-1420
(180) Vázquez, H.; Dappe, Y. J.; Ortega, J.; Flores, F. Energy level alignment at metal/organic semiconductor interfaces: "Pillow" effect, induced density of interface states, and charge neutrality level. *J. Chem. Phys.* **2007**, *126* (14), 144703
(181) Rissner, F.; Rangger, G. M.; Hofmann, O. T.; Track, A. M.; Heimel, G.; Zojer, E. Understanding the Electronic Structure of Metal/SAM/Organic−Semiconductor Heterojunctions. *ACS Nano* **2009**, *3* (11), 3513-3520
(182) Tkatchenko, A.; Romaner, L.; Hofmann, O. T.; Zojer, E.; Ambrosch-Draxl, C.; Scheffler, M. Van der Waals Interactions Between Organic Adsorbates and at Organic/Inorganic Interfaces. *MRS Bull.* **2010**, *35* (6), 435-442
(183) Runge, E.; Gross, E. K. U. Density-Functional Theory for Time-Dependent Systems. *Phys. Rev. Lett.* **1984**, *52* (12), 997-1000
(184) Adamo, C.; Scuseria, G. E.; Barone, V. Accurate excitation energies from time-dependent density functional theory: Assessing the PBE0 model. *J. Chem. Phys.* **1999**, *111* (7), 2889-2899
(185) Guillaumont, D.; Nakamura, S. Calculation of the absorption wavelength of dyes using time-dependent density-functional theory (TD-DFT). *Dyes Pigm.* **2000**, *46* (2), 85-92
(186) Ahmed, S.; Kalita, D. J. Charge transport in isoindigo-dithiophenepyrrole based D-A type oligomers: A DFT/TD-DFT study for the fabrication of fullerene-free organic solar cells. *J. Chem. Phys.* **2018**, *149* (23), 234906
(187) Issa, Y. M.; Abdel-Latif, S. A.; El-Ansary, A. L.; Hassib, H. B. The synthesis, spectroscopic characterization, DFT/TD-DFT/PCM calculations of the molecular structure and NBO of the novel charge-transfer complexes of pyrazine Schiff base derivatives with aromatic nitro compounds. *New J. Chem.* **2021**, *45* (3), 1482-1499
(188) Kümmel, S. Charge-Transfer Excitations: A Challenge for Time-Dependent Density Functional Theory That Has Been Met. *Adv. Energy Mater.* **2017**, *7* (16), 1700440
(189) Zhang, W.; Lan, Z.; Sun, Z.; Gaffney, K. J. Resolving Photo-Induced Twisted Intramolecular Charge Transfer with Vibrational Anisotropy and TDDFT. *J. Phys. Chem. B.* **2012**, *116* (37), 11527-11536
(190) García, G.; Adamo, C.; Ciofini, I. Evaluating push–pull dye efficiency using TD-DFT and charge transfer indices. *Phys. Chem. Chem. Phys.* **2013**, *15* (46), 20210
(191) Li, H.; Nieman, R.; Aquino, A. J. A.; Lischka, H.; Tretiak, S. Comparison of LC-TDDFT and ADC(2) Methods in Computations of Bright and Charge Transfer States in Stacked Oligothiophenes. *J. Chem. Theory. Comput.* **2014**, *10* (8), 3280-3289
(192) Marmolejo-Valencia, A. F.; Mata-Pinzón, Z.; Amador-Bedolla, C. Charge-transfer electronic states in organic solar cells: a TDDFT study. *Phys. Chem. Chem. Phys.* **2021**, *23* (31), 16806-16815
(193) Magyar, R. J.; Tretiak, S. Dependence of Spurious Charge-Transfer Excited States on Orbital Exchange in TDDFT: Large Molecules and Clusters. *J. Chem. Theory. Comput.* **2007**, *3* (3), 976-987
(194) Blaskovits, J. T.; Fumanal, M.; Vela, S.; Corminboeuf, C. Designing Singlet Fission Candidates from Donor–Acceptor Copolymers. *Chem. Mater.* **2020**, *32* (15), 6515-6524
(195) Fallon, K. J.; Budden, P.; Salvadori, E.; Ganose, A. M.; Savory, C. N.; Eyre, L.; Dowland, S.; Ai, Q.; Goodlett, S.; Risko, C.; et al. Exploiting Excited-State Aromaticity To Design Highly Stable Singlet Fission Materials. *J. Am. Chem. Soc.* **2019**, *141* (35), 13867-13876

(196) Vallett, P. J.; Snyder, J. L.; Damrauer, N. H. Tunable Electronic Coupling and Driving Force in Structurally Well-Defined Tetracene Dimers for Molecular Singlet Fission: A Computational Exploration Using Density Functional Theory. *J. Phys. Chem. A.* **2013**, *117* (42), 10824-10838
(197) Johnson, J. C.; Akdag, A.; Zamadar, M.; Chen, X.; Schwerin, A. F.; Paci, I.; Smith, M. B.; Havlas, Z.; Miller, J. R.; Ratner, M. A.; et al. Toward Designed Singlet Fission: Solution Photophysics of Two Indirectly Coupled Covalent Dimers of 1,3-Diphenylisobenzofuran. *J. Phys. Chem. B.* **2013**, *117* (16), 4680-4695
(198) Alagna, N.; Han, J.; Wollscheid, N.; Perez Lustres, J. L.; Herz, J.; Hahn, S.; Koser, S.; Paulus, F.; Bunz, U. H. F.; Dreuw, A.; et al. Tailoring Ultrafast Singlet Fission by the Chemical Modification of Phenazinothiadiazoles. *J. Am. Chem. Soc.* **2019**, *141* (22), 8834-8845
(199) Paci, I.; Johnson, J. C.; Chen, X.; Rana, G.; Popović, D.; David, D. E.; Nozik, A. J.; Ratner, M. A.; Michl, J. Singlet Fission for Dye-Sensitized Solar Cells: Can a Suitable Sensitizer Be Found? *J. Am. Chem. Soc.* **2006**, *128* (51), 16546-16553
(200) Japahuge, A.; Zeng, T. Theoretical Studies of Singlet Fission: Searching for Materials and Exploring Mechanisms. *ChemPlusChem* **2018**, *83* (4), 146-182
(201) Han, J.; Rehn, D. R.; Buckup, T.; Dreuw, A. Evaluation of Single-Reference DFT-Based Approaches for the Calculation of Spectroscopic Signatures of Excited States Involved in Singlet Fission. *J. Phys. Chem. A.* **2020**, *124* (41), 8446-8460
(202) Trinh, M. T.; Zhong, Y.; Chen, Q.; Schiros, T.; Jockusch, S.; Sfeir, M. Y.; Steigerwald, M.; Nuckolls, C.; Zhu, X. Intra- to Intermolecular Singlet Fission. *J. Phys. Chem. C.* **2015**, *119* (3), 1312-1319
(203) Grotjahn, R.; Maier, T. M.; Michl, J.; Kaupp, M. Development of a TDDFT-Based Protocol with Local Hybrid Functionals for the Screening of Potential Singlet Fission Chromophores. *J. Chem. Theory. Comput.* **2017**, *13* (10), 4984-4996
(204) Arsenyan, P.; Vigante, B.; Leitonas, K.; Volyniuk, D.; Andruleviciene, V.; Skhirtladze, L.; Belyakov, S.; Grazulevicius, J. V. Dual versus normal TADF of pyridines ornamented with multiple donor moieties and their performance in OLEDs. *J. Mater. Chem. C Mater* **2021**, *9* (11), 3928-3938
(205) Woo, S.-J.; Kim, Y.-H.; Kim, J.-J. Dihedral Angle Distribution of Thermally Activated Delayed Fluorescence Molecules in Solids Induces Dual Phosphorescence from Charge-Transfer and Local Triplet States. *Chem. Mater.* **2021**, *33* (14), 5618-5630
(206) Woo, S.-J.; Ha, Y.-H.; Kim, Y.-H.; Kim, J.-J. Effect of ortho-biphenyl substitution on the excited state dynamics of a multi-carbazole TADF molecule. *J. Mater. Chem. C Mater* **2020**, *8* (35), 12075-12084
(207) Hait, D.; Zhu, T.; Mcmahon, D. P.; Van Voorhis, T. Prediction of Excited-State Energies and Singlet–Triplet Gaps of Charge-Transfer States Using a Restricted Open-Shell Kohn–Sham Approach. *J. Chem. Theory. Comput.* **2016**, *12* (7), 3353-3359
(208) Woo, S.-J.; Kim, J.-J. TD-DFT and Experimental Methods for Unraveling the Energy Distribution of Charge-Transfer Triplet/Singlet States of a TADF Molecule in a Frozen Matrix. *J. Phys. Chem. A.* **2021**, *125* (5), 1234-1242
(209) Wex, B.; Kaafarani, B. R. Perspective on carbazole-based organic compounds as emitters and hosts in TADF applications. *J. Mater. Chem. C Mater* **2017**, *5* (34), 8622-8653
(210) Stratmann, R. E.; Scuseria, G. E.; Frisch, M. J. An efficient implementation of time-dependent density-functional theory for the calculation of excitation energies of large molecules. *J. Chem. Phys.* **1998**, *109* (19), 8218-8224
(211) Furche, F.; Ahlrichs, R. Adiabatic time-dependent density functional methods for excited state properties. *J. Chem. Phys.* **2002**, *117* (16), 7433-7447
(212) Cordova, F.; Doriol, L. J.; Ipatov, A.; Casida, M. E.; Filippi, C.; Vela, A. Troubleshooting time-dependent density-functional theory for photochemical applications: Oxirane. *J. Chem. Phys.* **2007**, *127* (16), 164111

(213) Casida, M. E. Time-dependent density functional response theory for molecules. In *Recent Advances In Density Functional Methods: (Part I)*, World Scientific, 1995; pp 155-192.
(214) Peach, M. J. G.; Tozer, D. J. Overcoming Low Orbital Overlap and Triplet Instability Problems in TDDFT. *J. Phys. Chem. A.* **2012**, *116* (39), 9783-9789
(215) Wang, Y.-L.; Wu, G.-S. Improving the TDDFT calculation of low-lying excited states for polycyclic aromatic hydrocarbons using the Tamm–Dancoff approximation. *Int. J. Quantum Chem* **2008**, *108* (3), 430-439
(216) Hirata, S.; Head-Gordon, M. Time-dependent density functional theory within the Tamm–Dancoff approximation. *Chem. Phys. Lett.* **1999**, *314* (3), 291-299
(217) Chantzis, A.; Laurent, A. D.; Adamo, C.; Jacquemin, D. Is the Tamm-Dancoff Approximation Reliable for the Calculation of Absorption and Fluorescence Band Shapes? *J. Chem. Theory. Comput.* **2013**, *9* (10), 4517-4525
(218) Rangel, T.; Hamed, S. M.; Bruneval, F.; Neaton, J. B. An assessment of low-lying excitation energies and triplet instabilities of organic molecules with an ab initio Bethe-Salpeter equation approach and the Tamm-Dancoff approximation. *J. Chem. Phys.* **2017**, *146* (19), 194108
(219) Zheng, Z.; Egger, D. A.; Brédas, J.-L.; Kronik, L.; Coropceanu, V. Effect of Solid-State Polarization on Charge-Transfer Excitations and Transport Levels at Organic Interfaces from a Screened Range-Separated Hybrid Functional. *J. Phys. Chem. Lett.* **2017**, *8* (14), 3277-3283
(220) Chen, X. K.; Wang, T.; Brédas, J. L. Suppressing Energy Loss due to Triplet Exciton Formation in Organic Solar Cells: The Role of Chemical Structures and Molecular Packing. *Adv. Energy Mater.* **2017**, *7* (15), 1602713
(221) Zheng, Z.; Brédas, J.-L.; Coropceanu, V. Description of the Charge Transfer States at the Pentacene/C60 Interface: Combining Range-Separated Hybrid Functionals with the Polarizable Continuum Model. *J. Phys. Chem. Lett.* **2016**, *7* (13), 2616-2621
(222) Silva-Junior, M. R.; Schreiber, M.; Sauer, S. P. A.; Thiel, W. Benchmarks of electronically excited states: Basis set effects on CASPT2 results. *J. Chem. Phys.* **2010**, *133* (17), 174318
(223) Peach, M. J. G.; Williamson, M. J.; Tozer, D. J. Influence of Triplet Instabilities in TDDFT. *J. Chem. Theory. Comput.* **2011**, *7* (11), 3578-3585
(224) Cai, Z.-L.; Sendt, K.; Reimers, J. R. Failure of density-functional theory and time-dependent density-functional theory for large extended π systems. *J. Chem. Phys.* **2002**, *117* (12), 5543-5549
(225) Savin, A. Beyond the Kohn–Sham Determinant. In *Recent Advances in Density Functional Methods*, Recent Advances in Computational Chemistry, 1995; pp 129-153.
(226) Toulouse, J.; Colonna, F.; Savin, A. Short-range exchange and correlation energy density functionals: Beyond the local-density approximation. *J. Chem. Phys.* **2005**, *122* (1), 014110
(227) Savin, A.; Flad, H.-J. R. Density functionals for the Yukawa electron-electron interaction. *Int. J. Quantum Chem* **1995**, *56* (4), 327-332
(228) Iikura, H.; Tsuneda, T.; Yanai, T.; Hirao, K. A long-range correction scheme for generalized-gradient-approximation exchange functionals. *J. Chem. Phys.* **2001**, *115* (8), 3540-3544
(229) Henderson, T. M.; Izmaylov, A. F.; Scuseria, G. E.; Savin, A. The importance of middle-range Hartree-Fock-type exchange for hybrid density functionals. *J. Chem. Phys.* **2007**, *127* (22), 221103
(230) Henderson, T. M.; Janesko, B. G.; Scuseria, G. E.; Savin, A. Locally range-separated hybrids as linear combinations of range-separated local hybrids. *Int. J. Quantum Chem* **2009**, *109* (9), 2023-2032
(231) Henderson, T. M.; Izmaylov, A. F.; Scalmani, G.; Scuseria, G. E. Can short-range hybrids describe long-range-dependent properties? *J. Chem. Phys.* **2009**, *131* (4), 044108-044108
(232) Janesko, B. G.; Krukau, A. V.; Scuseria, G. E. Self-consistent generalized Kohn-Sham local hybrid functionals of screened exchange: Combining local and range-separated hybridization. *J. Chem. Phys.* **2008**, *129* (12), 124110
(233) Kronik, L.; Stein, T.; Refaely-Abramson, S.; Baer, R. Excitation Gaps of Finite-Sized Systems from Optimally Tuned Range-Separated Hybrid Functionals. *J. Chem. Theory. Comput.* **2012**, *8* (5), 1515-1531

(234) Sachse, T.; Martínez, T. J.; Presselt, M. On combining the conductor-like screening model and optimally tuned range-separated hybrid density functionals. *J. Chem. Phys.* **2019**, *150* (17), 174117
(235) Garrett, K.; Sosa Vazquez, X.; Egri, S. B.; Wilmer, J.; Johnson, L. E.; Robinson, B. H.; Isborn, C. M. Optimum Exchange for Calculation of Excitation Energies and Hyperpolarizabilities of Organic Electro-optic Chromophores. *J. Chem. Theory. Comput.* **2014**, *10* (9), 3821-3831
(236) Refaely-Abramson, S.; Baer, R.; Kronik, L. Fundamental and excitation gaps in molecules of relevance for organic photovoltaics from an optimally tuned range-separated hybrid functional. *Phys. Rev. B.* **2011**, *84* (7), 075144
(237) Perdew, J. P.; Parr, R. G.; Levy, M.; Balduz, J. L. Density-Functional Theory for Fractional Particle Number: Derivative Discontinuities of the Energy. *Phys. Rev. Lett.* **1982**, *49* (23), 1691-1694
(238) Almbladh, C.-O.; Von Barth, U. Exact results for the charge and spin densities, exchange-correlation potentials, and density-functional eigenvalues. *Phys. Rev. B.* **1985**, *31* (6), 3231-3244
(239) Perdew, J. P.; Levy, M. Comment on "Significance of the highest occupied Kohn-Sham eigenvalue". *Phys. Rev. B.* **1997**, *56* (24), 16021-16028
(240) Körzdörfer, T.; Sears, J. S.; Sutton, C.; Brédas, J.-L. Long-range corrected hybrid functionals for π-conjugated systems: Dependence of the range-separation parameter on conjugation length. *J. Chem. Phys.* **2011**, *135* (20), 204107
(241) Sekino, H.; Maeda, Y.; Kamiya, M.; Hirao, K. Polarizability and second hyperpolarizability evaluation of long molecules by the density functional theory with long-range correction. *J. Chem. Phys.* **2007**, *126* (1), 014107
(242) Refaely-Abramson, S.; Baer, R.; Kronik, L. Fundamental and excitation gaps in molecules of relevance for organic photovoltaics from an optimally tuned range-separated hybrid functional. *Physical Review B* **2011**, *84* (7),
(243) Deleuze, M. S.; Claes, L.; Kryachko, E. S.; François, J.-P. Benchmark theoretical study of the ionization threshold of benzene and oligoacenes. *J. Chem. Phys.* **2003**, *119* (6), 3106-3119
(244) Hajgató, B.; Deleuze, M. S.; Tozer, D. J.; De Proft, F. A benchmark theoretical study of the electron affinities of benzene and linear acenes. *J. Chem. Phys.* **2008**, *129* (8), 084308
(245) Stein, T.; Kronik, L.; Baer, R. Prediction of charge-transfer excitations in coumarin-based dyes using a range-separated functional tuned from first principles. *J. Chem. Phys.* **2009**, *131* (24), 244119
(246) Karolewski, A.; Stein, T.; Baer, R.; Kümmel, S. Communication: Tailoring the optical gap in light-harvesting molecules. *J. Chem. Phys.* **2011**, *134* (15), 151101
(247) Stein, T.; Eisenberg, H.; Kronik, L.; Baer, R. Fundamental Gaps in Finite Systems from Eigenvalues of a Generalized Kohn-Sham Method. *Phys. Rev. Lett.* **2010**, *105* (26), 266802
(248) Pandey, L.; Doiron, C.; Sears, J. S.; Brédas, J.-L. Lowest excited states and optical absorption spectra of donor–acceptor copolymers for organic photovoltaics: a new picture emerging from tuned long-range corrected density functionals. *Phys. Chem. Chem. Phys.* **2012**, *14* (41), 14243
(249) Cho, E.; Coropceanu, V.; Brédas, J.-L. Electronic Structure of Multicomponent Organic Molecular Materials: Evaluation of Range-Separated Hybrid Functionals. *J. Chem. Theory. Comput.* **2020**, *16* (6), 3712-3719
(250) Grimme, S.; Parac, M. Substantial Errors from Time-Dependent Density Functional Theory for the Calculation of Excited States of Large π Systems. *ChemPhysChem* **2003**, *4* (3), 292-295
(251) Kuritz, N.; Stein, T.; Baer, R.; Kronik, L. Charge-Transfer-Like π→π* Excitations in Time-Dependent Density Functional Theory: A Conundrum and Its Solution. *J. Chem. Theory. Comput.* **2011**, *7* (8), 2408-2415
(252) Körzdörfer, T.; Brédas, J.-L. Organic Electronic Materials: Recent Advances in the DFT Description of the Ground and Excited States Using Tuned Range-Separated Hybrid Functionals. *Acc. Chem. Res.* **2014**, *47* (11), 3284-3291
(253) Onsager, L. Electric Moments of Molecules in Liquids. *J. Am. Chem. Soc.* **1936**, *58* (8), 1486-1493
(254) Kirkwood, J. G. Theory of Solutions of Molecules Containing Widely Separated Charges with Special Application to Zwitterions. *J. Chem. Phys.* **1934**, *2* (7), 351-361

(255) Bell, R. P. The electrostatic energy of dipole molecules in different media. *Trans. Faraday Soc.* **1931**, *27*, 797-802
(256) Born, M. Volumen und Hydratationswärme der Ionen. *Z. Phys.* **1920**, *1* (1), 45-48
(257) Caricato, M.; Mennucci, B.; Tomasi, J. Solvent Effects on the Electronic Spectra: An Extension of the Polarizable Continuum Model to the ZINDO Method. *J. Phys. Chem. A.* **2004**, *108* (29), 6248-6256
(258) Miertuš, S.; Scrocco, E.; Tomasi, J. Electrostatic interaction of a solute with a continuum. A direct utilizaion of AB initio molecular potentials for the prevision of solvent effects. *Chem. Phys.* **1981**, *55* (1), 117-129
(259) Maiti, B.; Schubert, A.; Sarkar, S.; Bhandari, S.; Wang, K.; Li, Z.; Geva, E.; Twieg, R. J.; Dunietz, B. D. Enhancing charge mobilities in organic semiconductors by selective fluorination: a design approach based on a quantum mechanical perspective. *Chem. Sci.* **2017**, *8* (10), 6947-6953
(260) Liu, Q.; Sun, H.; Blaikie, C.; Caporale, C.; Manzhos, S.; Feron, K.; Macleod, J. M.; Massi, M.; Bottle, S. E.; Bell, J.; et al. Naphthalene flanked diketopyrrolopyrrole based organic semiconductors for high performance organic field effect transistors. *New J. Chem.* **2018**, *42* (15), 12374-12385
(261) Sun, H.; Putta, A.; Billion, M. Arene Trifluoromethylation: An Effective Strategy to Obtain Air-Stable n-Type Organic Semiconductors with Tunable Optoelectronic and Electron Transfer Properties. *J. Phys. Chem. A.* **2012**, *116* (30), 8015-8022
(262) Sun, H.; Ryno, S.; Zhong, C.; Ravva, M. K.; Sun, Z.; Körzdörfer, T.; Brédas, J.-L. Ionization Energies, Electron Affinities, and Polarization Energies of Organic Molecular Crystals: Quantitative Estimations from a Polarizable Continuum Model (PCM)-Tuned Range-Separated Density Functional Approach. *J. Chem. Theory. Comput.* **2016**, *12* (6), 2906-2916
(263) Scalmani, G.; Frisch, M. J.; Mennucci, B.; Tomasi, J.; Cammi, R.; Barone, V. Geometries and properties of excited states in the gas phase and in solution: Theory and application of a time-dependent density functional theory polarizable continuum model. *J. Chem. Phys.* **2006**, *124* (9), 094107
(264) Cossi, M.; Barone, V. Time-dependent density functional theory for molecules in liquid solutions. *J. Chem. Phys.* **2001**, *115* (10), 4708-4717
(265) Phan Huu, D. K. A.; Dhali, R.; Pieroni, C.; Di Maiolo, F.; Sissa, C.; Terenziani, F.; Painelli, A. Antiadiabatic View of Fast Environmental Effects on Optical Spectra. *Phys. Rev. Lett.* **2020**, *124* (10), 107401
(266) Cammi, R.; Mennucci, B. Linear response theory for the polarizable continuum model. *J. Chem. Phys.* **1999**, *110* (20), 9877-9886
(267) Improta, R.; Barone, V.; Scalmani, G.; Frisch, M. J. A state-specific polarizable continuum model time dependent density functional theory method for excited state calculations in solution. *J. Chem. Phys.* **2006**, *125* (5), 054103
(268) Improta, R.; Scalmani, G.; Frisch, M. J.; Barone, V. Toward effective and reliable fluorescence energies in solution by a new state specific polarizable continuum model time dependent density functional theory approach. *J. Chem. Phys.* **2007**, *127* (7), 074504
(269) Marenich, A. V.; Cramer, C. J.; Truhlar, D. G.; Guido, C. A.; Mennucci, B.; Scalmani, G.; Frisch, M. J. Practical computation of electronic excitation in solution: vertical excitation model. *Chem. Sci.* **2011**, *2* (11), 2143
(270) Krumland, J.; Valencia, A. M.; Cocchi, C. Exploring organic semiconductors in solution: the effects of solvation, alkylization, and doping. *Phys. Chem. Chem. Phys.* **2021**, *23* (8), 4841-4855
(271) Klamt, A.; Schüürmann, G. COSMO: a new approach to dielectric screening in solvents with explicit expressions for the screening energy and its gradient. *J. Chem. Soc., Perkin Trans. 2* **1993**, (5), 799-805
(272) Bjorgaard, J. A.; Kuzmenko, V.; Velizhanin, K. A.; Tretiak, S. Solvent effects in time-dependent self-consistent field methods. I. Optical response calculations. *J. Chem. Phys.* **2015**, *142* (4), 044103

(273) Bhandari, S.; Cheung, M. S.; Geva, E.; Kronik, L.; Dunietz, B. D. Fundamental Gaps of Condensed-Phase Organic Semiconductors from Single-Molecule Calculations using Polarization-Consistent Optimally Tuned Screened Range-Separated Hybrid Functionals. *J. Chem. Theory. Comput.* **2018**, *14* (12), 6287-6294
(274) Joo, B.; Han, H.; Kim, E.-G. Solvation-Mediated Tuning of the Range-Separated Hybrid Functional: Self-Sufficiency through Screened Exchange. *J. Chem. Theory. Comput.* **2018**, *14* (6), 2823-2828
(275) Sun, J.; Lee, C.-W.; Kononov, A.; Schleife, A.; Ullrich, C. A. Real-Time Exciton Dynamics with Time-Dependent Density-Functional Theory. *Phys. Rev. Lett.* **2021**, *127* (7), 107401
(276) Li, X.; Govind, N.; Isborn, C.; Deprince, A. E.; Lopata, K. Real-Time Time-Dependent Electronic Structure Theory. *Chem. Rev.* **2020**, *120* (18), 9951-9993
(277) Yabana, K.; Bertsch, G. F. Time-dependent local-density approximation in real time: Application to conjugated molecules. *Int. J. Quantum Chem* **1999**, *75* (1), 55-66
(278) Lopata, K.; Govind, N. Modeling Fast Electron Dynamics with Real-Time Time-Dependent Density Functional Theory: Application to Small Molecules and Chromophores. *J. Chem. Theory. Comput.* **2011**, *7* (5), 1344-1355
(279) Cheng, C.-L.; Evans, J. S.; Van Voorhis, T. Simulating molecular conductance using real-time density functional theory. *Phys. Rev. B.* **2006**, *74* (15), 155112
(280) Lee, C. K.; Hua, C. C.; Chen, S. A. Parametrization of the Gay–Berne potential for conjugated oligomer with a high aspect ratio. *J. Chem. Phys.* **2010**, *133* (6), 064902
(281) Takimoto, Y.; Vila, F. D.; Rehr, J. J. Real-time time-dependent density functional theory approach for frequency-dependent nonlinear optical response in photonic molecules. *J. Chem. Phys.* **2007**, *127* (15), 154114
(282) Seiler, H.; Krynski, M.; Zahn, D.; Hammer, S.; Windsor, Y. W.; Vasileiadis, T.; Pflaum, J.; Ernstorfer, R.; Rossi, M.; Schwoerer, H. Nuclear dynamics of singlet exciton fission in pentacene single crystals. *Sci. Adv.* **2021**, *7* (26), 13946-13953
(283) Amos, A. T.; Hall, G. G.; Jones, H. Single determinant wave functions. *Proc. R. Soc. Lond. A Math. Phys. Sci.* **1961**, *263* (1315), 483-493
(284) Martin, R. L. Natural transition orbitals. *J. Chem. Phys.* **2003**, *118* (11), 4775-4777
(285) Badaeva, E. A.; Timofeeva, T. V.; Masunov, A.; Tretiak, S. Role of Donor−Acceptor Strengths and Separation on the Two-Photon Absorption Response of Cytotoxic Dyes: A TD-DFT Study. *J. Phys. Chem. A.* **2005**, *109* (32), 7276-7284
(286) Nayyar, I. H.; Batista, E. R.; Tretiak, S.; Saxena, A.; Smith, D. L.; Martin, R. L. Localization of Electronic Excitations in Conjugated Polymers Studied by DFT. *J. Phys. Chem. Lett.* **2011**, *2* (6), 566-571
(287) Zou, X.; Wen, G.; Hu, R.; Dong, G.; Zhang, C.; Zhang, W.; Huang, H.; Dang, W. An Insight into the Excitation States of Small Molecular Semiconductor Y6. *Molecules* **2020**, *25* (18), 4118
(288) Zimmerman, P. M.; Bell, F.; Casanova, D.; Head-Gordon, M. Mechanism for Singlet Fission in Pentacene and Tetracene: From Single Exciton to Two Triplets. *J. Am. Chem. Soc.* **2011**, *133* (49), 19944-19952
(289) Aizawa, N.; Pu, Y.-J.; Harabuchi, Y.; Nihonyanagi, A.; Ibuka, R.; Inuzuka, H.; Dhara, B.; Koyama, Y.; Nakayama, K.-I.; Maeda, S.; et al. Delayed fluorescence from inverted singlet and triplet excited states. *Nature* **2022**, *609* (7927), 502-506
(290) Moral, M.; Muccioli, L.; Son, W.-J.; Olivier, Y.; Sancho-García, J. C. Theoretical Rationalization of the Singlet–Triplet Gap in OLEDs Materials: Impact of Charge-Transfer Character. *J. Chem. Theory. Comput.* **2015**, *11* (1), 168-177
(291) Kang, H.; Ihn, S.-G.; Kim, I.; Chung, Y. S.; Jeon, S. O.; Sim, M.; Kim, J.; Lee, H.; Son, Y.; Son, W.-J.; et al. Designing Stable Deep-Blue Thermally Activated Delayed Fluorescence Emitters through Controlling the Intrinsic Stability of Triplet Excitons. *Adv. Opt. Mater.* **2022**, *10* (12), 2102309

(292) Zobel, J. P.; Nogueira, J. J.; González, L. Mechanism of Ultrafast Intersystem Crossing in 2-Nitronaphthalene. *Chemistry* **2018**, *24* (20), 5379-5387
(293) Wing, D.; Haber, J. B.; Noff, R.; Barker, B.; Egger, D. A.; Ramasubramaniam, A.; Louie, S. G.; Neaton, J. B.; Kronik, L. Comparing time-dependent density functional theory with many-body perturbation theory for semiconductors: Screened range-separated hybrids and the GW plus Bethe-Salpeter approach. *Phys. Rev. Mater.* **2019**, *3* (6), 064603
(294) Arhangelskis, M.; Jochym, D. B.; Bernasconi, L.; Friščić, T.; Morris, A. J.; Jones, W. Time-Dependent Density-Functional Theory for Modeling Solid-State Fluorescence Emission of Organic Multicomponent Crystals. *J. Phys. Chem. A.* **2018**, *122* (37), 7514-7521
(295) Hutter, J. Excited state nuclear forces from the Tamm–Dancoff approximation to time-dependent density functional theory within the plane wave basis set framework. *J. Chem. Phys.* **2003**, *118* (9), 3928-3934
(296) Refaely-Abramson, S.; Jain, M.; Sharifzadeh, S.; Neaton, J. B.; Kronik, L. Solid-state optical absorption from optimally tuned time-dependent range-separated hybrid density functional theory. *Phys. Rev. B.* **2015**, *92* (8), 081204
(297) Spano, F. C. Absorption and emission in oligo-phenylene vinylene nanoaggregates: The role of disorder and structural defects. *J. Chem. Phys.* **2002**, *116* (13), 5877-5891
(298) Spano, F. C. Excitons in conjugated oligomer aggregates, films, and crystals. *Annu. Rev. Phys. Chem.* **2006**, *57* (1), 217-243
(299) Ghosh, R.; Pochas, C. M.; Spano, F. C. Polaron Delocalization in Conjugated Polymer Films. *J. Phys. Chem. C.* **2016**, *120* (21), 11394-11406
(300) Hestand, N. J.; Spano, F. C. Molecular Aggregate Photophysics beyond the Kasha Model: Novel Design Principles for Organic Materials. *Acc. Chem. Res.* **2017**, *50* (2), 341-350
(301) Hoffmann, M.; Soos, Z. G. Optical absorption spectra of the Holstein molecular crystal for weak and intermediate electronic coupling. *Phys. Rev. B.* **2002**, *66* (2), 024305
(302) Holstein, T. Studies of polaron motion: Part I. The molecular-crystal model. *Ann. Phys. (NY)* **1959**, *8* (3), 325-342
(303) Holstein, T. Studies of polaron motion: Part II. The "small" polaron. *Ann. Phys. (NY)* **1959**, *8* (3), 343-389
(304) Hybertsen, M. S.; Louie, S. G. Electron correlation in semiconductors and insulators: Band gaps and quasiparticle energies. *Phys. Rev. B.* **1986**, *34* (8), 5390-5413
(305) Kronik, L.; Neaton, J. B. Excited-State Properties of Molecular Solids from First Principles. *Annu. Rev. Phys. Chem.* **2016**, *67* (1), 587-616
(306) Grossman, J. C.; Rohlfing, M.; Mitas, L.; Louie, S. G.; Cohen, M. L. High Accuracy Many-Body Calculational Approaches for Excitations in Molecules. *Phys. Rev. Lett.* **2001**, *86* (3), 472-475
(307) Sharifzadeh, S. Many-body perturbation theory for understanding optical excitations in organic molecules and solids. *J. Phys.: Condens. Matter* **2018**, *30* (15), 153002
(308) Faber, C.; Boulanger, P.; Attaccalite, C.; Duchemin, I.; Blase, X. Excited states properties of organic molecules: from density functional theory to the GW and Bethe-Salpeter Green's function formalisms. *Philos. Trans. A Math. Phys. Eng. Sci.* **2014**, *372* (2011), 20130271
(309) Salpeter, E. E.; Bethe, H. A. A Relativistic Equation for Bound-State Problems. *Phys. Rev.* **1951**, *84* (6), 1232-1242
(310) Strinati, G. Application of the Green's functions method to the study of the optical properties of semiconductors. *La Rivista del Nuovo Cimento* **1988**, *11* (12), 1-86
(311) Bruneval, F.; Hamed, S. M.; Neaton, J. B. A systematic benchmark of the ab initio Bethe-Salpeter equation approach for low-lying optical excitations of small organic molecules. *J. Chem. Phys.* **2015**, *142* (24), 244101
(312) Tiago, M. L.; Northrup, J. E.; Louie, S. G. Ab initio calculation of the electronic and optical properties of solid pentacene. *Phys. Rev. B.* **2003**, *67* (11), 115212

(313) Hummer, K.; Puschnig, P.; Ambrosch-Draxl, C. Lowest Optical Excitations in Molecular Crystals: Bound Excitons versus Free Electron-Hole Pairs in Anthracene. *Phys. Rev. Lett.* **2004**, *92* (14), 147402
(314) Sharifzadeh, S.; Biller, A.; Kronik, L.; Neaton, J. B. Quasiparticle and optical spectroscopy of the organic semiconductors pentacene and PTCDA from first principles. *Phys. Rev. B.* **2012**, *85* (12),
(315) Sharifzadeh, S.; Darancet, P.; Kronik, L.; Neaton, J. B. Low-Energy Charge-Transfer Excitons in Organic Solids from First-Principles: The Case of Pentacene. *J. Phys. Chem. Lett.* **2013**, *4* (13), 2197-2201
(316) Park, S. P.; Kim, S. S.; Kim, J. H.; Whang, C. N.; Im, S. Optical and luminescence characteristics of thermally evaporated pentacene films on Si. *Appl. Phys. Lett.* **2002**, *80* (16), 2872-2874
(317) Kepler, R. G. Charge Carrier Production and Mobility in Anthracene Crystals. *Phys. Rev.* **1960**, *119* (4), 1226-1229
(318) Leblanc, O. H. Hole and Electron Drift Mobilities in Anthracene. *J. Chem. Phys.* **1960**, *33* (2), 626-626
(319) Katz, J. L.; Rice, S. A.; Choi, S. I.; Jortner, J. On the Excess Electron and Hole Band Structures and Carrier Mobility in Naphthalene, Anthracene, and Several Polyphenyls. *J. Chem. Phys.* **1963**, *39* (7), 1683-1697
(320) Silbey, R.; Jortner, J.; Rice, S. A.; Vala, M. T. Exchange Effects on the Electron and Hole Mobility in Crystalline Anthracene and Naphthalene. *J. Chem. Phys.* **1965**, *42* (2), 733-737
(321) Nakada, I.; Ariga, K.; Ichimiya, A. The Electrical Conductivity of Anthracene. *J. Phys. Soc. Jpn.* **1964**, *19* (9), 1587-1591
(322) Pott, G. T.; Williams, D. F. Low-Temperature Electron Injection and Space-Charge-Limited Transients in Anthracene Crystals. *J. Chem. Phys.* **1969**, *51* (5), 1901-1906
(323) Fourny, J.; Delacôte, G. High-Temperature Dependence of Electron and Hole Mobilities in Anthracene Crystal. *J. Chem. Phys.* **1969**, *50* (2), 1028-1029
(324) Marcus, R. A. Chemical and Electrochemical Electron-Transfer Theory. *Annu. Rev. Phys. Chem.* **1964**, *15* (1), 155-196
(325) Hush, N. S. Adiabatic Rate Processes at Electrodes. I. Energy-Charge Relationships. *J. Chem. Phys.* **1958**, *28* (5), 962-972
(326) Marcus, R. A. On the Theory of Oxidation-Reduction Reactions Involving Electron Transfer. II. Applications to Data on the Rates of Isotopic Exchange Reactions. *J. Chem. Phys.* **1957**, *26* (4), 867-871
(327) Troisi, A.; Orlandi, G. Dynamics of the Intermolecular Transfer Integral in Crystalline Organic Semiconductors. *J. Phys. Chem. A.* **2006**, *110* (11), 4065-4070
(328) Liu, C.; Huang, K.; Park, W.-T.; Li, M.; Yang, T.; Liu, X.; Liang, L.; Minari, T.; Noh, Y.-Y. A unified understanding of charge transport in organic semiconductors: the importance of attenuated delocalization for the carriers. *Mater. Horiz.* **2017**, *4* (4), 608-618
(329) Fratini, S.; Mayou, D.; Ciuchi, S. The Transient Localization Scenario for Charge Transport in Crystalline Organic Materials. *Adv. Funct. Mater.* **2016**, *26* (14), 2292-2315
(330) Giannini, S.; Blumberger, J. Charge Transport in Organic Semiconductors: The Perspective from Nonadiabatic Molecular Dynamics. *Acc. Chem. Res.* **2022**, *55* (6), 819-830
(331) Fratini, S.; Nikolka, M.; Salleo, A.; Schweicher, G.; Sirringhaus, H. Charge transport in high-mobility conjugated polymers and molecular semiconductors. *Nat. Mater.* **2020**, 1-12
(332) Brédas, J. L.; Calbert, J. P.; Filho, D. A. d. S.; Cornil, J. Organic semiconductors: A theoretical characterization of the basic parameters governing charge transport. *PNAS* **2002**, *99* (9), 5804-5809
(333) Coropceanu, V.; Cornil, J.; da Silva Filho, D. A.; Olivier, Y.; Silbey, R.; Brédas, J.-L. Charge Transport in Organic Semiconductors. *Chem. Rev.* **2007**, *107* (4), 926-952
(334) Tessler, N.; Preezant, Y.; Rappaport, N.; Roichman, Y. Charge Transport in Disordered Organic Materials and Its Relevance to Thin-Film Devices: A Tutorial Review. *Adv. Mater.* **2009**, *21* (27), 2741-2761

(335) Wang, C.; Dong, H.; Jiang, L.; Hu, W. Organic semiconductor crystals. *Chem. Soc. Rev.* **2018**, *47* (2), 422-500
(336) Troisi, A. Charge transport in high mobility molecular semiconductors: classical models and new theories. *Chem. Soc. Rev.* **2011**, *40* (5), 2347
(337) Gryn'ova, G.; Lin, K.-H.; Corminboeuf, C. Read between the Molecules: Computational Insights into Organic Semiconductors. *J. Am. Chem. Soc.* **2018**, *140* (48), 16370-16386
(338) Huang, J.; Kertesz, M. Validation of intermolecular transfer integral and bandwidth calculations for organic molecular materials. *J. Chem. Phys.* **2005**, *122* (23), 234707
(339) Huang, J.; Kertesz, M. Intermolecular transfer integrals for organic molecular materials: can basis set convergence be achieved? *Chem. Phys. Lett.* **2004**, *390* (1), 110-115
(340) Sutton, C.; Sears, J. S.; Coropceanu, V.; Brédas, J.-L. Understanding the Density Functional Dependence of DFT-Calculated Electronic Couplings in Organic Semiconductors. *J. Phys. Chem. Lett.* **2013**, *4* (6), 919-924
(341) Valeev, E. F.; Coropceanu, V.; Da Silva Filho, D. A.; Salman, S.; Brédas, J. L. Effect of electronic polarization on charge-transport parameters in molecular organic semiconductors. *J. Am. Chem. Soc.* **2006**, *128* (30), 9882-9886
(342) Brédas, J. L.; Calbert, J. P.; Da Silva Filho, D. A.; Cornil, J. Organic semiconductors: A theoretical characterization of the basic parameters governing charge transport. *PNAS* **2002**, *99* (9), 5804-5809
(343) Coropceanu, V.; Li, H.; Winget, P.; Zhu, L.; Brédas, J.-L. Electronic-Structure Theory of Organic Semiconductors: Charge-Transport Parameters and Metal/Organic Interfaces. *Annu. Rev. Mater. Res.* **2013**, *43* (1), 63-87
(344) Kubas, A.; Gajdos, F.; Heck, A.; Oberhofer, H.; Elstner, M.; Blumberger, J. Electronic couplings for molecular charge transfer: benchmarking CDFT, FODFT and FODFTB against high-level ab initio calculations. II. *Phys. Chem. Chem. Phys.* **2015**, *17* (22), 14342-14354
(345) Kubas, A.; Hoffmann, F.; Heck, A.; Oberhofer, H.; Elstner, M.; Blumberger, J. Electronic couplings for molecular charge transfer: Benchmarking CDFT, FODFT, and FODFTB against high-level ab initio calculations. *J. Chem. Phys.* **2014**, *140* (10), 104105
(346) Thorley, K. J.; Risko, C. Mapping the configuration dependence of electronic coupling in organic semiconductors. *J. Mater. Chem. C Mater* **2016**, *4* (17), 3825-3832
(347) Valeev, E. F.; Coropceanu, V.; Da Silva Filho, D. A.; Salman, S.; Brédas, J.-L. Effect of Electronic Polarization on Charge-Transport Parameters in Molecular Organic Semiconductors. *J. Am. Chem. Soc.* **2006**, *128* (30), 9882-9886
(348) Nelsen, S. F.; Blackstock, S. C.; Kim, Y. Estimation of inner shell Marcus terms for amino nitrogen compounds by molecular orbital calculations. *J. Am. Chem. Soc.* **1987**, *109* (3), 677-682
(349) Malagoli, M.; Coropceanu, V.; Da Silva Filho, D. A.; Brédas, J. L. A multimode analysis of the gas-phase photoelectron spectra in oligoacenes. *J. Chem. Phys.* **2004**, *120* (16), 7490-7496
(350) Uejima, M.; Sato, T.; Tanaka, K.; Kaji, H. Vibronic coupling density analysis for the chain-length dependence of reorganization energies in oligofluorenes: a comparative study with oligothiophenes. *Phys. Chem. Chem. Phys.* **2013**, *15* (33), 14006
(351) Lin, K.-H.; Corminboeuf, C. FB-REDA: fragment-based decomposition analysis of the reorganization energy for organic semiconductors. *Phys. Chem. Chem. Phys.* **2020**, *22* (21), 11881-11890
(352) Huix-Rotllant, M.; Ferré, N. An Effective Procedure for Analyzing Molecular Vibrations in Terms of Local Fragment Modes. *J. Chem. Theory. Comput.* **2016**, *12* (10), 4768-4777
(353) Brückner, C.; Walter, C.; Stolte, M.; Braïda, B.; Meerholz, K.; Würthner, F.; Engels, B. Structure–Property Relationships for Exciton and Charge Reorganization Energies of Dipolar Organic Semiconductors: A Combined Valence Bond Self-Consistent Field and Time-Dependent Hartree-Fock and DFT Study of Merocyanine Dyes. *J. Phys. Chem. C.* **2015**, *119* (31), 17602-17611
(354) Brückner, C.; Engels, B. A theoretical description of charge reorganization energies in molecular organic P-type semiconductors. *J. Comput. Chem.* **2016**, *37* (15), 1335-1344

(355) Kümmel, S.; Kronik, L. Orbital-dependent density functionals: Theory and applications. *Rev. Mod. Phys.* **2008**, *80* (1), 3-60
(356) Koller, G.; Berkebile, S.; Oehzelt, M.; Puschnig, P.; Ambrosch-Draxl, C.; Netzer, F. P.; Ramsey, M. G. Intra- and Intermolecular Band Dispersion in an Organic Crystal. *Science* **2007**, *317* (5836), 351-355
(357) Zeidell, A. M.; Jennings, L.; Frederickson, C. K.; Ai, Q.; Dressler, J. J.; Zakharov, L. N.; Risko, C.; Haley, M. M.; Jurchescu, O. D. Organic Semiconductors Derived from Dinaphtho-Fused s-Indacenes: How Molecular Structure and Film Morphology Influence Thin-Film Transistor Performance. *Chem. Mater.* **2019**, *31* (17), 6962-6970
(358) Sato, H.; Abd. Rahman, S. A.; Yamada, Y.; Ishii, H.; Yoshida, H. Conduction band structure of high-mobility organic semiconductors and partially dressed polaron formation. *Nat. Mater.* **2022**, *21* (8), 910-916
(359) Beran, G. J. O. Modeling Polymorphic Molecular Crystals with Electronic Structure Theory. *Chem. Rev.* **2016**, *116* (9), 5567-5613
(360) Cheng, Y. C.; Silbey, R. J.; Da Silva Filho, D. A.; Calbert, J. P.; Cornil, J.; Brédas, J. L. Three-dimensional band structure and bandlike mobility in oligoacene single crystals: A theoretical investigation. *J. Chem. Phys.* **2003**, *118* (8), 3764-3774
(361) Fonari, A.; Sutton, C.; Brédas, J.-L.; Coropceanu, V. Impact of exact exchange in the description of the electronic structure of organic charge-transfer molecular crystals. *Phys. Rev. B.* **2014**, *90* (16), 165205
(362) Dori, N.; Menon, M.; Kilian, L.; Sokolowski, M.; Kronik, L.; Umbach, E. Valence electronic structure of gas-phase 3,4,9,10-perylene tetracarboxylic acid dianhydride: Experiment and theory. *Phys. Rev. B.* **2006**, *73* (19), 195208
(363) Sharifzadeh, S.; Biller, A.; Kronik, L.; Neaton, J. B. Quasiparticle and optical spectroscopy of the organic semiconductors pentacene and PTCDA from first principles. *Phys. Rev. B.* **2012**, *85* (12), 125307
(364) Cruz-Cabeza, A. J.; Reutzel-Edens, S. M.; Bernstein, J. Facts and fictions about polymorphism. *Chem. Soc. Rev.* **2015**, *44* (23), 8619-8635
(365) Cruz-Cabeza, A. J. Crystal structure prediction: are we there yet? *Acta. Crystallogr. B. Struct. Sci. Cryst. Eng. Mater.* **2016**, *72* (4), 437-438
(366) Bowskill, D. H.; Sugden, I. J.; Konstantinopoulos, S.; Adjiman, C. S.; Pantelides, C. C. Crystal Structure Prediction Methods for Organic Molecules: State of the Art. *Annu. Rev. Chem. Biomol. Eng.* **2021**, *12* (1), 593-623
(367) Woodley, S. M.; Catlow, R. Crystal structure prediction from first principles. *Nat. Mater.* **2008**, *7* (12), 937-946
(368) Price, S. L. Predicting crystal structures of organic compounds. *Chem. Soc. Rev.* **2014**, *43* (7), 2098-2111
(369) Oganov, A. R.; Lyakhov, A. O.; Valle, M. How Evolutionary Crystal Structure Prediction Works—and Why. *Acc. Chem. Res.* **2011**, *44* (3), 227-237
(370) Sánchez-Carrera, R. S.; Atahan, S.; Schrier, J.; Aspuru-Guzik, A. Theoretical Characterization of the Air-Stable, High-Mobility Dinaphtho[2,3-b:2′3′-f]thieno[3,2-b]-thiophene Organic Semiconductor. *J. Phys. Chem. C.* **2010**, *114* (5), 2334-2340
(371) Sokolov, A. N.; Atahan-Evrenk, S.; Mondal, R.; Akkerman, H. B.; Sánchez-Carrera, R. S.; Granados-Focil, S.; Schrier, J.; Mannsfeld, S. C. B.; Zoombelt, A. P.; Bao, Z.; et al. From computational discovery to experimental characterization of a high hole mobility organic crystal. *Nat. Commun.* **2011**, *2* (1), 437
(372) Case, D. H.; Campbell, J. E.; Bygrave, P. J.; Day, G. M. Convergence Properties of Crystal Structure Prediction by Quasi-Random Sampling. *J. Chem. Theory. Comput.* **2016**, *12* (2), 910-924
(373) Campbell, J. E.; Yang, J.; Day, G. M. Predicted energy–structure–function maps for the evaluation of small molecule organic semiconductors. *J. Mater. Chem. C Mater* **2017**, *5* (30), 7574-7584

(374) Yang, J.; De, S.; Campbell, J. E.; Li, S.; Ceriotti, M.; Day, G. M. Large-Scale Computational Screening of Molecular Organic Semiconductors Using Crystal Structure Prediction. *Chem. Mater.* **2018**, *30* (13), 4361-4371
(375) Curtis, F.; Li, X.; Rose, T.; Vázquez-Mayagoitia, Á.; Bhattacharya, S.; Ghiringhelli, L. M.; Marom, N. GAtor: A First-Principles Genetic Algorithm for Molecular Crystal Structure Prediction. *J. Chem. Theory. Comput.* **2018**, *14* (4), 2246-2264
(376) Tom, R.; Rose, T.; Bier, I.; O'Brien, H.; Vázquez-Mayagoitia, Á.; Marom, N. Genarris 2.0: A random structure generator for molecular crystals. *Comput. Phys. Commun.* **2020**, *250*, 107170
(377) Reilly, A. M.; Cooper, R. I.; Adjiman, C. S.; Bhattacharya, S.; Boese, A. D.; Brandenburg, J. G.; Bygrave, P. J.; Bylsma, R.; Campbell, J. E.; Car, R.; et al. Report on the sixth blind test of organic crystal structure prediction methods. *Acta Crystallographica* **2016**, *B72* (4), 439-459
(378) Yang, J.; Hu, W.; Usvyat, D.; Matthews, D.; Schütz, M.; Chan, G. K.-L. Ab initio determination of the crystalline benzene lattice energy to sub-kilojoule/mole accuracy. *Science* **2014**, *345* (6197), 640-643
(379) Beran, G. J. A new era for ab initio molecular crystal lattice energy prediction. *Angew. Chem. Int. Ed.* **2015**, *54* (2), 396-398
(380) Hunter, C. A.; Sanders, J. K. M. The nature of π-π interactions. *J. Am. Chem. Soc.* **1990**, *112* (14), 5525-5534
(381) Sherrill, C. D. Energy Component Analysis of π Interactions. *Acc. Chem. Res.* **2013**, *46* (4), 1020-1028
(382) Khaliullin, R. Z.; Cobar, E. A.; Lochan, R. C.; Bell, A. T.; Head-Gordon, M. Unravelling the Origin of Intermolecular Interactions Using Absolutely Localized Molecular Orbitals. *J. Phys. Chem. A.* **2007**, *111* (36), 8753-8765
(383) Kitaura, K.; Morokuma, K. A new energy decomposition scheme for molecular interactions within the Hartree-Fock approximation. *Int. J. Quantum Chem* **1976**, *10* (2), 325-340
(384) Su, P.; Li, H. Energy decomposition analysis of covalent bonds and intermolecular interactions. *J. Chem. Phys.* **2009**, *131* (1), 014102
(385) Mo, Y.; Gao, J.; Peyerimhoff, S. D. Energy decomposition analysis of intermolecular interactions using a block-localized wave function approach. *J. Chem. Phys.* **2000**, *112* (13), 5530-5538
(386) Mao, Y.; Loipersberger, M.; Horn, P. R.; Das, A.; Demerdash, O.; Levine, D. S.; Prasad Veccham, S.; Head-Gordon, T.; Head-Gordon, M. From Intermolecular Interaction Energies and Observable Shifts to Component Contributions and Back Again: A Tale of Variational Energy Decomposition Analysis. *Annu. Rev. Phys. Chem.* **2021**, *72* (1), 641-666
(387) Lai, Y.-Y.; Huang, V.-H.; Lee, H.-T.; Yang, H.-R. Stacking Principles on π- and Lamellar Stacking for Organic Semiconductors Evaluated by Energy Decomposition Analysis. *ACS Omega* **2018**, *3* (12), 18656-18662
(388) Mitoraj, M. P.; Michalak, A.; Ziegler, T. A Combined Charge and Energy Decomposition Scheme for Bond Analysis. *J. Chem. Theory. Comput.* **2009**, *5* (4), 962-975
(389) Jeziorski, B.; Moszynski, R.; Szalewicz, K. Perturbation Theory Approach to Intermolecular Potential Energy Surfaces of van der Waals Complexes. *Chem. Rev.* **1994**, *94* (7), 1887-1930
(390) Misquitta, A. J.; Podeszwa, R.; Jeziorski, B.; Szalewicz, K. Intermolecular potentials based on symmetry-adapted perturbation theory with dispersion energies from time-dependent density-functional calculations. *J. Chem. Phys.* **2005**, *123* (21), 214103
(391) Parrish, R. M.; Sherrill, C. D. Spatial assignment of symmetry adapted perturbation theory interaction energy components: The atomic SAPT partition. *J. Chem. Phys.* **2014**, *141* (4), 044115
(392) Hunter, C. A.; Lawson, K. R.; Perkins, J.; Urch, C. J. Aromatic interactions. *J. Chem. Soc., Perkin Trans. 2* **2001**, (5), 651-669
(393) Wheeler, S. E.; Houk, K. N. Substituent Effects in the Benzene Dimer are Due to Direct Interactions of the Substituents with the Unsubstituted Benzene. *J. Am. Chem. Soc.* **2008**, *130* (33), 10854-10855

(394) Parrish, R. M.; Sherrill, C. D. Quantum-Mechanical Evaluation of π–π versus Substituent−π Interactions in π Stacking: Direct Evidence for the Wheeler–Houk Picture. *J. Am. Chem. Soc.* **2014**, *136* (50), 17386-17389
(395) Ryno, S. M.; Risko, C.; Brédas, J.-L. Impact of Molecular Packing on Electronic Polarization in Organic Crystals: The Case of Pentacene vs TIPS-Pentacene. *J. Am. Chem. Soc.* **2014**, *136* (17), 6421-6427
(396) Purdum, G. E.; Telesz, N. G.; Jarolimek, K.; Ryno, S. M.; Gessner, T.; Davy, N. C.; Petty, A. J.; Zhen, Y.; Shu, Y.; Facchetti, A.; et al. Presence of Short Intermolecular Contacts Screens for Kinetic Stability in Packing Polymorphs. *J. Am. Chem. Soc.* **2018**, *140* (24), 7519-7525
(397) Bhat, V.; Gopan, G.; Nair, N. G.; Hariharan, M. γ-Herringbone Polymorph of 6,13-Bis(trimethylsilylethynyl)pentacene: A Potential Material for Enhanced Hole Mobility. *Chemistry* **2018**, *24* (34), 8679-8685
(398) Ji, L.-F.; Fan, J.-X.; Zhang, S.-F.; Ren, A.-M. Theoretical investigations into the charge transfer properties of thiophene α-substituted naphthodithiophene diimides: excellent n-channel and ambipolar organic semiconductors. *Phys. Chem. Chem. Phys.* **2017**, *19* (21), 13978-13993
(399) Sutton, C.; Marshall, M. S.; Sherrill, C. D.; Risko, C.; Brédas, J.-L. Rubrene: The Interplay between Intramolecular and Intermolecular Interactions Determines the Planarization of Its Tetracene Core in the Solid State. *J. Am. Chem. Soc.* **2015**, *137* (27), 8775-8782
(400) Ryno, S. M.; Risko, C.; Brédas, J.-L. Noncovalent Interactions and Impact of Charge Penetration Effects in Linear Oligoacene Dimers and Single Crystals. *Chem. Mater.* **2016**, *28* (11), 3990-4000
(401) Alder, B. J.; Wainwright, T. E. Phase Transition for a Hard Sphere System. *J. Chem. Phys.* **1957**, *27* (5), 1208-1209
(402) Rahman, A. Correlations in the Motion of Atoms in Liquid Argon. *Phys. Rev.* **1964**, *136* (2A), A405-A411
(403) Verlet, L. Computer "Experiments" on Classical Fluids. I. Thermodynamical Properties of Lennard-Jones Molecules. *Phys. Rev.* **1967**, *159* (1), 98-103
(404) Ruymgaart, A. P.; Elber, R. Revisiting Molecular Dynamics on a CPU/GPU system: Water Kernel and SHAKE Parallelization. *J. Chem. Theory. Comput.* **2012**, *8* (11), 4624-4636
(405) Anthopoulos, A.; Grimstead, I.; Brancale, A. GPU-accelerated molecular mechanics computations. *J. Comput. Chem.* **2013**, *34* (26), 2249-2260
(406) Barreales, G. N.; Novalbos, M.; Otaduy, M. A.; Sanchez, A. MDScale: Scalable multi-GPU bonded and short-range molecular dynamics. *J. Parallel Distrib. Comput.* **2021**, *157*, 243-255
(407) Larsson, P.; Hess, B.; Lindahl, E. Algorithm improvements for molecular dynamics simulations. *Wiley Interdiscip. Rev. Comput. Mol. Sci.* **2011**, *1* (1), 93-108
(408) Beljonne, D.; Cornil, J.; Muccioli, L.; Zannoni, C.; Brédas, J.-L.; Castet, F. Electronic Processes at Organic−Organic Interfaces: Insight from Modeling and Implications for Opto-electronic Devices. *Chem. Mater.* **2011**, *23* (3), 591-609
(409) Ciccotti, G.; Dellago, C.; Ferrario, M.; Hernández, E. R.; Tuckerman, M. E. Molecular simulations: past, present, and future (a Topical Issue in EPJB). *Eur. Phys. J. B.* **2022**, *95* (1), 3
(410) González, M. A. Force fields and molecular dynamics simulations. *École thématique de la Société Française de la Neutronique* **2011**, *12*, 169-200
(411) Clancy, P. Application of Molecular Simulation Techniques to the Study of Factors Affecting the Thin-Film Morphology of Small-Molecule Organic Semiconductors. *Chem. Mater.* **2011**, *23* (3), 522-543
(412) Jorgensen, W. L.; Maxwell, D. S.; Tirado-Rives, J. Development and Testing of the OPLS All-Atom Force Field on Conformational Energetics and Properties of Organic Liquids. *J. Am. Chem. Soc.* **1996**, *118* (45), 11225-11236
(413) Kaminski, G. A.; Friesner, R. A.; Tirado-Rives, J.; Jorgensen, W. L. Evaluation and Reparametrization of the OPLS-AA Force Field for Proteins via Comparison with Accurate Quantum Chemical Calculations on Peptides. *J. Phys. Chem. B.* **2001**, *105* (28), 6474-6487

(414) Wang, J.; Wolf, R. M.; Caldwell, J. W.; Kollman, P. A.; Case, D. A. Development and testing of a general amber force field. *J. Comput. Chem.* **2004**, *25* (9), 1157-1174
(415) Scott, W. R. P.; Hünenberger, P. H.; Tironi, I. G.; Mark, A. E.; Billeter, S. R.; Fennen, J.; Torda, A. E.; Huber, T.; Krüger, P.; van Gunsteren, W. F. The GROMOS Biomolecular Simulation Program Package. *J. Phys. Chem. A.* **1999**, *103* (19), 3596-3607
(416) Oostenbrink, C.; Villa, A.; Mark, A. E.; Van Gunsteren, W. F. A biomolecular force field based on the free enthalpy of hydration and solvation: The GROMOS force-field parameter sets 53A5 and 53A6. *J. Comput. Chem.* **2004**, *25* (13), 1656-1676
(417) MacKerell, A. D., Jr.; Bashford, D.; Bellott, M.; Dunbrack, R. L., Jr.; Evanseck, J. D.; Field, M. J.; Fischer, S.; Gao, J.; Guo, H.; Ha, S.; et al. All-Atom Empirical Potential for Molecular Modeling and Dynamics Studies of Proteins. *J. Phys. Chem. B.* **1998**, *102* (18), 3586-3616
(418) Mackerell Jr, A. D.; Feig, M.; Brooks Iii, C. L. Extending the treatment of backbone energetics in protein force fields: Limitations of gas-phase quantum mechanics in reproducing protein conformational distributions in molecular dynamics simulations. *J. Comput. Chem.* **2004**, *25* (11), 1400-1415
(419) Wang, J.; Cieplak, P.; Kollman, P. A. How well does a restrained electrostatic potential (RESP) model perform in calculating conformational energies of organic and biological molecules? *J. Comput. Chem.* **2000**, *21* (12), 1049-1074
(420) Duan, Y.; Wu, C.; Chowdhury, S.; Lee, M. C.; Xiong, G.; Zhang, W.; Yang, R.; Cieplak, P.; Luo, R.; Lee, T.; et al. A point-charge force field for molecular mechanics simulations of proteins based on condensed-phase quantum mechanical calculations. *J. Comput. Chem.* **2003**, *24* (16), 1999-2012
(421) Allinger, N. L.; Yuh, Y. H.; Lii, J. H. Molecular mechanics. The MM3 force field for hydrocarbons. 1. *J. Am. Chem. Soc.* **1989**, *111* (23), 8551-8566
(422) Lii, J. H.; Allinger, N. L. Molecular mechanics. The MM3 force field for hydrocarbons. 2. Vibrational frequencies and thermodynamics. *J. Am. Chem. Soc.* **1989**, *111* (23), 8566-8575
(423) Lii, J. H.; Allinger, N. L. Molecular mechanics. The MM3 force field for hydrocarbons. 3. The van der Waals' potentials and crystal data for aliphatic and aromatic hydrocarbons. *J. Am. Chem. Soc.* **1989**, *111* (23), 8576-8582
(424) DuBay, K. H.; Hall, M. L.; Hughes, T. F.; Wu, C.; Reichman, D. R.; Friesner, R. A. Accurate Force Field Development for Modeling Conjugated Polymers. *J. Chem. Theory. Comput.* **2012**, *8* (11), 4556-4569
(425) Borzdun, N. I.; Larin, S. V.; Falkovich, S. G.; Nazarychev, V. M.; Volgin, I. V.; Yakimansky, A. V.; Lyulin, A. V.; Negi, V.; Bobbert, P. A.; Lyulin, S. V. Molecular dynamics simulation of poly(3-hexylthiophene) helical structure In Vacuo and in amorphous polymer surrounding. *J. Polym. Sci., Part B: Polym. Phys.* **2016**, *54* (23), 2448-2456
(426) Casalegno, M.; Famulari, A.; Meille, S. V. Modeling of Poly(3-hexylthiophene) and Its Oligomer's Structure and Thermal Behavior with Different Force Fields: Insights into the Phase Transitions of Semiconducting Polymers. *Macromolecules* **2022**, *55* (7), 2398-2412
(427) Tsourtou, F. D.; Peristeras, L. D.; Apostolov, R.; Mavrantzas, V. G. Molecular Dynamics Simulation of Amorphous Poly(3-hexylthiophene). *Macromolecules* **2020**, *53* (18), 7810-7824
(428) Wolf, C. M.; Kanekal, K. H.; Yimer, Y. Y.; Tyagi, M.; Omar-Diallo, S.; Pakhnyuk, V.; Luscombe, C. K.; Pfaendtner, J.; Pozzo, L. D. Assessment of molecular dynamics simulations for amorphous poly(3-hexylthiophene) using neutron and X-ray scattering experiments. *Soft Matter* **2019**, *15* (25), 5067-5083
(429) Wolf, C. M.; Guio, L.; Scheiwiller, S.; Pakhnyuk, V.; Luscombe, C.; Pozzo, L. D. Strategies for the Development of Conjugated Polymer Molecular Dynamics Force Fields Validated with Neutron and X-ray Scattering. *ACS Polym. Au* **2021**, *1* (3), 134-152
(430) Rissler, J. Effective conjugation length of π-conjugated systems. *Chem. Phys. Lett.* **2004**, *395* (1), 92-96
(431) Lynch, P.; Neill, L. O.; Whelan, J.; McNamara, M.; Byrne, H. J. Structural property relationships in conjugated polymers. In *Proc.SPIE*, 2005; Vol. 5826, pp 242-252. DOI: 10.1117/12.598779.

(432) Risko, C.; McGehee, M. D.; Brédas, J.-L. A quantum-chemical perspective into low optical-gap polymers for highly-efficient organic solar cells. *Chem. Sci.* **2011**, *2* (7), 1200-1218
(433) Jiang, L.; Hirst, J. D.; Do, H. Structure–Property Relationships in Amorphous Thieno[3,2-b]thiophene–Diketopyrrolopyrrole–Thiophene-Containing Polymers. *J. Phys. Chem. C.* **2022**, *126* (26), 10842-10854
(434) Bhatta, R. S.; Yimer, Y. Y.; Tsige, M.; Perry, D. S. Conformations and torsional potentials of poly(3-hexylthiophene) oligomers: Density functional calculations up to the dodecamer. *Computational and Theoretical Chemistry* **2012**, *995*, 36-42
(435) Munshi, J.; Farooq Ghumman, U.; Iyer, A.; Dulal, R.; Chen, W.; Chien, T.; Balasubramanian, G. Composition and processing dependent miscibility of P3HT and PCBM in organic solar cells by coarse-grained molecular simulations. *Comput. Mater. Sci.* **2018**, *155*, 112-115
(436) Callen, H. B.; Welton, T. A. Irreversibility and Generalized Noise. *Phys. Rev.* **1951**, *83* (1), 34-40
(437) Weber, J. Fluctuation Dissipation Theorem. *Phys. Rev.* **1956**, *101* (6), 1620-1626
(438) Kubo, R. The fluctuation-dissipation theorem. *Rep. Prog. Phys.* **1966**, *29* (1), 255
(439) Gross, J.; Ivanov, M.; Janke, W. Comparing atomistic and coarse-grained simulations of P3HT. *J. Phys. Conf. Ser.* **2016**, *750*, 012009
(440) Root, S. E.; Savagatrup, S.; Pais, C. J.; Arya, G.; Lipomi, D. J. Predicting the Mechanical Properties of Organic Semiconductors Using Coarse-Grained Molecular Dynamics Simulations. *Macromolecules* **2016**, *49* (7), 2886-2894
(441) Jackson, N. E. Coarse-Graining Organic Semiconductors: The Path to Multiscale Design. *J. Phys. Chem. B.* **2021**, *125* (2), 485-496
(442) Webb, M. A.; Delannoy, J.-Y.; de Pablo, J. J. Graph-Based Approach to Systematic Molecular Coarse-Graining. *J. Chem. Theory. Comput.* **2019**, *15* (2), 1199-1208
(443) Jackson, N. E.; Bowen, A. S.; Antony, L. W.; Webb, M. A.; Vishwanath, V.; de Pablo, J. J. Electronic structure at coarse-grained resolutions from supervised machine learning. *Sci. Adv.* **2019**, *5* (3), eaav1190
(444) Li, Z.; Wellawatte, G. P.; Chakraborty, M.; Gandhi, H. A.; Xu, C.; White, A. D. Graph neural network based coarse-grained mapping prediction. *Chem. Sci.* **2020**, *11* (35), 9524-9531
(445) Chakraborty, M.; Xu, C.; White, A. D. Encoding and selecting coarse-grain mapping operators with hierarchical graphs. *J. Chem. Phys.* **2018**, *149* (13), 134106
(446) Chakraborty, M.; Xu, J.; White, A. D. Is preservation of symmetry necessary for coarse-graining? *Phys. Chem. Chem. Phys.* **2020**, *22* (26), 14998-15005
(447) Khot, A.; Shiring, S. B.; Savoie, B. M. Evidence of information limitations in coarse-grained models. *J. Chem. Phys.* **2019**, *151* (24), 244105
(448) Nüske, F.; Boninsegna, L.; Clementi, C. Coarse-graining molecular systems by spectral matching. *J. Chem. Phys.* **2019**, *151* (4), 044116
(449) Lukyanov, A. Charge transport in amorphous organic semiconductors. Ph.D. Thesis, Mainz, 2011. http://dx.doi.org/10.25358/openscience-4787.
(450) Potestio, R.; Peter, C.; Kremer, K. Computer Simulations of Soft Matter: Linking the Scales. *Entropy* **2014**, *16* (8), 4199-4245
(451) Tschöp, W.; Kremer, K.; Batoulis, J.; Bürger, T.; Hahn, O. Simulation of polymer melts. I. Coarse-graining procedure for polycarbonates. *Acta Polym.* **1998**, *49* (2-3), 61-74
(452) Reith, D.; Pütz, M.; Müller-Plathe, F. Deriving effective mesoscale potentials from atomistic simulations. *J. Comput. Chem.* **2003**, *24* (13), 1624-1636
(453) Lyubartsev, A. P.; Laaksonen, A. Calculation of effective interaction potentials from radial distribution functions: A reverse Monte Carlo approach. *Phys. Rev. E.* **1995**, *52* (4), 3730-3737
(454) Soper, A. K. Empirical potential Monte Carlo simulation of fluid structure. *Chem. Phys.* **1996**, *202* (2), 295-306
(455) Ercolessi, F.; Adams, J. B. Interatomic Potentials from First-Principles Calculations: The Force-Matching Method. *Europhys Lett.* **1994**, *26* (8), 583-588

(456) Izvekov, S.; Voth, G. A. Multiscale coarse graining of liquid-state systems. *J. Chem. Phys.* **2005**, *123* (13), 134105
(457) Noid, W. G.; Chu, J.-W.; Ayton, G. S.; Voth, G. A. Multiscale Coarse-Graining and Structural Correlations: Connections to Liquid-State Theory. *J. Phys. Chem. B.* **2007**, *111* (16), 4116-4127
(458) Shell, M. S. The relative entropy is fundamental to multiscale and inverse thermodynamic problems. *J. Chem. Phys.* **2008**, *129* (14), 144108
(459) Kullback, S.; Leibler, R. A. On Information and Sufficiency. *Ann. Math. Stat.* **1951**, *22* (1), 79-86
(460) Scherer, C.; Andrienko, D. Comparison of systematic coarse-graining strategies for soluble conjugated polymers. *Eur. Phys. J. Spec. Top.* **2016**, *225* (8), 1441-1461
(461) Huang, D. M.; Faller, R.; Do, K.; Moulé, A. J. Coarse-Grained Computer Simulations of Polymer/Fullerene Bulk Heterojunctions for Organic Photovoltaic Applications. *J. Chem. Theory. Comput.* **2010**, *6* (2), 526-537
(462) Lee, C.-K.; Pao, C.-W.; Chu, C.-W. Multiscale molecular simulations of the nanoscale morphologies of P3HT:PCBM blends for bulk heterojunction organic photovoltaic cells. *Energy Environ. Sci.* **2011**, *4* (10), 4124-4132
(463) Lee, C. K.; Hua, C. C.; Chen, S. A. Hybrid Solvents Incubated π−π Stacking in Quenched Conjugated Polymer Resolved by Multiscale Computation. *Macromolecules* **2011**, *44* (2), 320-324
(464) Lee, C.-K.; Pao, C.-W. Solubility of [6,6]-Phenyl-C61-butyric Acid Methyl Ester and Optimal Blending Ratio of Bulk Heterojunction Polymer Solar Cells. *J. Phys. Chem. C.* **2012**, *116* (23), 12455-12461
(465) Lee, C. K.; Hua, C. C.; Chen, S. A. An ellipsoid-chain model for conjugated polymer solutions. *J. Chem. Phys.* **2012**, *136* (8), 084901
(466) Lee, C. K.; Hua, C. C.; Chen, S. A. Phase Transition and Gels in Conjugated Polymer Solutions. *Macromolecules* **2013**, *46* (5), 1932-1938
(467) Carrillo, J.-M. Y.; Kumar, R.; Goswami, M.; Sumpter, B. G.; Brown, W. M. New insights into the dynamics and morphology of P3HT:PCBM active layers in bulk heterojunctions. *Phys. Chem. Chem. Phys.* **2013**, *15* (41), 17873-17882
(468) Jankowski, E.; Marsh, H. S.; Jayaraman, A. Computationally Linking Molecular Features of Conjugated Polymers and Fullerene Derivatives to Bulk Heterojunction Morphology. *Macromolecules* **2013**, *46* (14), 5775-5785
(469) Lee, C.-K.; Pao, C.-W. Nanomorphology Evolution of P3HT/PCBM Blends during Solution-Processing from Coarse-Grained Molecular Simulations. *J. Phys. Chem. C.* **2014**, *118* (21), 11224-11233
(470) To, T. T.; Adams, S. Modelling of P3HT:PCBM interface using coarse-grained forcefield derived from accurate atomistic forcefield. *Phys. Chem. Chem. Phys.* **2014**, *16* (10), 4653-4663
(471) Böckmann, M.; Schemme, T.; de Jong, D. H.; Denz, C.; Heuer, A.; Doltsinis, N. L. Structure of P3HT crystals, thin films, and solutions by UV/Vis spectral analysis. *Phys. Chem. Chem. Phys.* **2015**, *17* (43), 28616-28625
(472) Chen, C.-W.; Huang, C.-I. Effects of intra/inter-molecular potential parameters, length and grafting density of side-chains on the self-assembling behavior of poly(3′-alkylthiophene)s in the ordered state. *Polymer* **2015**, *77*, 189-198
(473) Negi, V.; Lyulin, A.; Bobbert, P. Solvent-Dependent Structure Formation in Drying P3HT:PCBM Films Studied by Molecular Dynamics Simulations. *Macromol. Theory Simul.* **2016**, *25* (6), 550-558
(474) Alessandri, R.; Uusitalo, J. J.; de Vries, A. H.; Havenith, R. W. A.; Marrink, S. J. Bulk Heterojunction Morphologies with Atomistic Resolution from Coarse-Grain Solvent Evaporation Simulations. *J. Am. Chem. Soc.* **2017**, *139* (10), 3697-3705
(475) Choi, Y. K.; Lee, D.; Lee, S. Y.; Shin, T. J.; Park, J.; Ahn, D. J. Conjugated Polymer Nanoparticles in Aqueous Media by Assembly with Phospholipids via Dense Alkyl Chain Packing. *Macromolecules* **2017**, *50* (17), 6935-6944

(476) Munshi, J.; Dulal, R.; Chien, T.; Chen, W.; Balasubramanian, G. Solution Processing Dependent Bulk Heterojunction Nanomorphology of P3HT/PCBM Thin Films. *ACS Appl. Mater. Interfaces.* **2019**, *11* (18), 17056-17067
(477) Munshi, J.; Ghumman, U. F.; Iyer, A.; Dulal, R.; Chen, W.; Chien, T.; Balasubramanian, G. Effect of polydispersity on the bulk-heterojunction morphology of P3HT:PCBM solar cells. *J. Polym. Sci., Part B: Polym. Phys.* **2019**, *57* (14), 895-903
(478) Munshi, J.; Chien, T.; Chen, W.; Balasubramanian, G. Elasto-morphology of P3HT:PCBM bulk heterojunction organic solar cells. *Soft Matter* **2020**, *16* (29), 6743-6751
(479) Cohen, A. E.; Jackson, N. E.; de Pablo, J. J. Anisotropic Coarse-Grained Model for Conjugated Polymers: Investigations into Solution Morphologies. *Macromolecules* **2021**, *54* (8), 3780-3789
(480) Pantawane, S.; Gekle, S. Temperature-Dependent Conformation Behavior of Isolated Poly(3-hexylthiopene) Chains. *Polymers* **2022**, *14* (3), 550
(481) Boehm, B. J.; Huang, D. M. A simple predictor of interface orientation of fluids of disk-like anisotropic particles and its implications for organic semiconductors. *Soft Matter* **2022**, *18* (9), 1843-1857
(482) Yang, Y. I.; Shao, Q.; Zhang, J.; Yang, L.; Gao, Y. Q. Enhanced sampling in molecular dynamics. *J. Chem. Phys.* **2019**, *151* (7), 070902
(483) Liao, Q. Chapter Four - Enhanced sampling and free energy calculations for protein simulations. In *Progress in Molecular Biology and Translational Science*, Strodel, B., Barz, B. Eds.; Vol. 170; Academic Press, 2020; pp 177-213.
(484) Laio, A.; Parrinello, M. Escaping free-energy minima. *PNAS* **2002**, *99* (20), 12562-12566
(485) Valsson, O.; Tiwary, P.; Parrinello, M. Enhancing Important Fluctuations: Rare Events and Metadynamics from a Conceptual Viewpoint. *Annu. Rev. Phys. Chem.* **2016**, *67* (1), 159-184
(486) Valsson, O.; Parrinello, M. Variational Approach to Enhanced Sampling and Free Energy Calculations. *Phys. Rev. Lett.* **2014**, *113* (9), 090601
(487) Torrie, G. M.; Valleau, J. P. Nonphysical sampling distributions in Monte Carlo free-energy estimation: Umbrella sampling. *J. Comput. Phys.* **1977**, *23* (2), 187-199
(488) Grubmüller, H.; Tavan, P. Molecular dynamics of conformational substates for a simplified protein model. *J. Chem. Phys.* **1994**, *101* (6), 5047-5057
(489) Huber, T.; Torda, A. E.; van Gunsteren, W. F. Local elevation: A method for improving the searching properties of molecular dynamics simulation. *J. Comput. Aided Mol. Des.* **1994**, *8* (6), 695-708
(490) Lu, H.; Schulten, K. Steered molecular dynamics simulations of force-induced protein domain unfolding. *Proteins* **1999**, *35* (4), 453-463
(491) Swendsen, R. H.; Wang, J.-S. Replica Monte Carlo Simulation of Spin-Glasses. *Phys. Rev. Lett.* **1986**, *57* (21), 2607-2609
(492) Sugita, Y.; Okamoto, Y. Replica-exchange molecular dynamics method for protein folding. *Chem. Phys. Lett.* **1999**, *314* (1), 141-151
(493) Gao, Y. Q. An integrate-over-temperature approach for enhanced sampling. *J. Chem. Phys.* **2008**, *128* (6), 064105
(494) Sørensen, M. R.; Voter, A. F. Temperature-accelerated dynamics for simulation of infrequent events. *J. Chem. Phys.* **2000**, *112* (21), 9599-9606
(495) Hamelberg, D.; Mongan, J.; McCammon, J. A. Accelerated molecular dynamics: A promising and efficient simulation method for biomolecules. *J. Chem. Phys.* **2004**, *120* (24), 11919-11929
(496) Maragliano, L.; Vanden-Eijnden, E. A temperature accelerated method for sampling free energy and determining reaction pathways in rare events simulations. *Chem. Phys. Lett.* **2006**, *426* (1), 168-175
(497) Nakajima, N.; Nakamura, H.; Kidera, A. Multicanonical Ensemble Generated by Molecular Dynamics Simulation for Enhanced Conformational Sampling of Peptides. *J. Phys. Chem. B.* **1997**, *101* (5), 817-824

(498) Hansen, H. S.; Hünenberger, P. H. Using the local elevation method to construct optimized umbrella sampling potentials: Calculation of the relative free energies and interconversion barriers of glucopyranose ring conformers in water. *J. Comput. Chem.* **2010**, *31* (1), 1-23
(499) Barducci, A.; Bonomi, M.; Parrinello, M. Metadynamics. *Wiley Interdiscip. Rev. Comput. Mol. Sci.* **2011**, *1* (5), 826-843
(500) Kästner, J. Umbrella sampling. *Wiley Interdiscip. Rev. Comput. Mol. Sci.* **2011**, *1* (6), 932-942
(501) Kumar, S.; Rosenberg, J. M.; Bouzida, D.; Swendsen, R. H.; Kollman, P. A. The weighted histogram analysis method for free-energy calculations on biomolecules. I. The method. *J. Comput. Chem.* **1992**, *13* (8), 1011-1021
(502) Yang, Y. I.; Parrinello, M. Refining Collective Coordinates and Improving Free Energy Representation in Variational Enhanced Sampling. *J. Chem. Theory. Comput.* **2018**, *14* (6), 2889-2894
(503) Park, S.; Khalili-Araghi, F.; Tajkhorshid, E.; Schulten, K. Free energy calculation from steered molecular dynamics simulations using Jarzynski's equality. *J. Chem. Phys.* **2003**, *119* (6), 3559-3566
(504) Park, S.; Schulten, K. Calculating potentials of mean force from steered molecular dynamics simulations. *J. Chem. Phys.* **2004**, *120* (13), 5946-5961
(505) Chodera, J. D.; Singhal, N.; Pande, V. S.; Dill, K. A.; Swope, W. C. Automatic discovery of metastable states for the construction of Markov models of macromolecular conformational dynamics. *J. Chem. Phys.* **2007**, *126* (15), 155101
(506) Perkett, M. R.; Hagan, M. F. Using Markov state models to study self-assembly. *J. Chem. Phys.* **2014**, *140* (21), 214101
(507) Husic, B. E.; Pande, V. S. Markov State Models: From an Art to a Science. *J. Am. Chem. Soc.* **2018**, *140* (7), 2386-2396
(508) Konovalov, K. A.; Unarta, I. C.; Cao, S.; Goonetilleke, E. C.; Huang, X. Markov State Models to Study the Functional Dynamics of Proteins in the Wake of Machine Learning. *JACS Au* **2021**, *1* (9), 1330-1341
(509) Perez, D.; Uberuaga, B. P.; Shim, Y.; Amar, J. G.; Voter, A. F. Chapter 4 Accelerated Molecular Dynamics Methods: Introduction and Recent Developments. In *Annual Reports in Computational Chemistry*, Wheeler, R. A. Ed.; Vol. 5; Elsevier, 2009; pp 79-98.
(510) Voter, A. F. Hyperdynamics: Accelerated Molecular Dynamics of Infrequent Events. *Phys. Rev. Lett.* **1997**, *78* (20), 3908-3911
(511) Zamora, R. J.; Uberuaga, B. P.; Perez, D.; Voter, A. F. The Modern Temperature-Accelerated Dynamics Approach. *Annu. Rev. Chem. Biomol. Eng.* **2016**, *7* (1), 87-110
(512) Yang, L.; Liu, C.-W.; Shao, Q.; Zhang, J.; Gao, Y. Q. From Thermodynamics to Kinetics: Enhanced Sampling of Rare Events. *Acc. Chem. Res.* **2015**, *48* (4), 947-955
(513) You, Z.; Li, L.; Lu, J.; Ge, H. Integrated tempering enhanced sampling method as the infinite switching limit of simulated tempering. *J. Chem. Phys.* **2018**, *149* (8), 084114
(514) Berg, B. A.; Neuhaus, T. Multicanonical algorithms for first order phase transitions. *Phys. Lett. B* **1991**, *267* (2), 249-253
(515) Berg, B. A.; Neuhaus, T. Multicanonical ensemble: A new approach to simulate first-order phase transitions. *Phys. Rev. Lett.* **1992**, *68* (1), 9-12
(516) Berg, B. A.; Celik, T. New approach to spin-glass simulations. *Phys. Rev. Lett.* **1992**, *69* (15), 2292-2295
(517) Wang, F.; Landau, D. P. Efficient, Multiple-Range Random Walk Algorithm to Calculate the Density of States. *Phys. Rev. Lett.* **2001**, *86* (10), 2050-2053
(518) Tsallis, C.; Stariolo, D. A. Generalized simulated annealing. *Physica A: Statistical Mechanics and its Applications* **1996**, *233* (1), 395-406
(519) Bernardi, M.; Giulianini, M.; Grossman, J. C. Self-Assembly and Its Impact on Interfacial Charge Transfer in Carbon Nanotube/P3HT Solar Cells. *ACS Nano* **2010**, *4* (11), 6599-6606

(520) Adachi, T.; Brazard, J.; Ono, R. J.; Hanson, B.; Traub, M. C.; Wu, Z.-Q.; Li, Z.; Bolinger, J. C.; Ganesan, V.; Bielawski, C. W.; et al. Regioregularity and Single Polythiophene Chain Conformation. *J. Phys. Chem. Lett.* **2011**, *2* (12), 1400-1404
(521) Bounos, G.; Ghosh, S.; Lee, A. K.; Plunkett, K. N.; DuBay, K. H.; Bolinger, J. C.; Zhang, R.; Friesner, R. A.; Nuckolls, C.; Reichman, D. R.; et al. Controlling Chain Conformation in Conjugated Polymers Using Defect Inclusion Strategies. *J. Am. Chem. Soc.* **2011**, *133* (26), 10155-10160
(522) Torras, J.; Sanchez-Navas, C.; Bertran, O.; Alemán, C. On the modeling of aggregates of an optically active regioregular polythiophene. *Phys. Chem. Chem. Phys.* **2012**, *14* (6), 1881-1891
(523) Hu, Z.; Adachi, T.; Lee, Y.-G.; Haws, R. T.; Hanson, B.; Ono, R. J.; Bielawski, C. W.; Ganesan, V.; Rossky, P. J.; Vanden Bout, D. A. Effect of the Side-Chain-Distribution Density on the Single-Conjugated-Polymer-Chain Conformation. *ChemPhysChem* **2013**, *14* (18), 4143-4148
(524) Janke, W. Computer Simulation Studies of Polymer Adsorption and Aggregation – From Flexible to Stiff. *Phys. Procedia.* **2015**, *68*, 69-79
(525) Ivanov, M.; Gross, J.; Janke, W. Single-chain behavior of poly(3-hexylthiophene). *Eur. Phys. J. Spec. Top.* **2017**, *226* (4), 667-681
(526) Oberthür, N.; Gross, J.; Janke, W. Two-dimensional Monte Carlo simulations of coarse-grained poly(3-hexylthiophene) (P3HT) adsorbed on striped substrates. *J. Chem. Phys.* **2018**, *149* (14), 144903
(527) Tsourtou, F. D.; Peroukidis, S. D.; Peristeras, L. D.; Mavrantzas, V. G. Monte Carlo Algorithm Based on Internal Bridging Moves for the Atomistic Simulation of Thiophene Oligomers and Polymers. *Macromolecules* **2018**, *51* (21), 8406-8423
(528) Fortino, M.; Cozza, C.; Bonomi, M.; Pietropaolo, A. Multi-replica biased sampling for photoswitchable π-conjugated polymers. *J. Chem. Phys.* **2021**, *154* (17), 174108
(529) Mortuza, S. M.; Banerjee, S. Molecular modeling study of agglomeration of [6,6]-phenyl-C61-butyric acid methyl ester in solvents. *J. Chem. Phys.* **2012**, *137* (24), 244308
(530) Goldey, M. B.; Reid, D.; de Pablo, J.; Galli, G. Planarity and multiple components promote organic photovoltaic efficiency by improving electronic transport. *Phys. Chem. Chem. Phys.* **2016**, *18* (46), 31388-31399
(531) Bourdick, A.; Reichenberger, M.; Stradomska, A.; Bazan, G. C.; Nguyen, T.-Q.; Köhler, A.; Gekle, S. Elucidating Aggregation Pathways in the Donor–Acceptor Type Molecules p-DTS(FBTTh2)2 and p-SIDT(FBTTh2)2. *J. Phys. Chem. B.* **2018**, *122* (39), 9191-9201
(532) Reid, D. R.; Jackson, N. E.; Bourque, A. J.; Snyder, C. R.; Jones, R. L.; de Pablo, J. J. Aggregation and Solubility of a Model Conjugated Donor–Acceptor Polymer. *J. Phys. Chem. Lett.* **2018**, *9* (16), 4802-4807
(533) Schwermann, C.; Doltsinis, N. L. Exciton transfer free energy from Car–Parrinello molecular dynamics. *Phys. Chem. Chem. Phys.* **2020**, *22* (19), 10526-10535
(534) Wedler, S.; Bourdick, A.; Athanasopoulos, S.; Gekle, S.; Panzer, F.; McDowell, C.; Nguyen, T.-Q.; Bazan, G. C.; Köhler, A. What is the role of planarity and torsional freedom for aggregation in a π-conjugated donor–acceptor model oligomer? *J. Mater. Chem. C Mater* **2020**, *8* (14), 4944-4955
(535) Park, K. S.; Xue, Z.; Patel, B. B.; An, H.; Kwok, J. J.; Kafle, P.; Chen, Q.; Shukla, D.; Diao, Y. Chiral emergence in multistep hierarchical assembly of achiral conjugated polymers. *Nat. Commun.* **2022**, *13* (1), 2738
(536) Wu, C. H.; Hua, C. C. Solvation-Shell-Induced Entropic Repulsion and Insights into Solvent Quality of Crystalline Conjugated Polymer Solutions. *Macromolecules* **2022**, *55* (13), 5382-5389
(537) Ghosh, A.; Jana, B.; Chakraborty, S.; Maiti, S.; Jana, B.; Ghosh, H. N.; Patra, A. Exciton Dynamics and Formation Mechanism of MEH-PPV Polymer-Based Nanostructures. *J. Phys. Chem. C.* **2017**, *121* (38), 21062-21072
(538) Cozza, C.; Bonomi, M.; Pietropaolo, A. A Versatile Computational Strategy To Characterize the Free-Energy Landscape of Excited States in Oligofluorenes. *J. Chem. Theory. Comput.* **2018**, *14* (11), 5441-5445

(539) Wang, X.; Tang, X.; yang, X.; Wang, Y.; Zhang, P.; Dong, X.; Yang, D.; Lü, X.; Zheng, H.; Li, K.; et al. High-Pressure Synthesis of Highly Conjugated Polymers via Synergistic Polymerization of Phenylpropiolic Acid. *ACS Appl. Polym. Mater.* **2022**, *4* (7), 5246-5252
(540) Elmer, S. P.; Park, S.; Pande, V. S. Foldamer dynamics expressed via Markov state models. I. Explicit solvent molecular-dynamics simulations in acetonitrile, chloroform, methanol, and water. *J. Chem. Phys.* **2005**, *123* (11), 114902
(541) Thurston, B. A.; Tovar, J. D.; Ferguson, A. L. Thermodynamics, morphology, and kinetics of early-stage self-assembly of π-conjugated oligopeptides. *Mol. Simul.* **2016**, *42* (12), 955-975
(542) Hu, D.; Yu, J.; Wong, K.; Bagchi, B.; Rossky, P. J.; Barbara, P. F. Collapse of stiff conjugated polymers with chemical defects into ordered, cylindrical conformations. *Nature* **2000**, *405* (6790), 1030-1033
(543) Vukmirović, N.; Wang, L.-W. Electronic Structure of Disordered Conjugated Polymers: Polythiophenes. *J. Phys. Chem. B.* **2009**, *113* (2), 409-415
(544) Khoshkhoo, M. S.; Taromi, F. A.; Kowsari, E.; Shalamzari, E. K. Contribution of chromophores with different numbers of repeat units to overall emission of MEH–PPV: An experimental and simulation study. *Polymer* **2013**, *54* (15), 4017-4029
(545) Jackson, N. E.; Kohlstedt, K. L.; Savoie, B. M.; Olvera de la Cruz, M.; Schatz, G. C.; Chen, L. X.; Ratner, M. A. Conformational Order in Aggregates of Conjugated Polymers. *J. Am. Chem. Soc.* **2015**, *137* (19), 6254-6262
(546) Lee, F. L.; Barati Farimani, A.; Gu, K. L.; Yan, H.; Toney, M. F.; Bao, Z.; Pande, V. S. Solution-Phase Conformation and Dynamics of Conjugated Isoindigo-Based Donor–Acceptor Polymer Single Chains. *J. Phys. Chem. Lett.* **2017**, *8* (22), 5479-5486
(547) Cheung, D. L.; McMahon, D. P.; Troisi, A. Computational Study of the Structure and Charge-Transfer Parameters in Low-Molecular-Mass P3HT. *J. Phys. Chem. B.* **2009**, *113* (28), 9393-9401
(548) Barford, W.; Lidzey, D. G.; Makhov, D. V.; Meijer, A. J. H. Exciton localization in disordered poly(3-hexylthiophene). *J. Chem. Phys.* **2010**, *133* (4), 044504
(549) Batagin-Neto, A.; Oliveira, E. F.; Graeff, C. F. O.; Lavarda, F. C. Modelling polymers with side chains: MEH-PPV and P3HT. *Mol. Simul.* **2013**, *39* (4), 309-321
(550) Qin, T.; Troisi, A. Relation between Structure and Electronic Properties of Amorphous MEH-PPV Polymers. *J. Am. Chem. Soc.* **2013**, *135* (30), 11247-11256
(551) Do, K.; Saleem, Q.; Ravva, M. K.; Cruciani, F.; Kan, Z.; Wolf, J.; Hansen, M. R.; Beaujuge, P. M.; Brédas, J.-L. Impact of Fluorine Substituents on π-Conjugated Polymer Main-Chain Conformations, Packing, and Electronic Couplings. *Adv. Mater.* **2016**, *28* (37), 8197-8205
(552) Lemaur, V.; Cornil, J.; Lazzaroni, R.; Sirringhaus, H.; Beljonne, D.; Olivier, Y. Resilience to Conformational Fluctuations Controls Energetic Disorder in Conjugated Polymer Materials: Insights from Atomistic Simulations. *Chem. Mater.* **2019**, *31* (17), 6889-6899
(553) Prodhan, S.; Qiu, J.; Ricci, M.; Roscioni, O. M.; Wang, L.; Beljonne, D. Design Rules to Maximize Charge-Carrier Mobility along Conjugated Polymer Chains. *J. Phys. Chem. Lett.* **2020**, *11* (16), 6519-6525
(554) Karunasena, C.; Li, S.; Heifner, M. C.; Ryno, S. M.; Risko, C. Reconsidering the Roles of Noncovalent Intramolecular "Locks" in π-Conjugated Molecules. *Chem. Mater.* **2021**, *33* (23), 9139-9151
(555) Chaudhari, S. R.; Griffin, J. M.; Broch, K.; Lesage, A.; Lemaur, V.; Dudenko, D.; Olivier, Y.; Sirringhaus, H.; Emsley, L.; Grey, C. P. Donor–acceptor stacking arrangements in bulk and thin-film high-mobility conjugated polymers characterized using molecular modelling and MAS and surface-enhanced solid-state NMR spectroscopy. *Chem. Sci.* **2017**, *8* (4), 3126-3136
(556) Cherniawski, B. P.; Lopez, S. A.; Burnett, E. K.; Yavuz, I.; Zhang, L.; Parkin, S. R.; Houk, K. N.; Briseno, A. L. The effect of hexyl side chains on molecular conformations, crystal packing, and charge transport of oligothiophenes. *J. Mater. Chem. C Mater* **2017**, *5* (3), 582-588
(557) Lukose, B.; Bobbili, S. V.; Clancy, P. Factors affecting tacticity and aggregation of P3HT polymers in P3HT:PCBM blends. *Mol. Simul.* **2017**, *43* (10-11), 743-755

(558) Meirovitch, H. Calculation of the Free Energy and the Entropy of Macromolecular Systems by Computer Simulation. In *Reviews in Computational Chemistry*, Kenny B. Lipkowitz, D. B. B. Ed.; Vol. 12; 1998; pp 1-74.
(559) Meirovitch, H. Recent developments in methodologies for calculating the entropy and free energy of biological systems by computer simulation. *Curr. Opin. Struct. Biol.* **2007**, *17* (2), 181-186
(560) Meirovitch, H. Methods for calculating the absolute entropy and free energy of biological systems based on ideas from polymer physics. *J. Mol. Recognit.* **2010**, *23* (2), 153-172
(561) Kumar, S.; Rosenberg, J. M.; Bouzida, D.; Swendsen, R. H.; Kollman, P. A. Multidimensional free-energy calculations using the weighted histogram analysis method. *J. Comput. Chem.* **1995**, *16* (11), 1339-1350
(562) Beveridge, D. L.; DiCapua, F. M. Free Energy Via Molecular Simulation: Applications to Chemical and Biomolecular Systems. *Annu. Rev. Biophys. Biophys. Chem.* **1989**, *18* (1), 431-492
(563) Jorgensen, W. L. Free energy calculations: a breakthrough for modeling organic chemistry in solution. *Acc. Chem. Res.* **1989**, *22* (5), 184-189
(564) Kollman, P. Free energy calculations: Applications to chemical and biochemical phenomena. *Chem. Rev.* **1993**, *93* (7), 2395-2417
(565) Kirkwood, J. G. Statistical Mechanics of Fluid Mixtures. *J. Chem. Phys.* **1935**, *3* (5), 300-313
(566) Zwanzig, R. W. High-Temperature Equation of State by a Perturbation Method. I. Nonpolar Gases. *J. Chem. Phys.* **1954**, *22* (8), 1420-1426
(567) Fasnacht, M.; Swendsen, R. H.; Rosenberg, J. M. Adaptive integration method for Monte Carlo simulations. *Phys. Rev. E.* **2004**, *69* (5), 056704
(568) Jarzynski, C. Nonequilibrium Equality for Free Energy Differences. *Phys. Rev. Lett.* **1997**, *78* (14), 2690-2693
(569) Bennett, C. H. Efficient estimation of free energy differences from Monte Carlo data. *J. Comput. Phys.* **1976**, *22* (2), 245-268
(570) Gō, N.; Scheraga, H. A. Analysis of the Contribution of Internal Vibrations to the Statistical Weights of Equilibrium Conformations of Macromolecules. *J. Chem. Phys.* **1969**, *51* (11), 4751-4767
(571) Gō, N.; Scheraga, H. A. On the Use of Classical Statistical Mechanics in the Treatment of Polymer Chain Conformation. *Macromolecules* **1976**, *9* (4), 535-542
(572) Karplus, M.; Kushick, J. N. Method for estimating the configurational entropy of macromolecules. *Macromolecules* **1981**, *14* (2), 325-332
(573) Baron, R.; van Gunsteren, W. F.; Hünenberger, P. H. Estimating the configurational entropy from molecular dynamics simulations: anharmonicity and correlation corrections to the quasi-harmonic approximation. *Trends Phys Chem* **2006**, *11*, 87-122
(574) Wang, J.; Brüschweiler, R. 2D Entropy of Discrete Molecular Ensembles. *J. Chem. Theory. Comput.* **2006**, *2* (1), 18-24
(575) Meirovitch, H. Calculation of entropy with computer simulation methods. *Chem. Phys. Lett.* **1977**, *45* (2), 389-392
(576) White, R. P.; Meirovitch, H. Lower and upper bounds for the absolute free energy by the hypothetical scanning Monte Carlo method: Application to liquid argon and water. *J. Chem. Phys.* **2004**, *121* (22), 10889-10904
(577) White, R. P.; Meirovitch, H. Calculation of the entropy of random coil polymers with the hypothetical scanning Monte Carlo method. *J. Chem. Phys.* **2005**, *123* (21), 214908
(578) Schlitter, J. Estimation of absolute and relative entropies of macromolecules using the covariance matrix. *Chem. Phys. Lett.* **1993**, *215* (6), 617-621
(579) Guilbert, A. A. Y.; Zbiri, M.; Dunbar, A. D. F.; Nelson, J. Quantitative Analysis of the Molecular Dynamics of P3HT:PCBM Bulk Heterojunction. *J. Phys. Chem. B.* **2017**, *121* (38), 9073-9080
(580) Qian, Y.; Guo, M.; Li, C.; Bi, K.; Chen, Y. New Insight on the Interface between Polythiophene and Semiconductors via Molecular Dynamics Simulations. *ACS Appl. Mater. Interfaces.* **2019**, *11* (33), 30470-30476

(581) Wu, C. H.; Hua, C. C.; Wang, C. I. Effects of solvation shell relaxation on chain association mechanisms in poly(3-hexylthiophene) solutions. *Phys. Chem. Chem. Phys.* **2021**, *23* (20), 12005-12014
(582) Wu, E. C.-K.; Salamat, C. Z.; Tolbert, S. H.; Schwartz, B. J. Molecular Dynamics Study of the Thermodynamics of Integer Charge Transfer vs Charge-Transfer Complex Formation in Doped Conjugated Polymers. *ACS Appl. Mater. Interfaces.* **2022**, *14* (23), 26988-27001
(583) Leclère, P.; Calderone, A.; Marsitzky, D.; Francke, V.; Geerts, Y.; Müllen, K.; Brédas, J. L.; Lazzaroni, R. Highly Regular Organization of Conjugated Polymer Chains via Block Copolymer Self-Assembly. *Adv. Mater.* **2000**, *12* (14), 1042-1046
(584) Marcon, V.; Raos, G.; Allegra, G. Tetrathiophene on Graphite: Molecular Dynamics Simulations. *Macromol. Theory Simul.* **2004**, *13* (6), 497-505
(585) Sumpter, B. G.; Kumar, P.; Mehta, A.; Barnes, M. D.; Shelton, W. A.; Harrison, R. J. Computational Study of the Structure, Dynamics, and Photophysical Properties of Conjugated Polymers and Oligomers under Nanoscale Confinement. *J. Phys. Chem. B.* **2005**, *109* (16), 7671-7685
(586) Martinelli, N. G.; Savini, M.; Muccioli, L.; Olivier, Y.; Castet, F.; Zannoni, C.; Beljonne, D.; Cornil, J. Modeling Polymer Dielectric/Pentacene Interfaces: On the Role of Electrostatic Energy Disorder on Charge Carrier Mobility. *Adv. Funct. Mater.* **2009**, *19* (20), 3254-3261
(587) Meredig, B.; Salleo, A.; Gee, R. Ordering of Poly(3-hexylthiophene) Nanocrystallites on the Basis of Substrate Surface Energy. *ACS Nano* **2009**, *3* (10), 2881-2886
(588) Vukmirović, N.; Wang, L.-W. Charge Carrier Motion in Disordered Conjugated Polymers: A Multiscale Ab Initio Study. *Nano Lett.* **2009**, *9* (12), 3996-4000
(589) Dag, S.; Wang, L.-W. Packing Structure of Poly(3-hexylthiophene) Crystal: Ab Initio and Molecular Dynamics Studies. *J. Phys. Chem. B.* **2010**, *114* (18), 5997-6000
(590) Melis, C.; Colombo, L.; Mattoni, A. Self-Assembling of Poly(3-hexylthiophene). *J. Phys. Chem. C.* **2011**, *115* (2), 576-581
(591) Obata, S.; Shimoi, Y. Molecular Arrangements of Regioregular and Regiorandom Poly(3-hexylthiophene): Molecular Dynamics Simulations. *Trans. Mater. Res. Soc* **2012**, *37* (2), 311-314
(592) Obata, S.; Shimoi, Y. Control of molecular orientations of poly(3-hexylthiophene) on self-assembled monolayers: molecular dynamics simulations. *Phys. Chem. Chem. Phys.* **2013**, *15* (23), 9265-9270
(593) Pani, R. C.; Bond, B. D.; Krishnan, G.; Yingling, Y. G. Correlating fullerene diffusion with the polythiophene morphology: molecular dynamics simulations. *Soft Matter* **2013**, *9* (42), 10048-10055
(594) Poelking, C.; Cho, E.; Malafeev, A.; Ivanov, V.; Kremer, K.; Risko, C.; Brédas, J.-L.; Andrienko, D. Characterization of Charge-Carrier Transport in Semicrystalline Polymers: Electronic Couplings, Site Energies, and Charge-Carrier Dynamics in Poly(bithiophene-alt-thienothiophene) [PBTTT]. *J. Phys. Chem. C.* **2013**, *117* (4), 1633-1640
(595) Poelking, C.; Andrienko, D. Effect of Polymorphism, Regioregularity and Paracrystallinity on Charge Transport in Poly(3-hexylthiophene) [P3HT] Nanofibers. *Macromolecules* **2013**, *46* (22), 8941-8956
(596) Wang, C. I.; Hsu, C. H.; Hua, C. C.; Chen, S. A. Molecular dynamics study of pair interactions, interfacial microstructure, and nanomorphology of C60/MEH-PPV hybrids. *J. Polym. Res.* **2013**, *20* (7), 188
(597) Alberga, D.; Mangiatordi, G. F.; Torsi, L.; Lattanzi, G. Effects of Annealing and Residual Solvents on Amorphous P3HT and PBTTT Films. *J. Phys. Chem. C.* **2014**, *118* (16), 8641-8655
(598) Alberga, D.; Perrier, A.; Ciofini, I.; Mangiatordi, G. F.; Lattanzi, G.; Adamo, C. Morphological and charge transport properties of amorphous and crystalline P3HT and PBTTT: insights from theory. *Phys. Chem. Chem. Phys.* **2015**, *17* (28), 18742-18750

(599) Tummala, N. R.; Risko, C.; Bruner, C.; Dauskardt, R. H.; Brédas, J.-L. Entanglements in P3HT and their influence on thin-film mechanical properties: Insights from molecular dynamics simulations. *J. Polym. Sci., Part B: Polym. Phys.* **2015**, *53* (13), 934-942
(600) de Magalhães, C. E. T.; Savedra, R. M. L.; Dias, K. S.; Ramos, R.; Siqueira, M. F. Structural dependence of MEH-PPV chromism in solution. *J. Mol. Model.* **2017**, *23* (3), 91
(601) Han, G.; Guo, Y.; Duan, R.; Shen, X.; Yi, Y. Importance of side-chain anchoring atoms on electron donor/fullerene interfaces for high-performance organic solar cells. *J. Mater. Chem. A Mater* **2017**, *5* (19), 9316-9321
(602) Henry, M. M.; Jones, M. L.; Oosterhout, S. D.; Braunecker, W. A.; Kemper, T. W.; Larsen, R. E.; Kopidakis, N.; Toney, M. F.; Olson, D. C.; Jankowski, E. Simplified Models for Accelerated Structural Prediction of Conjugated Semiconducting Polymers. *J. Phys. Chem. C.* **2017**, *121* (47), 26528-26538
(603) Lan, Y.-B.; Sher, P.-H.; Lee, C.-K.; Pao, C.-W.; Tsao, C.-S.; Huang, Y.-C.; Huang, P.-T.; Wu, C.-I.; Wang, J.-K. Revealing Ordered Polymer Packing during Freeze-Drying Fabrication of a Bulk Heterojunction Poly(3-hexylthiophene-2,5-diyl):[6,6]-Phenyl-C61-butyric Acid Methyl Ester Layer: In Situ Optical Spectroscopy, Molecular Dynamics Simulation, and X-ray Diffraction. *J. Phys. Chem. C.* **2017**, *121* (27), 14826-14834
(604) Root, S. E.; Jackson, N. E.; Savagatrup, S.; Arya, G.; Lipomi, D. J. Modelling the morphology and thermomechanical behaviour of low-bandgap conjugated polymers and bulk heterojunction films. *Energy Environ. Sci.* **2017**, *10* (2), 558-569
(605) Casalegno, M.; Nicolini, T.; Famulari, A.; Raos, G.; Po, R.; Meille, S. V. Atomistic modelling of entropy driven phase transitions between different crystal modifications in polymers: the case of poly(3-alkylthiophenes). *Phys. Chem. Chem. Phys.* **2018**, *20* (46), 28984-28989
(606) Zhugayevych, A.; Mazaleva, O.; Naumov, A.; Tretiak, S. Lowest-Energy Crystalline Polymorphs of P3HT. *J. Phys. Chem. C.* **2018**, *122* (16), 9141-9151
(607) Gertsen, A. S.; Sørensen, M. K.; Andreasen, J. W. Nanostructure of organic semiconductor thin films: Molecular dynamics modeling with solvent evaporation. *Phys. Rev. Mater.* **2020**, *4* (7), 075405
(608) Lee, T.; Sanzogni, A. V.; Burn, P. L.; Mark, A. E. Evolution and Morphology of Thin Films Formed by Solvent Evaporation: An Organic Semiconductor Case Study. *ACS Appl. Mater. Interfaces.* **2020**, *12* (36), 40548-40557
(609) Reisjalali, M.; Burgos-Mármol, J. J.; Manurung, R.; Troisi, A. Local structuring of diketopyrrolopyrrole (DPP)-based oligomers from molecular dynamics simulations. *Phys. Chem. Chem. Phys.* **2021**, *23* (35), 19693-19707
(610) Callaway, C. P.; Bombile, J. H.; Mask, W.; Ryno, S. M.; Risko, C. Thermomechanical enhancement of DPP-4T through purposeful π-conjugation disruption. *J. Polym. Sci.* **2022**, *60* (3), 559-568
(611) Savedra, R. M. L.; de Morais, M. N. B. L.; Siqueira, M. F. On the microstructures of the bulk of P3HT amorphous films obtained from two protocols: Insights from molecular dynamics simulations. *J. Mol. Graphics Modell.* **2022**, *117*, 108279
(612) Do, K.; Huang, D. M.; Faller, R.; Moulé, A. J. A comparative MD study of the local structure of polymer semiconductors P3HT and PBTTT. *Phys. Chem. Chem. Phys.* **2010**, *12* (44), 14735-14739
(613) Choudhary, D.; Clancy, P.; Shetty, R.; Escobedo, F. A Computational Study of the Sub-monolayer Growth of Pentacene. *Adv. Funct. Mater.* **2006**, *16* (13), 1768-1775
(614) Lee, C. K.; Hua, C. C.; Chen, S. A. Single-Chain and Aggregation Properties of Semiconducting Polymer Solutions Investigated by Coarse-Grained Langevin Dynamics Simulation. *J. Phys. Chem. B.* **2008**, *112* (37), 11479-11489
(615) Root, S. E.; Savagatrup, S.; Printz, A. D.; Rodriquez, D.; Lipomi, D. J. Mechanical Properties of Organic Semiconductors for Stretchable, Highly Flexible, and Mechanically Robust Electronics. *Chem. Rev.* **2017**, *117* (9), 6467-6499

(616) Li, S.; Ryno, S. M.; Risko, C. Exploring thermal transitions in anthradithiophene-based organic semiconductors to reveal structure-packing relationships. *J. Mater. Chem. C Mater* **2018**, *6* (40), 10924-10934
(617) Zhang, S.; Alesadi, A.; Selivanova, M.; Cao, Z.; Qian, Z.; Luo, S.; Galuska, L.; Teh, C.; Ocheje, M. U.; Mason, G. T.; et al. Toward the Prediction and Control of Glass Transition Temperature for Donor–Acceptor Polymers. *Adv. Funct. Mater.* **2020**, *30* (27), 2002221
(618) Yoshimoto, Y.; Sugiyama, S.; Shimada, S.; Kaneko, T.; Takagi, S.; Kinefuchi, I. Molecular Insights into the Mechanical Properties of Polymer–Fullerene Bulk Heterojunctions for Organic Photovoltaic Applications. *Macromolecules* **2021**, *54* (2), 958-969
(619) Tummala, N. R.; Bruner, C.; Risko, C.; Brédas, J.-L.; Dauskardt, R. H. Molecular-Scale Understanding of Cohesion and Fracture in P3HT:Fullerene Blends. *ACS Appl. Mater. Interfaces.* **2015**, *7* (18), 9957-9964
(620) Rodriquez, D.; Kim, J.-H.; Root, S. E.; Fei, Z.; Boufflet, P.; Heeney, M.; Kim, T.-S.; Lipomi, D. J. Comparison of Methods for Determining the Mechanical Properties of Semiconducting Polymer Films for Stretchable Electronics. *ACS Appl. Mater. Interfaces.* **2017**, *9* (10), 8855-8862
(621) Dias, K. d. S.; Savedra, R. M. L.; de Magalhães, C. E. T.; Siqueira, M. F. Solvent influence on molecular interactions in the bulk of fluorene copolymer films. *RSC Adv.* **2020**, *10* (35), 20772-20777
(622) Kröger, M. Shortest multiple disconnected path for the analysis of entanglements in two- and three-dimensional polymeric systems. *Comput. Phys. Commun.* **2005**, *168* (3), 209-232
(623) Shanbhag, S.; Kröger, M. Primitive Path Networks Generated by Annealing and Geometrical Methods: Insights into Differences. *Macromolecules* **2007**, *40* (8), 2897-2903
(624) Karayiannis, N. C.; Kröger, M. Combined Molecular Algorithms for the Generation, Equilibration and Topological Analysis of Entangled Polymers: Methodology and Performance. *Int. J. Mol. Sci.* **2009**, *10* (11), 5054-5089
(625) Hoy, R. S.; Foteinopoulou, K.; Kröger, M. Topological analysis of polymeric melts: Chain-length effects and fast-converging estimators for entanglement length. *Phys. Rev. E.* **2009**, *80* (3), 031803
(626) Wang, X.; Wang, W.; Yang, C.; Han, D.; Fan, H.; Zhang, J. Thermal transport in organic semiconductors. *J. Appl. Phys.* **2021**, *130* (17), 170902
(627) Zhang, T.; Wu, X.; Luo, T. Polymer Nanofibers with Outstanding Thermal Conductivity and Thermal Stability: Fundamental Linkage between Molecular Characteristics and Macroscopic Thermal Properties. *J. Phys. Chem. C.* **2014**, *118* (36), 21148-21159
(628) Peierls, R. On the Kinetic Theory of Thermal Conduction in Crystals. *Ann. Phys.* **1929**, *395* (8), 1055-1101
(629) Peierls, R. E. Transport Phenomena. In *Quantum Theory of Solids*, Oxford University Press, 1955; pp 115-142.
(630) Callaway, J. Model for Lattice Thermal Conductivity at Low Temperatures. *Phys. Rev.* **1959**, *113* (4), 1046-1051
(631) Ziman, J. M. *Electrons and Phonons*; Oxford University Press, 1960. DOI: 10.1093/acprof:oso/9780198507796.003.0002.
(632) Holland, M. G. Analysis of Lattice Thermal Conductivity. *Phys. Rev.* **1963**, *132* (6), 2461-2471
(633) Hamilton, R. A. H.; Parrott, J. E. Variational Calculation of the Thermal Conductivity of Germanium. *Phys. Rev.* **1969**, *178* (3), 1284-1292
(634) Srivastava, G. P. *The physics of phonons*; Institute of Physics Publishing, 1990.
(635) Omini, M.; Sparavigna, A. An iterative approach to the phonon Boltzmann equation in the theory of thermal conductivity. *Physica B: Condensed Matter* **1995**, *212* (2), 101-112
(636) Omini, M.; Sparavigna, A. Beyond the isotropic-model approximation in the theory of thermal conductivity. *Phys. Rev. B.* **1996**, *53* (14), 9064-9073
(637) Pascual-Gutiérrez, J. A.; Murthy, J. Y.; Viskanta, R. Thermal conductivity and phonon transport properties of silicon using perturbation theory and the environment-dependent interatomic potential. *J. Appl. Phys.* **2009**, *106* (6), 063532

(638) Fugallo, G.; Lazzeri, M.; Paulatto, L.; Mauri, F. Ab initio variational approach for evaluating lattice thermal conductivity. *Phys. Rev. B.* **2013**, *88* (4), 045430
(639) Green, M. S. Markoff Random Processes and the Statistical Mechanics of Time-Dependent Phenomena. II. Irreversible Processes in Fluids. *J. Chem. Phys.* **1954**, *22* (3), 398-413
(640) Kubo, R. Statistical-Mechanical Theory of Irreversible Processes. I. General Theory and Simple Applications to Magnetic and Conduction Problems. *J. Phys. Soc. Jpn.* **1957**, *12* (6), 570-586
(641) Kubo, R.; Toda, M.; Hashitsume, N. *Statistical physics II*; Springer, 1991. DOI: 10.1007/978-3-642-58244-8.
(642) Hoover, W. G.; Evans, D. J.; Hickman, R. B.; Ladd, A. J. C.; Ashurst, W. T.; Moran, B. Lennard-Jones triple-point bulk and shear viscosities. Green-Kubo theory, Hamiltonian mechanics, and nonequilibrium molecular dynamics. *Phys. Rev. A.* **1980**, *22* (4), 1690-1697
(643) Evans, D. J.; Morriss, G. P. Nonlinear-response theory for steady planar Couette flow. *Phys. Rev. A.* **1984**, *30* (3), 1528-1530
(644) Lampin, E.; Palla, P. L.; Francioso, P. A.; Cleri, F. Thermal conductivity from approach-to-equilibrium molecular dynamics. *J. Appl. Phys.* **2013**, *114* (3), 033525
(645) Melis, C.; Dettori, R.; Vandermeulen, S.; Colombo, L. Calculating thermal conductivity in a transient conduction regime: theory and implementation. *Eur. Phys. J. B.* **2014**, *87* (4), 96
(646) Puligheddu, M.; Gygi, F.; Galli, G. First-principles simulations of heat transport. *Phys. Rev. Mater.* **2017**, *1* (6), 060802
(647) McGaughey, A. J. H.; Kaviany, M. Thermal conductivity decomposition and analysis using molecular dynamics simulations. Part I. Lennard-Jones argon. *International Journal of Heat and Mass Transfer* **2004**, *47* (8), 1783-1798
(648) McGaughey, A. J. H.; Kaviany, M. Thermal conductivity decomposition and analysis using molecular dynamics simulations: Part II. Complex silica structures. *International Journal of Heat and Mass Transfer* **2004**, *47* (8), 1799-1816
(649) McGaughey, A. J. H.; Kaviany, M. Quantitative validation of the Boltzmann transport equation phonon thermal conductivity model under the single-mode relaxation time approximation. *Phys. Rev. B.* **2004**, *69* (9), 094303
(650) Macdowell, L. G. On the calculation of the frequency sum rules of the heat flux correlation function. *Molecular Physics* **1999**, *96* (5), 881-884
(651) Khadem, M. H.; Wemhoff, A. P. Comparison of Green–Kubo and NEMD heat flux formulations for thermal conductivity prediction using the Tersoff potential. *Comput. Mater. Sci.* **2013**, *69*, 428-434
(652) Carbogno, C.; Ramprasad, R.; Scheffler, M. Ab Initio Green-Kubo Approach for the Thermal Conductivity of Solids. *Phys. Rev. Lett.* **2017**, *118* (17), 175901
(653) Boone, P.; Babaei, H.; Wilmer, C. E. Heat Flux for Many-Body Interactions: Corrections to LAMMPS. *J. Chem. Theory. Comput.* **2019**, *15* (10), 5579-5587
(654) Surblys, D.; Matsubara, H.; Kikugawa, G.; Ohara, T. Application of atomic stress to compute heat flux via molecular dynamics for systems with many-body interactions. *Phys. Rev. E.* **2019**, *99* (5), 051301
(655) Jund, P.; Jullien, R. Molecular-dynamics calculation of the thermal conductivity of vitreous silica. *Phys. Rev. B.* **1999**, *59* (21), 13707-13711
(656) Ikeshoji, T.; Hafskjold, B. Non-equilibrium molecular dynamics calculation of heat conduction in liquid and through liquid-gas interface. *Molecular Physics* **1994**, *81* (2), 251-261
(657) Müller-Plathe, F. A simple nonequilibrium molecular dynamics method for calculating the thermal conductivity. *J. Chem. Phys.* **1997**, *106* (14), 6082-6085
(658) Müller-Plathe, F.; Reith, D. Cause and effect reversed in non-equilibrium molecular dynamics: an easy route to transport coefficients. *Computational and Theoretical Polymer Science* **1999**, *9* (3), 203-209
(659) Schelling, P. K.; Phillpot, S. R.; Keblinski, P. Comparison of atomic-level simulation methods for computing thermal conductivity. *Phys. Rev. B.* **2002**, *65* (14), 144306

(660) Shi, W.; Shuai, Z.; Wang, D. Tuning Thermal Transport in Chain-Oriented Conducting Polymers for Enhanced Thermoelectric Efficiency: A Computational Study. *Adv. Funct. Mater.* **2017**, *27* (40), 1702847
(661) Genovese, C.; Antidormi, A.; Dettori, R.; Caddeo, C.; Mattoni, A.; Colombo, L.; Melis, C. Linking morphology to thermal conductivity in PEDOT: an atomistic investigation. *Journal of Physics D: Applied Physics* **2017**, *50* (49), 494002
(662) Crnjar, A.; Melis, C.; Colombo, L. Assessing the anomalous superdiffusive heat transport in a single one-dimensional PEDOT chain. *Phys. Rev. Mater.* **2018**, *2* (1), 015603
(663) Maeno, S.; Cannon, J. J.; Shiga, T.; Shiomi, J. Molecular dynamics study on heat conduction in poly(3,4-ethylenedioxythiophene). *Japanese Journal of Applied Physics* **2018**, *57* (10), 101601
(664) Yu, X.; Li, R.; Shiga, T.; Feng, L.; An, M.; Zhang, L.; Shiomi, J.; Yang, N. Hybrid Thermal Transport Characteristics of Doped Organic Semiconductor Poly(3,4-ethylenedioxythiophene):Tosylate. *J. Phys. Chem. C.* **2019**, *123* (43), 26735-26741
(665) Cappai, A.; Antidormi, A.; Bosin, A.; Narducci, D.; Colombo, L.; Melis, C. Impact of synthetic conditions on the anisotropic thermal conductivity of poly(3,4-ethylenedioxythiophene) (PEDOT): A molecular dynamics investigation. *Phys. Rev. Mater.* **2020**, *4* (3), 035401
(666) Shi, W.; Chen, J.; Xi, J.; Wang, D.; Shuai, Z. Search for Organic Thermoelectric Materials with High Mobility: The Case of 2,7-Dialkyl[1]benzothieno[3,2-b][1]benzothiophene Derivatives. *Chem. Mater.* **2014**, *26* (8), 2669-2677
(667) Gueye, M. N.; Vercouter, A.; Jouclas, R.; Guérin, D.; Lemaur, V.; Schweicher, G.; Lenfant, S.; Antidormi, A.; Geerts, Y.; Melis, C.; et al. Thermal conductivity of benzothieno-benzothiophene derivatives at the nanoscale. *Nanoscale* **2021**, *13* (6), 3800-3807
(668) Lv, W.; Winters, R. M.; DeAngelis, F.; Weinberg, G.; Henry, A. Understanding Divergent Thermal Conductivity in Single Polythiophene Chains Using Green–Kubo Modal Analysis and Sonification. *J. Phys. Chem. A.* **2017**, *121* (30), 5586-5596
(669) Zheng, H.; Wu, K.; Chen, W.; Nan, B.; Qu, Z.; Lu, M. High Intrinsic Thermal Conductivity of Polythiophene by Reducing Steric Hindrance and Enhancing p-π Conjugation. *Macromolecular Chemistry and Physics* **2021**, *222* (10), 2000418
(670) Car, R.; Parrinello, M. Unified Approach for Molecular Dynamics and Density-Functional Theory. *Phys. Rev. Lett.* **1985**, *55* (22), 2471-2474
(671) Kratzer, P. Monte Carlo and Kinetic Monte Carlo Methods – A Tutorial. In *Multiscale Simulation Methods in Molecular Sciences - Lecture Notes*, Grotendorst, J., Attig, N., Blügel, S., Marx, D. Eds.; Vol. 42; John von Neumann-Institut für Computing, 2009; pp 51-76.
(672) Andersen, M.; Panosetti, C.; Reuter, K. A Practical Guide to Surface Kinetic Monte Carlo Simulations. *Front. Chem.* **2019**, *7*, 202
(673) Cheimarios, N.; To, D.; Kokkoris, G.; Memos, G.; Boudouvis, A. G. Monte Carlo and Kinetic Monte Carlo Models for Deposition Processes: A Review of Recent Works. *Front. Phys.* **2021**, *9*, 631918
(674) Groves, C.; Greenham, N. C. Monte Carlo Simulations of Organic Photovoltaics. In *Multiscale Modelling of Organic and Hybrid Photovoltaics*, Beljonne, D., Cornil, J. Eds.; Springer Berlin Heidelberg, 2014; pp 257-278.
(675) Shuai, Z.; Geng, H.; Xu, W.; Liao, Y.; André, J.-M. From charge transport parameters to charge mobility in organic semiconductors through multiscale simulation. *Chem. Soc. Rev.* **2014**, *43* (8), 2662-2679
(676) Bjorgaard, J. A.; Köse, M. E. Simulations of singlet exciton diffusion in organic semiconductors: a review. *RSC Adv.* **2015**, *5* (11), 8432-8445
(677) Groves, C. Simulating charge transport in organic semiconductors and devices: a review. *Rep. Prog. Phys.* **2016**, *80* (2), 026502
(678) Lu, N.; Li, L.; Liu, M. A review of carrier thermoelectric-transport theory in organic semiconductors. *Phys. Chem. Chem. Phys.* **2016**, *18* (29), 19503-19525

(679) Baranovskii, S. D. Mott Lecture: Description of Charge Transport in Disordered Organic Semiconductors: Analytical Theories and Computer Simulations. *Phys. Status Solidi A* **2018**, *215* (12), 1700676
(680) Zhang, X.; Li, Z.; Lu, G. First-principles simulations of exciton diffusion in organic semiconductors. *Phys. Rev. B.* **2011**, *84* (23), 235208
(681) Hoffmann, S. T.; Athanasopoulos, S.; Beljonne, D.; Bässler, H.; Köhler, A. How do Triplets and Charges Move in Disordered Organic Semiconductors? A Monte Carlo Study Comprising the Equilibrium and Nonequilibrium Regime. *J. Phys. Chem. C.* **2012**, *116* (31), 16371-16383
(682) Yao, Y.; Si, W.; Hou, X.; Wu, C.-Q. Monte Carlo simulation based on dynamic disorder model in organic semiconductors: From coherent to incoherent transport. *J. Chem. Phys.* **2012**, *136* (23), 234106
(683) van der Kaap, N. J.; Koster, L. J. A. Massively parallel kinetic Monte Carlo simulations of charge carrier transport in organic semiconductors. *J. Comput. Phys.* **2016**, *307*, 321-332
(684) Kaiser, W.; Popp, J.; Rinderle, M.; Albes, T.; Gagliardi, A. Generalized Kinetic Monte Carlo Framework for Organic Electronics. *Algorithms* **2018**, *11* (4), 37
(685) Deng, W.-Q.; Goddard, W. A. Predictions of Hole Mobilities in Oligoacene Organic Semiconductors from Quantum Mechanical Calculations. *J. Phys. Chem. B.* **2004**, *108* (25), 8614-8621
(686) Grimm, S.; Tabatabai, D.; Scherer, A.; Michaelis, J.; Frank, I. Chromophore Localization in Conjugated Polymers: Molecular Dynamics Simulation. *J. Phys. Chem. B.* **2007**, *111* (42), 12053-12058
(687) Troisi, A. Prediction of the Absolute Charge Mobility of Molecular Semiconductors: the Case of Rubrene. *Adv. Mater.* **2007**, *19* (15), 2000-2004
(688) Lan, Y.-K.; Huang, C.-I. A Theoretical Study of the Charge Transfer Behavior of the Highly Regioregular Poly-3-hexylthiophene in the Ordered State. *J. Phys. Chem. B.* **2008**, *112* (47), 14857-14862
(689) Vukmirović, N.; Wang, L.-W. Charge patching method for electronic structure of organic systems. *J. Chem. Phys.* **2008**, *128* (12), 121102
(690) Idé, J.; Méreau, R.; Ducasse, L.; Castet, F.; Olivier, Y.; Martinelli, N.; Cornil, J.; Beljonne, D. Supramolecular Organization and Charge Transport Properties of Self-Assembled π−π Stacks of Perylene Diimide Dyes. *J. Phys. Chem. B.* **2011**, *115* (18), 5593-5603
(691) Liu, T.; Cheung, D. L.; Troisi, A. Structural variability and dynamics of the P3HT/PCBM interface and its effects on the electronic structure and the charge-transfer rates in solar cells. *Phys. Chem. Chem. Phys.* **2011**, *13* (48), 21461-21470
(692) D'Avino, G.; Mothy, S.; Muccioli, L.; Zannoni, C.; Wang, L.; Cornil, J.; Beljonne, D.; Castet, F. Energetics of Electron–Hole Separation at P3HT/PCBM Heterojunctions. *J. Phys. Chem. C.* **2013**, *117* (25), 12981-12990
(693) Idé, J.; Méreau, R.; Ducasse, L.; Castet, F.; Bock, H.; Olivier, Y.; Cornil, J.; Beljonne, D.; D'Avino, G.; Roscioni, O. M.; et al. Charge Dissociation at Interfaces between Discotic Liquid Crystals: The Surprising Role of Column Mismatch. *J. Am. Chem. Soc.* **2014**, *136* (7), 2911-2920
(694) Liu, T.; Troisi, A. Understanding the Microscopic Origin of the Very High Charge Mobility in PBTTT: Tolerance of Thermal Disorder. *Adv. Funct. Mater.* **2014**, *24* (7), 925-933
(695) Olivier, Y.; Niedzialek, D.; Lemaur, V.; Pisula, W.; Müllen, K.; Koldemir, U.; Reynolds, J. R.; Lazzaroni, R.; Cornil, J.; Beljonne, D. 25th Anniversary Article: High-Mobility Hole and Electron Transport Conjugated Polymers: How Structure Defines Function. *Adv. Mater.* **2014**, *26* (14), 2119-2136
(696) Qiu, M.; Brandt, R. G.; Niu, Y.; Bao, X.; Yu, D.; Wang, N.; Han, L.; Yu, L.; Xia, S.; Yang, R. Theoretical Study on the Rational Design of Cyano-Substituted P3HT Materials for OSCs: Substitution Effect on the Improvement of Photovoltaic Performance. *J. Phys. Chem. C.* **2015**, *119* (16), 8501-8511

(697) Tummala, N. R.; Zheng, Z.; Aziz, S. G.; Coropceanu, V.; Brédas, J.-L. Static and Dynamic Energetic Disorders in the C60, PC61BM, C70, and PC71BM Fullerenes. *J. Phys. Chem. Lett.* **2015**, *6* (18), 3657-3662
(698) Ravva, M. K.; Wang, T.; Brédas, J.-L. Nature of the Binding Interactions between Conjugated Polymer Chains and Fullerenes in Bulk Heterojunction Organic Solar Cells. *Chem. Mater.* **2016**, *28* (22), 8181-8189
(699) Pan, Q.-Q.; Li, S.-B.; Duan, Y.-C.; Wu, Y.; Zhang, J.; Geng, Y.; Zhao, L.; Su, Z.-M. Exploring what prompts ITIC to become a superior acceptor in organic solar cell by combining molecular dynamics simulation with quantum chemistry calculation. *Phys. Chem. Chem. Phys.* **2017**, *19* (46), 31227-31235
(700) Rice, B.; Guilbert, A. A. Y.; Frost, J. M.; Nelson, J. Polaron States in Fullerene Adducts Modeled by Coarse-Grained Molecular Dynamics and Tight Binding. *J. Phys. Chem. Lett.* **2018**, *9* (22), 6616-6623
(701) Guilbert, A. A. Y.; Zbiri, M.; Finn, P. A.; Jenart, M.; Fouquet, P.; Cristiglio, V.; Frick, B.; Nelson, J.; Nielsen, C. B. Mapping Microstructural Dynamics up to the Nanosecond of the Conjugated Polymer P3HT in the Solid State. *Chem. Mater.* **2019**, *31* (23), 9635-9651
(702) Wang, T.; Coropceanu, V.; Brédas, J.-L. All-Polymer Solar Cells: Impact of the Length of the Branched Alkyl Side Chains on the Polymer Acceptors on the Interchain Packing and Electronic Properties in Amorphous Blends. *Chem. Mater.* **2019**, *31* (16), 6239-6248
(703) Mombrú, D.; Romero, M.; Faccio, R.; Mombrú, Á. W. Ab Initio Molecular Dynamics Assessment on the Mixed Ionic–Electronic Transport for Crystalline Poly(3-Hexylthiophene) Using Full Explicit Lithium-Based Dopants and Additives. *Macromolecules* **2022**, *55* (1), 113-124
(704) Marcus, R. A. Electron transfer reactions in chemistry. Theory and experiment. *Rev. Mod. Phys.* **1993**, *65* (3), 599-610
(705) Miller, A.; Abrahams, E. Impurity Conduction at Low Concentrations. *Phys. Rev.* **1960**, *120* (3), 745-755
(706) Cheung, D. L.; Troisi, A. Modelling charge transport in organic semiconductors: from quantum dynamics to soft matter. *Phys. Chem. Chem. Phys.* **2008**, *10* (39), 5941-5952
(707) Nelson, J.; Kwiatkowski, J. J.; Kirkpatrick, J.; Frost, J. M. Modeling Charge Transport in Organic Photovoltaic Materials. *Acc. Chem. Res.* **2009**, *42* (11), 1768-1778
(708) McMahon, D. P.; Troisi, A. Organic Semiconductors: Impact of Disorder at Different Timescales. *ChemPhysChem* **2010**, *11* (10), 2067-2074
(709) Rühle, V.; Junghans, C.; Lukyanov, A.; Kremer, K.; Andrienko, D. Versatile Object-Oriented Toolkit for Coarse-Graining Applications. *J. Chem. Theory. Comput.* **2009**, *5* (12), 3211-3223
(710) Rühle, V.; Lukyanov, A.; May, F.; Schrader, M.; Vehoff, T.; Kirkpatrick, J.; Baumeier, B.; Andrienko, D. Microscopic Simulations of Charge Transport in Disordered Organic Semiconductors. *J. Chem. Theory. Comput.* **2011**, *7* (10), 3335-3345
(711) Kirkpatrick, J.; Marcon, V.; Nelson, J.; Kremer, K.; Andrienko, D. Charge Mobility of Discotic Mesophases: A Multiscale Quantum and Classical Study. *Phys. Rev. Lett.* **2007**, *98* (22), 227402
(712) Martinelli, N. G.; Olivier, Y.; Athanasopoulos, S.; Ruiz Delgado, M.-C.; Pigg, K. R.; da Silva Filho, D. A.; Sánchez-Carrera, R. S.; Venuti, E.; Della Valle, R. G.; Brédas, J.-L.; et al. Influence of Intermolecular Vibrations on the Electronic Coupling in Organic Semiconductors: The Case of Anthracene and Perfluoropentacene. *ChemPhysChem* **2009**, *10* (13), 2265-2273
(713) Lukyanov, A.; Andrienko, D. Extracting nondispersive charge carrier mobilities of organic semiconductors from simulations of small systems. *Phys. Rev. B.* **2010**, *82* (19), 193202
(714) MacKenzie, R. C. I.; Frost, J. M.; Nelson, J. A numerical study of mobility in thin films of fullerene derivatives. *J. Chem. Phys.* **2010**, *132* (6), 064904
(715) Vehoff, T.; Chung, Y. S.; Johnston, K.; Troisi, A.; Yoon, D. Y.; Andrienko, D. Charge Transport in Self-Assembled Semiconducting Organic Layers: Role of Dynamic and Static Disorder. *J. Phys. Chem. C.* **2010**, *114* (23), 10592-10597

(716) Wang, L.; Li, Q.; Shuai, Z.; Chen, L.; Shi, Q. Multiscale study of charge mobility of organic semiconductor with dynamic disorders. *Phys. Chem. Chem. Phys.* **2010**, *12* (13), 3309-3314
(717) Geng, H.; Peng, Q.; Wang, L.; Li, H.; Liao, Y.; Ma, Z.; Shuai, Z. Toward Quantitative Prediction of Charge Mobility in Organic Semiconductors: Tunneling Enabled Hopping Model. *Adv. Mater.* **2012**, *24* (26), 3568-3572
(718) Bashir, A.; Heck, A.; Narita, A.; Feng, X.; Nefedov, A.; Rohwerder, M.; Müllen, K.; Elstner, M.; Wöll, C. Charge carrier mobilities in organic semiconductors: crystal engineering and the importance of molecular contacts. *Phys. Chem. Chem. Phys.* **2015**, *17* (34), 21988-21996
(719) Qiu, M.; Zhu, D.; Yan, L.; Wang, N.; Han, L.; Bao, X.; Du, Z.; Niu, Y.; Yang, R. Strategy to Manipulate Molecular Orientation and Charge Mobility in D–A Type Conjugated Polymer through Rational Fluorination for Improvements of Photovoltaic Performances. *J. Phys. Chem. C.* **2016**, *120* (40), 22757-22765
(720) Paterson, A. F.; Li, R.; Markina, A.; Tsetseris, L.; MacPhee, S.; Faber, H.; Emwas, A.-H.; Panidi, J.; Bristow, H.; Wadsworth, A.; et al. N-Doping improves charge transport and morphology in the organic non-fullerene acceptor O-IDTBR. *J. Mater. Chem. C Mater* **2021**, *9* (13), 4486-4495
(721) Dilmurat, R.; Lemaur, V.; Olivier, Y.; Gali, S. M.; Beljonne, D. Tuning Short Contacts between Polymer Chains To Enhance Charge Transport in Amorphous Donor–Acceptor Polymers. *J. Phys. Chem. C.* **2022**, *126* (6), 3118-3126
(722) Franck, J.; Dymond, E. G. Elementary processes of photochemical reactions. *Trans. Faraday Soc.* **1926**, *21* (February), 536-542
(723) Webster, D. L. Minutes of the Stanford Meeting, March 6, 1926. *Phys. Rev.* **1926**, *27* (5), 637-644
(724) Condon, E. A Theory of Intensity Distribution in Band Systems. *Phys. Rev.* **1926**, *28* (6), 1182-1201
(725) Condon, E. U. Nuclear Motions Associated with Electron Transitions in Diatomic Molecules. *Phys. Rev.* **1928**, *32* (6), 858-872
(726) Emin, D.; Holstein, T. Adiabatic Theory of an Electron in a Deformable Continuum. *Phys. Rev. Lett.* **1976**, *36* (6), 323-326
(727) Munn, R. W.; Silbey, R. Theory of electronic transport in molecular crystals. II. Zeroth order states incorporating nonlocal linear electron–phonon coupling. *J. Chem. Phys.* **1985**, *83* (4), 1843-1853
(728) Martinelli, N. G.; Idé, J.; Sánchez-Carrera, R. S.; Coropceanu, V.; Brédas, J.-L.; Ducasse, L.; Castet, F.; Cornil, J.; Beljonne, D. Influence of Structural Dynamics on Polarization Energies in Anthracene Single Crystals. *J. Phys. Chem. C.* **2010**, *114* (48), 20678-20685
(729) Coropceanu, V.; Li, Y.; Yi, Y.; Zhu, L.; Brédas, J.-L. Intrinsic charge transport in single crystals of organic molecular semiconductors: A theoretical perspective. *MRS Bull.* **2013**, *38* (1), 57-64
(730) Sánchez-Carrera, R. S.; Paramonov, P.; Day, G. M.; Coropceanu, V.; Brédas, J.-L. Interaction of Charge Carriers with Lattice Vibrations in Oligoacene Crystals from Naphthalene to Pentacene. *J. Am. Chem. Soc.* **2010**, *132* (41), 14437-14446
(731) Yi, Y.; Coropceanu, V.; Brédas, J.-L. Nonlocal electron-phonon coupling in the pentacene crystal: Beyond the Γ-point approximation. *J. Chem. Phys.* **2012**, *137* (16), 164303
(732) Tu, Z.; Yi, Y.; Coropceanu, V.; Brédas, J.-L. Impact of Phonon Dispersion on Nonlocal Electron–Phonon Couplings in Organic Semiconductors: The Naphthalene Crystal as a Case Study. *J. Phys. Chem. C.* **2018**, *122* (1), 44-49
(733) Harrelson, T. F.; Dettmann, M.; Scherer, C.; Andrienko, D.; Moulé, A. J.; Faller, R. Computing inelastic neutron scattering spectra from molecular dynamics trajectories. *Sci. Rep.* **2021**, *11* (1), 7938
(734) Reimers, J. R. A practical method for the use of curvilinear coordinates in calculations of normal-mode-projected displacements and Duschinsky rotation matrices for large molecules. *J. Chem. Phys.* **2001**, *115* (20), 9103-9109
(735) Togo, A.; Tanaka, I. First principles phonon calculations in materials science. *Scripta Materialia* **2015**, *108*, 1-5

(736) Marcus, R. A. On the Theory of Oxidation-Reduction Reactions Involving Electron Transfer. I. *J. Chem. Phys.* **1956**, *24* (5), 966-978
(737) Marcus, R. A. Exchange reactions and electron transfer reactions including isotopic exchange. Theory of oxidation-reduction reactions involving electron transfer. Part 4.—A statistical-mechanical basis for treating contributions from solvent, ligands, and inert salt. *Discuss. Faraday Soc.* **1960**, *29* (0), 21-31
(738) Marcus, R. A. On the Theory of Electron-Transfer Reactions. VI. Unified Treatment for Homogeneous and Electrode Reactions. *J. Chem. Phys.* **1965**, *43* (2), 679-701
(739) Marcus, R. A. Theoretical relations among rate constants, barriers, and Broensted slopes of chemical reactions. *J. Phys. Chem.* **1968**, *72* (3), 891-899
(740) Marcus, R. A.; Sutin, N. Electron transfers in chemistry and biology. *Biochim. Biophys. Acta Bioenerg.* **1985**, *811* (3), 265-322
(741) Bajorath, J. Integration of virtual and high-throughput screening. *Nature Reviews Drug Discovery* **2002**, *1* (11), 882-894
(742) Subramaniam, S.; Mehrotra, M.; Gupta, D. Virtual high throughput screening (vHTS) – A perspective. *Bioinformation* **2008**, *3* (1), 14-17
(743) Mayr, L. M.; Bojanic, D. Novel trends in high-throughput screening. *Current Opinion in Pharmacology* **2009**, *9* (5), 580-588
(744) Greeley, J.; Jaramillo, T. F.; Bonde, J.; Chorkendorff, I.; Nørskov, J. K. Computational high-throughput screening of electrocatalytic materials for hydrogen evolution. *Nat. Mater.* **2006**, *5* (11), 909-913
(745) Jain, A.; Hautier, G.; Moore, C. J.; Ping Ong, S.; Fischer, C. C.; Mueller, T.; Persson, K. A.; Ceder, G. A high-throughput infrastructure for density functional theory calculations. *Comput. Mater. Sci.* **2011**, *50* (8), 2295-2310
(746) Setyawan, W.; Gaume, R. M.; Lam, S.; Feigelson, R. S.; Curtarolo, S. High-Throughput Combinatorial Database of Electronic Band Structures for Inorganic Scintillator Materials. *ACS Comb. Sci* **2011**, *13*, 382-390
(747) Saal, J. E.; Kirklin, S.; Aykol, M.; Meredig, B.; Wolverton, C. Materials Design and Discovery with High-Throughput Density Functional Theory: The Open Quantum Materials Database (OQMD). *JOM* **2013**, *65* (11), 1501-1509
(748) Pyzer-Knapp, E. O.; Suh, C.; Gómez-Bombarelli, R.; Aguilera-Iparraguirre, J.; Aspuru-Guzik, A. What Is High-Throughput Virtual Screening? A Perspective from Organic Materials Discovery. *Annu. Rev. Mater. Res.* **2015**, *45* (1), 195-216
(749) Hachmann, J.; Olivares-Amaya, R.; Atahan-Evrenk, S.; Amador-Bedolla, C.; Sánchez-Carrera, R. S.; Gold-Parker, A.; Vogt, L.; Brockway, A. M.; Aspuru-Guzik, A. The Harvard Clean Energy Project: Large-Scale Computational Screening and Design of Organic Photovoltaics on the World Community Grid. *J. Phys. Chem. Lett.* **2011**, *2* (17), 2241-2251
(750) Hachmann, J.; Olivares-Amaya, R.; Jinich, A.; Appleton, A. L.; Blood-Forsythe, M. A.; Seress, L. R.; Román-Salgado, C.; Trepte, K.; Atahan-Evrenk, S.; Er, S.; et al. Lead candidates for high-performance organic photovoltaics from high-throughput quantum chemistry – the Harvard Clean Energy Project. *Energy Environ. Sci.* **2014**, *7* (2), 698-704
(751) Wilbraham, L.; Berardo, E.; Turcani, L.; Jelfs, K. E.; Zwijnenburg, M. A. High-Throughput Screening Approach for the Optoelectronic Properties of Conjugated Polymers. *J. Chem. Inf. Model.* **2018**, *58* (12), 2450-2459
(752) Schober, C.; Reuter, K.; Oberhofer, H. Virtual Screening for High Carrier Mobility in Organic Semiconductors. *J. Phys. Chem. Lett.* **2016**, *7* (19), 3973-3977
(753) Nematiaram, T.; Padula, D.; Landi, A.; Troisi, A. On the Largest Possible Mobility of Molecular Semiconductors and How to Achieve It. *Adv. Funct. Mater.* **2020**, *30* (30), 2001906-2001906
(754) Omar, Ö. H.; Nematiaram, T.; Troisi, A.; Padula, D. Organic materials repurposing, a data set for theoretical predictions of new applications for existing compounds. *Sci. Data.* **2022**, *9* (1), 54

(755) Ai, Q.; Bhat, V.; Ryno, S. M.; Jarolimek, K.; Sornberger, P.; Smith, A.; Haley, M. M.; Anthony, J. E.; Risko, C. OCELOT: An infrastructure for data-driven research to discover and design crystalline organic semiconductors. *The Journal of Chemical Physics* **2021**, *154* (17), 174705
(756) Groom, C. R.; Bruno, I. J.; Lightfoot, M. P.; Ward, S. C. The Cambridge Structural Database. *Acta Crystallographica Section B* **2016**, *72* (2), 171-179
(757) Hoerl, A. E.; Kennard, R. W. Ridge Regression: Biased Estimation for Nonorthogonal Problems. *Technometrics* **1970**, *12* (1), 55-67
(758) Cortes, C.; Vapnik, V. Support-vector networks. *Mach. Learn.* **1995**, *20* (3), 273-297
(759) Wu, X.; Kumar, V.; Ross Quinlan, J.; Ghosh, J.; Yang, Q.; Motoda, H.; Mclachlan, G. J.; Ng, A.; Liu, B.; Yu, P. S.; et al. Top 10 algorithms in data mining. *Knowl. Inf. Syst.* **2008**, *14* (1), 1-37
(760) Mcculloch, W. S.; Pitts, W. A logical calculus of the ideas immanent in nervous activity. *Bull. Math. Biophys.* **1943**, *5* (4), 115-133
(761) Bhat, V.; Sornberger, P.; Pokuri, B. S. S.; Duke, R.; Ganapathysubramanian, B.; Risko, C. Electronic, redox, and optical property prediction of organic π-conjugated molecules through a hierarchy of machine learning approaches. *Chem. Sci.* **2023**, *14* (1), 203-213
(762) Westermayr, J.; Marquetand, P. Machine Learning for Electronically Excited States of Molecules. *Chem. Rev.* **2021**, *121* (16), 9873-9926
(763) Lederer, J.; Kaiser, W.; Mattoni, A.; Gagliardi, A. Machine Learning–Based Charge Transport Computation for Pentacene. *Adv. Theory Simul.* **2019**, *2* (2), 1800136
(764) Borysov, S. S.; Geilhufe, R. M.; Balatsky, A. V. Organic materials database: An open-access online database for data mining. *PLoS One* **2017**, *12* (2), e0171501
(765) Wang, H.; Ma, C.; Zhou, L. A Brief Review of Machine Learning and Its Application. In *2009 International Conference on Information Engineering and Computer Science*, 19-20 Dec. 2009, 2009; pp 1-4. DOI: 10.1109/ICIECS.2009.5362936.
(766) Jordan, M. I.; Mitchell, T. M. Machine learning: Trends, perspectives, and prospects. *Science* **2015**, *349* (6245), 255-260
(767) Sun, W.; Zheng, Y.; Yang, K.; Zhang, Q.; Shah, A. A.; Wu, Z.; Sun, Y.; Feng, L.; Chen, D.; Xiao, Z.; et al. Machine learning and assisted molecular design and efficiency prediction for high-performance organic photovoltaic materials. *Sci. Adv.* **2019**, *5* (11), eaay4275
(768) Rogers, D.; Hahn, M. Extended-Connectivity Fingerprints. *J. Chem. Inf. Model.* **2010**, *50* (5), 742-754
(769) Durant, J. L.; Leland, B. A.; Henry, D. R.; Nourse, J. G. Reoptimization of MDL Keys for Use in Drug Discovery. *J. Chem. Inf. Comput.* **2002**, *42* (6), 1273-1280
(770) Pyzer-Knapp, E. O.; Li, K.; Aspuru-Guzik, A. Learning from the Harvard Clean Energy Project: The Use of Neural Networks to Accelerate Materials Discovery. *Adv. Funct. Mater.* **2015**, *25* (41), 6495-6502
(771) Duvenaud, D. K.; Maclaurin, D.; Aguilera-Iparraguirre, J.; Gómez-Bombarelli, R.; Hirzel, T. D.; Aspuru-Guzik, A.; Adams, R. P. Convolutional Networks on Graphs for Learning Molecular Fingerprints. *ArXiv* **2015**, *abs/1509.09292*,
(772) Bengio, Y.; Courville, A. C.; Vincent, P. Representation Learning: A Review and New Perspectives. *IEEE Trans. Pattern. Anal. Mach. Intell.* **2013**, *35* (8), 1798-1828
(773) Weininger, D. SMILES, a chemical language and information system. 1. Introduction to methodology and encoding rules. *J. Chem. Inf. Comput.* **1988**, *28* (1), 31-36
(774) Kingma, D. P.; Welling, M. An Introduction to Variational Autoencoders. *ArXiv* **2019**, *abs/1906.02691*,
(775) Gómez-Bombarelli, R.; Wei, J. N.; Duvenaud, D.; Hernández-Lobato, J. M.; Sánchez-Lengeling, B.; Sheberla, D.; Aguilera-Iparraguirre, J.; Hirzel, T. D.; Adams, R. P.; Aspuru-Guzik, A. Automatic Chemical Design Using a Data-Driven Continuous Representation of Molecules. *ACS Cent. Sci.* **2018**, *4* (2), 268-276
(776) Ramakrishnan, R.; Dral, P. O.; Rupp, M.; von Lilienfeld, O. A. Quantum chemistry structures and properties of 134 kilo molecules. *Sci. Data.* **2014**, *1* (1), 140022

(777) Schütt, K.; Kindermans, P.-J.; Felix, H. E. S.; Chmiela, S.; Tkatchenko, A.; Müller, K.-R. SchNet: A continuous-filter convolutional neural network for modeling quantum interactions. *ArXiv* **2017**, *abs/1706.08566*,
(778) Schütt, K. T.; Sauceda, H. E.; Kindermans, P.-J.; Tkatchenko, A.; Müller, K.-R. SchNet – A deep learning architecture for molecules and materials. *J. Chem. Phys.* **2018**, *148* (24), 241722
(779) Gilmer, J.; Schoenholz, S. S.; Riley, P. F.; Vinyals, O.; Dahl, G. E. Neural Message Passing for Quantum Chemistry. *ArXiv* **2017**, *abs/1704.01212*,
(780) Chen, C.; Ye, W.; Zuo, Y.; Zheng, C.; Ong, S. P. Graph Networks as a Universal Machine Learning Framework for Molecules and Crystals. *Chem. Mater.* **2019**, *31* (9), 3564-3572
(781) Qiao, Z.; Welborn, M.; Anandkumar, A.; Manby, F. R.; Miller, T. F. OrbNet: Deep learning for quantum chemistry using symmetry-adapted atomic-orbital features. *J. Chem. Phys.* **2020**, *153* (12), 124111
(782) Choudhary, K.; DeCost, B. Atomistic Line Graph Neural Network for improved materials property predictions. *Npj Comput. Mater.* **2021**, *7* (1), 185
(783) Klicpera, J.; Giri, S.; Margraf, J. T.; Gunnemann, S. Fast and Uncertainty-Aware Directional Message Passing for Non-Equilibrium Molecules. *ArXiv* **2020**, *abs/2011.14115*,
(784) Unke, O. T.; Meuwly, M. PhysNet: A Neural Network for Predicting Energies, Forces, Dipole Moments, and Partial Charges. *J. Chem. Theory. Comput.* **2019**, *15* (6), 3678-3693
(785) Lu, C.; Liu, Q.; Sun, Q.; Hsieh, C.-Y.; Zhang, S.; Shi, L.; Lee, C.-K. Deep Learning for Optoelectronic Properties of Organic Semiconductors. *J. Phys. Chem. C.* **2020**, *124* (13), 7048-7060
(786) Ito, D.; Shirasawa, R.; Hattori, S.; Tomiya, S.; Tanaka, G. Prediction of Molecular Packing Motifs in Organic Crystals by Neural Graph Fingerprints. In *Neural Information Processing*, Springer International Publishing, 2018; pp 26-34.
(787) Sun, W.; Li, M.; Li, Y.; Wu, Z.; Sun, Y.; Lu, S.; Xiao, Z.; Zhao, B.; Sun, K. The Use of Deep Learning to Fast Evaluate Organic Photovoltaic Materials. *Adv. Theory Simul.* **2019**, *2* (1), 1800116
(788) Albawi, S.; Mohammed, T. A.; Al-Zawi, S. Understanding of a convolutional neural network. In *2017 International Conference on Engineering and Technology (ICET)*, 21-23 Aug. 2017, 2017; pp 1-6. DOI: 10.1109/ICEngTechnol.2017.8308186.
(789) Atahan-Evrenk, S.; Atalay, F. B. Prediction of Intramolecular Reorganization Energy Using Machine Learning. *J. Phys. Chem. A.* **2019**, *123* (36), 7855-7863
(790) Olsthoorn, B.; Geilhufe, R. M.; Borysov, S. S.; Balatsky, A. V. Band Gap Prediction for Large Organic Crystal Structures with Machine Learning. *Adv. Quantum Technol.* **2019**, *2* (7-8), 1900023
(791) Wang, C.-I.; Joanito, I.; Lan, C.-F.; Hsu, C.-P. Artificial neural networks for predicting charge transfer coupling. *J. Chem. Phys.* **2020**, *153* (21), 214113
(792) Bartók, A. P.; Kondor, R.; Csányi, G. On representing chemical environments. *Phys. Rev. B.* **2013**, *87* (18), 184115
(793) Rupp, M.; Tkatchenko, A.; Müller, K.-R.; Von Lilienfeld, O. A. Fast and Accurate Modeling of Molecular Atomization Energies with Machine Learning. *Phys. Rev. Lett.* **2012**, *108* (5), 058301
(794) Jørgensen, P. B.; Mesta, M.; Shil, S.; García Lastra, J. M.; Jacobsen, K. W.; Thygesen, K. S.; Schmidt, M. N. Machine learning-based screening of complex molecules for polymer solar cells. *J. Chem. Phys.* **2018**, *148* (24), 241735
(795) Sherstinsky, A. Fundamentals of Recurrent Neural Network (RNN) and Long Short-Term Memory (LSTM) Network. *ArXiv* **2018**, *abs/1808.03314*,
(796) Kim, K.; Kang, S.; Yoo, J.; Kwon, Y.; Nam, Y.; Lee, D.; Kim, I.; Choi, Y.-S.; Jung, Y.; Kim, S.; et al. Deep-learning-based inverse design model for intelligent discovery of organic molecules. *Npj Comput. Mater.* **2018**, *4* (1), 67
(797) Nigam, A.; Pollice, R.; Krenn, M.; Gomes, G. D. P.; Aspuru-Guzik, A. Beyond generative models: superfast traversal, optimization, novelty, exploration and discovery (STONED) algorithm for molecules using SELFIES. *Chem. Sci.* **2021**, *12* (20), 7079-7090

(798) Guo, M.; Shou, W.; Makatura, L.; Erps, T.; Foshey, M.; Matusik, W. Polygrammar: Grammar for Digital Polymer Representation and Generation. *Adv. Sci.* **2022**, *9* (23), 2101864
(799) Krenn, M.; Häse, F.; Nigam, A.; Friederich, P.; Aspuru-Guzik, A. SELFIES: a robust representation of semantically constrained graphs with an example application in chemistry. *ArXiv* **2019**, *abs/1905.13741*,
(800) Zang, C.; Wang, F. MoFlow: An Invertible Flow Model for Generating Molecular Graphs. *ArXiv* **2020**, *abs/2006.10137*,
(801) Frey, N. C.; Gadepally, V. N.; Ramsundar, B. FastFlows: Flow-Based Models for Molecular Graph Generation. *ArXiv* **2022**, *abs/2201.12419*,
(802) Satorras, V. G.; Hoogeboom, E.; Fuchs, F. B.; Posner, I.; Welling, M. E(n) Equivariant Normalizing Flows. *ArXiv* **2021**, *abs/2105.09016*,
(803) Hoogeboom, E.; Satorras, V. G.; Vignac, C. e.; Welling, M. Equivariant Diffusion for Molecule Generation in 3D. In *International Conference on Machine Learning*, 2022.
(804) Guarino, M. DiPol-GAN : Generating Molecular Graphs Adversarially with Relational Differentiable Pooling. 2019.
(805) Prykhodko, O.; Johansson, S. V.; Kotsias, P.-C.; Arús-Pous, J.; Bjerrum, E. J.; Engkvist, O.; Chen, H. A de novo molecular generation method using latent vector based generative adversarial network. *J. Cheminform.* **2019**, *11* (1), 74
(806) De Cao, N.; Kipf, T. MolGAN: An implicit generative model for small molecular graphs. *ArXiv* **2018**, *abs/1805.11973*,
(807) Maziarka, Ł.; Pocha, A.; Kaczmarczyk, J.; Rataj, K.; Danel, T.; Warchoł, M. Mol-CycleGAN: a generative model for molecular optimization. *J. Cheminform.* **2020**, *12* (1), 2
(808) Vasudevan, R.; Pilania, G.; Balachandran, P. V. Machine learning for materials design and discovery. *J. Appl. Phys.* **2021**, *129* (7), 070401
(809) Abroshan, H.; Kwak, H. S.; An, Y.; Brown, C.; Chandrasekaran, A.; Winget, P.; Halls, M. D. Active Learning Accelerates Design and Optimization of Hole-Transporting Materials for Organic Electronics. *Front. Chem.* **2021**, *9*, 800371
(810) Kunkel, C.; Margraf, J. T.; Chen, K.; Oberhofer, H.; Reuter, K. Active discovery of organic semiconductors. *Nat. Commun.* **2021**, *12* (1), 2422
(811) Smith, J. S.; Nebgen, B.; Lubbers, N.; Isayev, O.; Roitberg, A. E. Less is more: Sampling chemical space with active learning. *J. Chem. Phys.* **2018**, *148* (24), 241733
(812) Manzhos, S.; Carrington, T. Neural Network Potential Energy Surfaces for Small Molecules and Reactions. *Chem. Rev.* **2021**, *121* (16), 10187-10217
(813) Unke, O. T.; Chmiela, S.; Sauceda, H. E.; Gastegger, M.; Poltavsky, I.; Schütt, K. T.; Tkatchenko, A.; Müller, K.-R. Machine Learning Force Fields. *Chem. Rev.* **2021**, *121* (16), 10142-10186
(814) Smith, J. S.; Isayev, O.; Roitberg, A. E. ANI-1: an extensible neural network potential with DFT accuracy at force field computational cost. *Chem. Sci.* **2017**, *8* (4), 3192-3203
(815) Devereux, C.; Smith, J. S.; Huddleston, K. K.; Barros, K.; Zubatyuk, R.; Isayev, O.; Roitberg, A. E. Extending the Applicability of the ANI Deep Learning Molecular Potential to Sulfur and Halogens. *J. Chem. Theory. Comput.* **2020**, *16* (7), 4192-4202
(816) Zubatyuk, R.; Smith, J. S.; Leszczynski, J.; Isayev, O. Accurate and transferable multitask prediction of chemical properties with an atoms-in-molecules neural network. *Sci. Adv.* **2019**, *5* (8), eaav6490
(817) Bader, R. F. W. Atoms in molecules. *Acc. Chem. Res.* **1985**, *18* (1), 9-15
(818) Zubatyuk, R.; Smith, J. S.; Nebgen, B. T.; Tretiak, S.; Isayev, O. Teaching a neural network to attach and detach electrons from molecules. *Nat. Commun.* **2021**, *12* (1), 4870
(819) Liu, Z.; Zubatiuk, T.; Roitberg, A.; Isayev, O. Auto3D: Automatic Generation of the Low-Energy 3D Structures with ANI Neural Network Potentials. *J. Chem. Inf. Model.* **2022**, *62* (22), 5373-5382
(820) Gao, X.; Ramezanghorbani, F.; Isayev, O.; Smith, J. S.; Roitberg, A. E. TorchANI: A Free and Open Source PyTorch-Based Deep Learning Implementation of the ANI Neural Network Potentials. *J. Chem. Inf. Model.* **2020**, *60* (7), 3408-3415

(821) Aspuru-Guzik, A.; Dutoi, A. D.; Love, P. J.; Head-Gordon, M. Simulated Quantum Computation of Molecular Energies. *Science* **2005**, *309* (5741), 1704-1707
(822) Yoshida, R.; Lötstedt, E.; Yamanouchi, K. Quantum computing of Hückel molecular orbitals of π-electron systems. *J. Chem. Phys.* **2022**, *156* (18), 184117
(823) Kowalski, K.; Bair, R.; Bauman, N. P.; Boschen, J. S.; Bylaska, E. J.; Daily, J.; De Jong, W. A.; Dunning, T.; Govind, N.; Harrison, R. J.; et al. From NWChem to NWChemEx: Evolving with the Computational Chemistry Landscape. *Chem. Rev.* **2021**, *121* (8), 4962-4998
(824) *Simulation Environment for Atomistic and Molecular Simulations (SEAMM)*. 2018. https://github.com/molssi-seamm/seamm (accessed 2022-10-09).
(825) Wilkinson, M. D.; Dumontier, M.; Aalbersberg, I. J.; Appleton, G.; Axton, M.; Baak, A.; Blomberg, N.; Boiten, J.-W.; da Silva Santos, L. B.; Bourne, P. E.; et al. The FAIR Guiding Principles for scientific data management and stewardship. *Sci. Data.* **2016**, *3* (1), 160018